AN ABSTRACT OF THE THESIS OF

Stephen L. Albright for the degree of Doctor of Philosophy in Mechanical Engineering presented on February 19, 1990.

Title: Kinematics of Arthropod Legs: Modeling and Measurement

Abstract approved:

Redacted for Privacy

Eugene F. Fichter

Redacted for Privacy

Charles E. Smith

This thesis presents a method for determining the kinematic geometry of arthropod legs. A kinematic description makes possible the analysis of arthropod leg motion, as a prelude to investigating how various arthropod species are able to negotiate diverse terrains. Such knowledge will aid in design of legged vehicles.

The focus is on three areas: leg modeling, leg measurement for model-parameter determination, and effects of model-parameter accuracy. Three characteristics are considered important to arthropod leg modeling. The model must show proportionality to differences in leg geometry, physically resemble the leg being modeled and be adaptable

to various joint types found in arthropods. In successfully addressing all these concerns, the model presented in this work is an improvement over other available models.

Measuring the small arthropod leg requires specialized equipment design and measurement technique. A microscope mounted over a positioner which measures three translations and two rotations makes it possible to determine position, orientation and range-of-motion of each successive joint. Model parameters are calculated from these measurements.

Measurement errors in positioning equipment are quantified. A technique for representing these measurement errors as errors in the position and orientation of each joint axis is presented. Joint axis errors are superposed to form an error volume surrounding the foot position. Foot-position error can be used to evaluate accuracy of leg-model parameters computed from the measurement method.

This technique was used to measure the right middle leg of a darkling beetle and proved to be an effective tool for quantifying kinematic parameters of a small articulated biological mechanism. Such methods may also prove useful for measuring small engineering mechanisms.

Kinematics of Arthropod Legs: Modeling and Measurement

by

Stephen L. Albright

A THESIS

submitted to

Oregon State University

in partial fulfillment of
the requirements for the
degree of

Doctor of Philosophy

Completed February 19, 1990

Commencement June 1990

APPROVED:

Redacted for Privacy

Professor of Industrial and General Engineering in charge of co-major

Redacted for Privacy

Professor of Mechanical Engineering in charge of co-major

Redacted for Privacy

Head of Department of Mechanical Engineering

Redacted for Privacy

Dean of Graduate School

Date thesis is presented February 19, 1990

ACKNOWLEDGEMENT

Special thanks are first due to Dr. Eugene F. Fichter, my major advisor. His hours of guidance not only helped me with the thesis, but taught me the fundamentals of scientific investigation.

I would also like to thank Dr. Becky Fichter for her useful suggestions in the laboratory and her educating me on the biological aspects of this work. Additional thanks are extended to my committee members, Dr. Charles E. Smith, Dr. Andrzej Olas and Dr. Lorin Davis for their advice and encouragement.

Final thanks go to Susan Albright for her professional preparation of technical illustrations in this thesis.

The majority of my financial support during the course of this work came from the Boeing Engineering Educator Fellowship. Support also came from the National Science Foundation Engineering Division under grant numbers MSM-8613337 and MSM-8711182.

TABLE OF CONTENTS

LIST OF FIGURES

LIST OF TABLES

KINEMATICS OF ARTHROPOD LEGS: MODELING AND MEASUREMENT

1. INTRODUCTION

This research into the kinematics of arthropod legs was born out of current interest in legged vehicles. Legged vehicles or walking machines have the potential advantage over wheeled or tracked vehicles of being able to travel in difficult terrains. Their capabilities in climbing steep inclines, maneuvering around obstacles or traversing narrow beams could be useful in environments hazardous to humans such as areas where toxic chemical or radioactive material are present. Other suggested uses are for maintenance of space stations or underwater structures.

Walking machines presently built are only able to move on smooth, nearly horizontal surfaces with few obstacles. A review of these machines was given by Song and Waldron (1989). They note three areas which are crucial to development of a practical walking machine: "control of legged vehicles, gait study and actuation, and leg design." Leg design is becoming more sophisticated but it's complexity is still limited by current control technology so movement in difficult terrains is not yet possible. As control capabilities advance and allow greater control sophistication, mobility of legged vehicles will increase. In preparation for control advances, studies of various leg characteristics necessary for specific movements or motion

of a walking machine is timely.

Design ideas for man-made locomotion, whether it be aerial or terrestrial, have often come from nature. Arthropods, having the ability to travel in extremely diverse environments, provide an excellent opportunity to investigate successful leg design. These animals have an external skeletal structure and relatively simple joints which allow a practical study of their leg geometries and movements.

Several biologists over the years have researched the walking characteristics of arthropods. Most of their attention has been focused on gaits or on muscle and neural control (Fichter, Fichter and Albright, 1987). Until now, no attempt has been made to describe the entire arthropod leg as a force-transmitting mechanism. Without knowledge of the kinematic structure of the leg, it is difficult to investigate why arthropod legs perform so well under such varied environmental conditions.

Presented in this thesis is a method for quantifying the kinematic geometry of arthropod legs. Attention is given first to development of a mathematical model which provides both a kinematic and physical description of the leg. This is followed by presentation of the method and instrumentation used to determine model parameters. Errors in the measuring equipment pertinent to accurate model-parameter determination are then discussed and quantified.

Finally, measurement errors are represented as dimensional errors in each joint axis of the leg and translated to foot position errors, allowing evaluation of the effect of measurement errors on predicted foot position.

Work in this thesis closely relates to research in robot calibration and positioning accuracy. The objective of robot calibration is to measure and model true characteristics of a robot arm in order to improve its positioning accuracy. Errors in positioning generally arise from three sources: dimensional errors, variations between the actual and modeled dimensional relationships of successive joint axes; dynamic errors, deviations due to elastic deflections of links; and joint servo errors, errors in positioning the joints of an arm.

Of the three error sources, robot calibration is used to reduce dimensional errors through measurement of the arm. This has required researchers to develop kinematic models whose parameters are measurable. Since many calibration procedures use numerical techniques to determine model parameters from arm measurements, changes in model parameters must be continuous or change proportionately with slight changes in robot geometry. Several models have been developed which successfully address this problem but often bear no resemblance to the physical appearance of the arm being described. For arthropod legs, it is not only necessary for parameters of a kinematic model to be

measurable but the model must also provide a way to compare legs of different arthropod species or different legs on the same animal. Hence, two important characteristics of arthropod leg models are proportionality and physical resemblance.

A third characteristic not commonly addressed in robot modeling but potentially important to arthropod modeling is adaptability to varying joint types. Most robot links are connected by revolute or prismatic joints and so models have been limited to these two types. Although the predominate joint in arthropods is a revolute, many two and three degree-of-freedom joints do exist. The model described in chapter two of this thesis was developed to address all three of the above concerns.

The accuracy of model parameters relies on the measuring method used in determining them. Measurement for robot calibration purposes has been approached in two ways. The most common is to measure the hand or wrist of a robot in several different positions then numerically determine model parameters which would allow these positions. A more recent approach is to measure the position and orientation of each joint axis individually starting with the joint near the base, fixing its position then measuring the next joint. This technique results in a description of successive joint axis geometries from which many models can be determined analytically. This technique also allows individual

examination of joint motion and leaves flexibility in choice of joint models. The leg measurement method described in chapter three is based on the idea of individual joint measurement. Design of the equipment and techniques used required special consideration of the small size of arthropod legs.

The values of the model parameters determined from measurement of a leg are only as good as the apparatus used for measuring. In chapter four, examination and calibration of the apparatus is discussed. Errors which affect the model were quantified so they could be later used to evaluate accuracy of model parameters.

An important difference between robot arms and arthropod legs is in the ability to remotely control a robot. This allows researchers to test their calibration methods directly. Not having this advantage with arthropod legs, accuracy of the model-parameter values were evaluated using knowledge of the measurement device accuracy. In chapter five, measurement errors of a joint axis are represented as dimensional errors in position and orientation of link model coordinate frames. These errors are then translated to foot position error. Since dimensional errors are defined by a range of values, foot position error is described as an error volume surrounding the foot. It is this volume that can be used to evaluate the effect of errors in model parameters.

Methods presented in this thesis make it possible to describe the kinematic geometry of arthropod legs and therefore provide opportunities for various other studies. For instance, leg movements can be simulated to investigate options various arthropods have for mobility. Geometrical differences between legs of an individual specimen can be evaluated in terms of their functional use. It is anticipated that these and other studies will reveal concepts usable in leg designs of future walking machines.

Results herein are not limited to the study of arthropods. A natural extension of the leg measurement technique is to use it for describing small mechanical mechanisms. The error analysis method of chapter 5 offers a way to investigate the effects dimensional errors have on positioning precision of mechanical manipulators. All such investigations begin with the development of an appropriate model which is the subject of the next chapter.

2. LEG MODELING

2.1. Overview

Arthropod legs consist of 4 to 8 segments and are usually connected by hinge or revolute joints (Fichter and Fichter, 1988). Each joint is typically made up of two ball and socket joints with a single axis of rotation running through their centers. Manton (1973, 1977) described these as pivot joints. Although joints with more degrees of freedom exist, they do not occur often in arthropods because they require more controlling musculature (Manton, 1958).

To analyze position, motion and force capabilities of these legs, a model must be developed that will mathematically describe their kinematic structure. This model needs to accurately represent the motion in each joint and the geometric relationship between successive joint axes.

Models of this nature have been used extensively in analysis of mechanical mechanisms. Their mathematical form is typically a series of transformation matrices, one matrix for each mechanical link. Individual matrices define rotations and translations that transform a joint-axis coordinate frame to its succeeding joint-axis frame. Models from which these transformations are formulated vary but all give a direct relationship between displacement in the joints and position of the mechanism.

Control or prediction of position and motion of a

mechanism is a common use of a kinematic model, although using models for such purposes is difficult to do accurately. The issue of accurate modeling has received much attention in robotics. For robot mechanisms, errors generally arise from three sources: dimensional errors, which are variations between the actual and modeled dimensional relationships; dynamic errors, which are deviations due to elastic deflections of links; and joint servo errors, defined as errors in positioning the joints of an arm. These errors can be reduced by various calibration and compensation techniques which improve model accuracy.

Of the model improvement techniques, those directed toward increasing dimensional accuracy are the most useful at this stage in the modeling of arthropod legs for the following reasons. Compensation for joint servo errors is useful for control of mechanical mechanisms but has little significance for a biological mechanism for which automatic control is not an issue. Elastic deformations certainly occur in anatomical legs, but until leg geometry can be accurately described, these deflections are of secondary importance.

Improving dimensional accuracy of a robot kinematic model is ordinarily accomplished by a procedure called robot calibration. Robot calibration closely relates to leg modeling in this case because the objective of each is to obtain an accurate kinematic description of a mechanism

through measurement. The calibration techniques proposed by researchers involve a variety of kinematic models. From a knowledge of the mechanical models used, a model appropriate for analyzing arthropod legs was developed. Described in this chapter are the criteria for modeling arthropod legs, prior work done in robot modeling for calibration and the resulting arthropod leg model.

2.2 Model Criteria

The leg model will be used in motion studies and as a comparative tool for a wide variety of arthropods. Each leg studied is likely to produce different motions and display different features. Reasons for these differences may be evaluated in terms of variations in leg model parameters. For instance, if a physical feature of a leg is important for a particular motion, then it is important that the model reflect that feature so the feature can be compared to those in other legs. Therefore, in order to make clear comparisons, kinematic parameters must resemble physical characteristics of the leg. These characteristics are segment length and relative orientations of a leg segment's joint axes. It should be noted that the physical resemblance criterion in kinematic models is not necessary to describe motion of a mechanism. This criterion is only important in providing a clear physical description.

Additionally, if kinematic parameters are to be used as

a comparison tool then small differences in leg geometry should be proportionately reflected in the model parameters. Without proportionality, small differences in the physical features of a leg could cause large changes in model parameters and comparisons would be difficult to make.

A final consideration is the adaptability of a leg model to a variety of arthropod leg joints. Although revolute joints are most common in arthropods, some appear to have more degrees-of-freedom (DOF) such as the two and three DOF joints sometimes found at leg extremes (Fichter and Fichter, 1988). For this reason the arthropod leg model should have the flexibility to model other joint types.

In summary, the model representing an arthropod leg should have three characteristics:

1. It should resemble the physical properties of the leg.
2. Its parameters should change proportionately to changes in leg geometry.
3. It should be adaptable to other less common joint types likely to exist in some arthropods.

Criteria important to calibrating mechanical mechanisms are similar in some respects to those mentioned above. For that reason, a review of robot calibration and modeling follows.

2.3. Model Review

Most models used in robot calibration are based on one introduced by Denavit and Hartenberg (1955). In general, six model parameters are required to describe the orientation and position relationships between successive coordinate frames. However, two coordinate frame constraints used in the Denavit-Hartenberg model (D-H model) reduce this number to four (Figure 2.1). The first constraint positions the origin of frame i at the intersection of joint axis i+1 and the common perpendicular between joint axes i and i+1. The second constraint requires that coordinate x_i be parallel to the common perpendicular, a_i. The four parameters of the D-H model are joint displacement θ_i, joint-offset d_i, link-length a_i and link-twist α_i. The transformation from frame i-1 to frame i for the D-H model is as follows.

1. rotate about z by θ_i so x is parallel to the succeeding common perpendicular.
2. translate along z by d_i to the intersection of joint axis i and the common perpendicular.
3. translate along x by a_i to the intersection of joint axis i+1 and the common perpendicular.
4. rotate about x by α_i so z is coincident with joint axis i+1.

The two constraints of the D-H model described above create calibration difficulties when consecutive joint axes

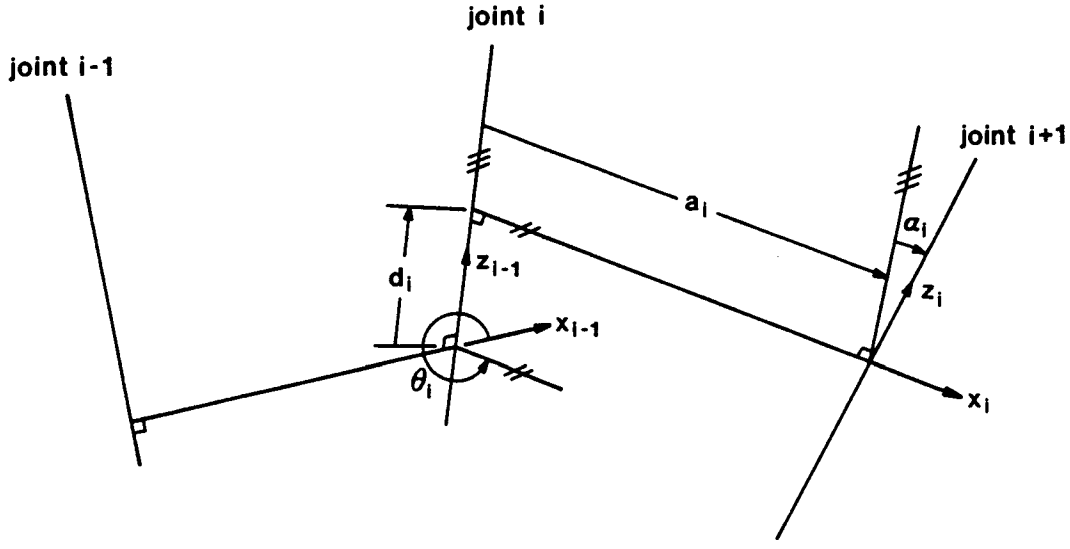

Figure 2.1. Denavit-Hartenberg four-parameter model.

are nearly parallel. Under these conditions the kinematic parameters of the model do not vary proportionately with variations in joint axis alignment. When consecutive joints are parallel, the common perpendicular has an infinite number of possible positions. If joint axis i+1, originally parallel to joint axis i, is rotated slightly about coordinate y_i, the values of three of the four parameters change radically (Figure 2.2). The joint-offset d_i becomes extremely large, the link-length becomes zero and the orientation of x_i shifts 90°. Since many of the robot calibration procedures rely on numerical determination of parameters, convergence problems occur when parameter values do not change proportionately with small changes in link geometry.

This problem has prompted many researchers to modify the D-H model to avoid proportionality problems and make robot calibration possible. Hayati (1983), and Judd and Knasinski (1987) presented an alternative for finding the geometric errors in the nominal D-H model of a robot. When consecutive joint axes were parallel or nearly parallel they added a final rotation about y to avoid proportionality difficulties (Figure 2.3). Their model was formulated as follows.

1. The intersection of joint axis i+1 with the xy_{i-1} plane is the origin of the ith coordinate system. Frame i-1 is then moved to frame i.

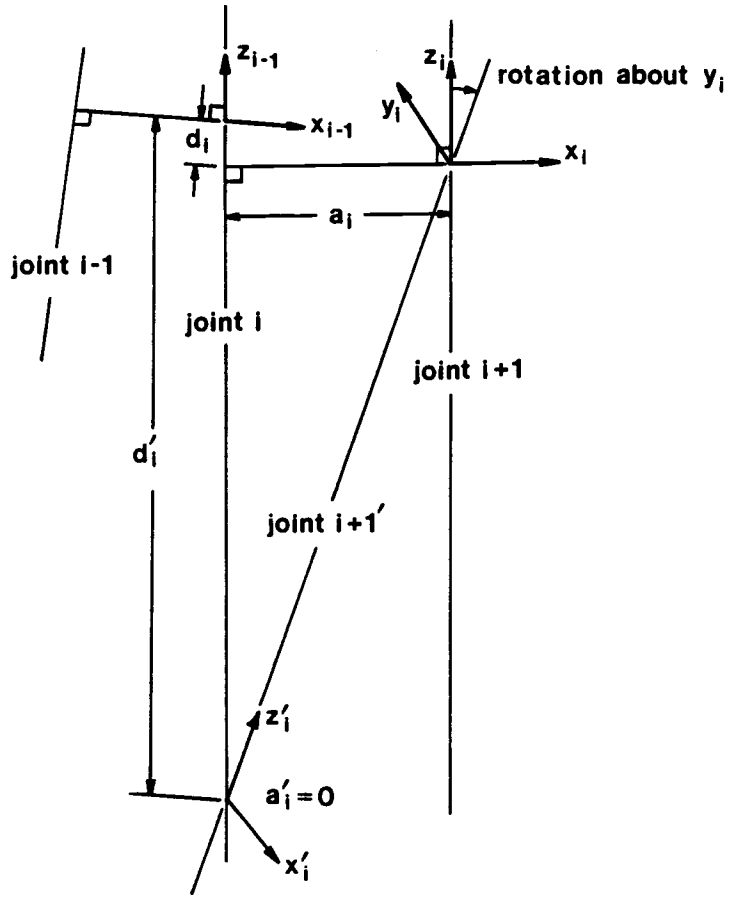

Figure 2.2. Parallel and nearly parallel joint axes in D-H model.

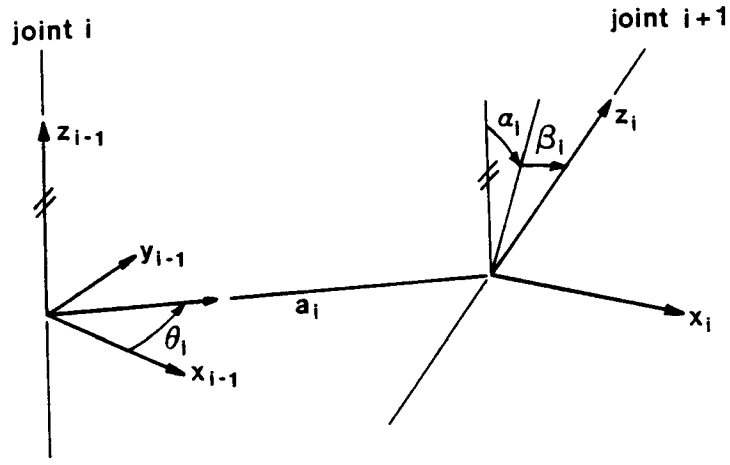

Figure 2.3. Four-parameter model used by Hayati, and Judd and Knasinski.

2. rotate about z by θ_i so x passes through joint axis i+1.

3. translate along x by a_i to origin of frame i.

4. rotate about x by α_i so z_i lies in the plane xz.

5. rotate about y by β_i so z is coincident with z_i.

For revolute joints their modified model eliminated the need for a joint-offset and so still required only four parameters. Judd and Knasinski suggest that with this modified model "...direct physical interpretation can be attached to the parameters found." This is only true for robot arms whose joints are nearly parallel. Hayati points out that this model breaks down when consecutive joint axes are perpendicular or nearly perpendicular. In the perpendicular configuration the origin of frame i can not be determined because joint axis i+1 does not intersect the xy_{i-1} plane.

Hsu and Everett (1985), and Veitschegger and Wu (1987) use a model similar to the one described above but retain the offset of the D-H model which solves the problem addressed by Hayati. Using the offset parameter they are able to translate frame i-1 along z so the origin of frame i lies in plane xy_{i-1}. They then used their model for all axis configurations.

Another approach is to determine errors in the nominal D-H model parameters. Ibarra and Perreira (1986) used the difference between the measured pose and the predicted pose

of a robot to determine D-H error parameters. Vaishnav and Magrab (1987) suggested determining 9 errors for each coordinate frame on a joint axis. These errors identified the skewness of a frame's coordinate axes and the distances between them assuming they do not intersect. The model of Mooring and Tang (1984) involves a "displacement matrix" transformation from the nominal joint axis to the actual. Their calibration procedure involved determining the elements of this matrix which reflected the misalignment of a joint axis.

Whitney, Lozinski and Rouke (1984) avoided the proportionality problem by not adhering to the D-H model. Consecutive coordinate frames were related to one another by six parameters, three orthogonal translations and three Euler angles. They define the coordinate systems attached to each joint axis as having the y coordinate along the axis and the x coordinate along the arm.

Sheth and Uicker (1971) modified the D-H model for reasons other than calibration. However, their model is worth mentioning here because its attributes have been used by other researchers for robot calibration purposes. They noted the D-H model was limited to use with lower pairs and had restrictive link notation because it relied on the geometry of the previous link. Two corrective actions were taken. First, three parameters were added to a modified D-H notation so the geometric description or "shape" of the

rigid link did not depend on that of the previous link (Figure 2.4). The common perpendicular was still used but the location of the coordinate frame's origin and the orientation of its x axis became arbitrary. Second, they separated notation into two parts, one consisting of constant parameters and the other representing variables of the joint or "pair".

Constant parameters were used to form a "shape matrix", **T**, defining link geometry independent of adjacent links; variable parameters, describing joint motion, appeared in a separate "pair matrix", Φ. Formulation of their shape matrix using link H of Figure 2.4 was as follows.

1. translate frame uvw_j along w_j by c_{jk} to the intersection of axis w_j and the common perpendicular of axes w_j and z_k.
2. rotate about w by γ_{jk} so u is parallel to the common perpendicular.
3. translate along u by a_{jk} to the intersection of axis z_k and the common perpendicular.
4. rotate about u by α_{jk} so w is parallel to axis z_k.
5. rotate about w by β_{jk} so u is parallel to axis x_k.
6. translate along w by b_{jk} to the origin of frame xyz_k.

Since the **T** matrix defined two arbitrarily oriented coordinate systems, it could be used to formulate pair matrices. Sheth and Uicker demonstrated this formulation with the six common lower pairs: revolute, prismatic,

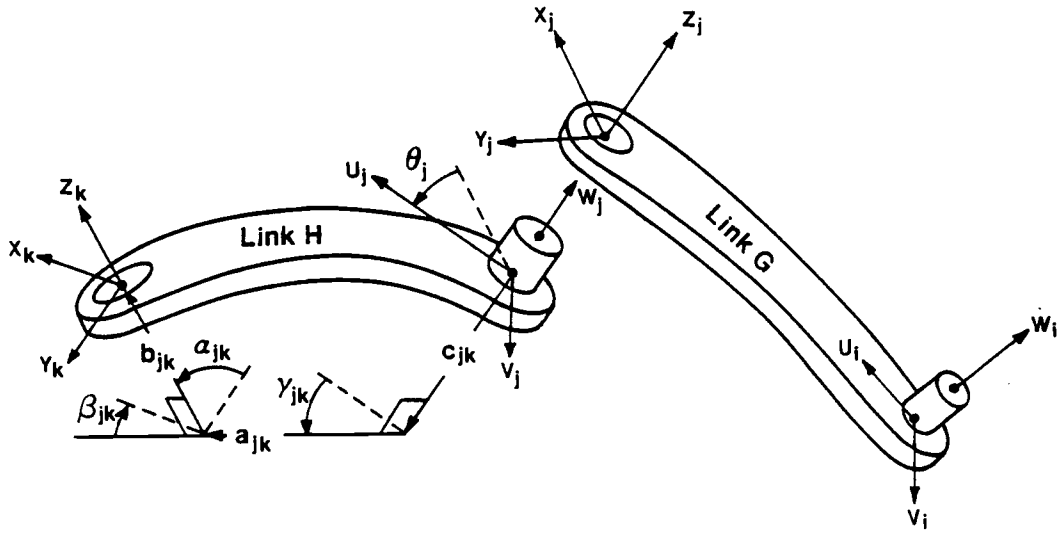

Figure 2.4. Sheth and Uicker six parameter Shape model and single Pair model (Sheth and Uicker's Fig.2).

cylindrical, screw, spherical and planar. They used a gear pair to exemplify higher pairs.

Stone (1987) used a "signature" model (referred to herein as the S-model) for robot calibration which closely resembled Sheth and Uicker's shape matrix model with one exception. The first fixed rotation parameter of the shape matrix model becomes a joint variable in the S-model. The S-model has similar proportionality characteristics to those of the D-H model because it also uses the common perpendicular of two consecutive joint axes. Stone avoided calibration difficulties of this by measuring the position and orientation of each joint frame individually with respect to a world coordinate system. These data were then used to develop a transformation matrix for each link. Since the S-model, like the Sheth and Uicker model, defined two arbitrarily oriented coordinate systems, its parameters could be extracted from the measured link matrices. Hemami (1989), in a review of Stone's book, saw the strength of the S-model in its ability to arbitrarily select the position of a joint frame. This allowed the origin to be selected on the link so its coordinates could be measured directly.

The model which Chen and Chao (1986) used for robot calibration resembled the Sheth and Uicker model in that they used separate transformation matrices for the fixed (shape) and variable (pair) model parameters. One transformation characterized the nominal design of the robot

and the errors between the nominal and actual robot. The other characterized the joint rotation. The separate pair matrix and shape matrix was also used by Broderick and Cipra (1988). In their calibration technique they developed a shape matrix for each of n links of a manipulator using n+1 measurements of the end-effector. Their shape matrix was not made of specific parameters such as that of Sheth and Uicker but simply provided a geometric relationship between consecutive joint coordinate frames.

With so many different models used for robot calibration some researchers have developed model evaluation criteria. Everett, Driels and Mooring (1987) argue that models using lower kinematic pairs (e.g. revolute or prismatic joints) should possess three properties: completeness, equivalence and proportionality. For completeness "...the model must contain a sufficient number of parameters to completely specify the motion of the robot under study." Also "...the model must contain a sufficient number of independent coefficients to express any possible variation in the kinematic structure of the robot." Equivalence was described as "...the ability to establish a relationship between the functional form of the model and that of any other acceptable model." The concept of proportionality has been discussed above.

Ziegert and Datseris (1988) looked at several considerations in kinematic modeling for robot calibration.

They observed that "...there is no advantage to systems which determine a unique frame location..." to describe the location of the end effector. They also pointed out that geometric parameters for any kinematic model can be determined if the global location of the joint axes are known. This leads to their conclusion that the calibration should involve the global determination of the joint axes.

This review does not cover all existing models used for robot calibration but does cover the major concerns for correcting dimensional errors. In developing a model appropriate for arthropod legs, recognition should be given to three differences that exist between legs and mechanical manipulators. First, nominal design parameters of manipulators are known prior to their calibration while nothing is known of the kinematic geometry of arthropod legs. This excludes using a model in which error parameters are determined. Second, the joint axes of most mechanical manipulators are nearly parallel or perpendicular to one another while the joint axes of arthropod legs are typically skew. When joint axes of a mechanism are skew, the descriptive parameters of many of the models mentioned above would bear little physical resemblance to the actual mechanism. Third, the joints of manipulators have been restricted to revolute and prismatic but this is not the case for arthropods. Although revolute joints are predominate, other lower and possibly higher pairs should be

anticipated in arthropods. With these considerations and the previous leg model criteria in mind, the following leg model was developed.

2.4. A-Model

The arthropod leg model, herein called the A-model, uses four fixed parameters and from one to a possible six variable parameters depending on the degrees-of-freedom in the joint. Using four fixed parameters instead of five is compatible with the measuring technique as seen in the next chapter. To allow the necessary flexibility for modeling various joint types, fixed and variable parameters are separated into two transformation matrices for each segment as done by Sheth and Uicker. Shape matrix **S** uses the four fixed parameters to describe the leg segment shape. Motion between leg segments is described in pair matrix **$**. For a leg of n segments, the matrix

$$\mathbf{A} = \mathbf{B}\cdot\$_1\cdot\mathbf{S}_1\cdot\$_2\cdot\mathbf{S}_2\cdot\ldots\cdot\$_{n-1}\cdot\mathbf{S}_{n-1} \qquad (2.1)$$

describes the foot position with respect to a coordinate system fixed in the arthropod body. Matrix **B** is the transformation relating the body coordinate frame to the first joint coordinate frame of the leg. The formulation of **B**, **$** and **S** are best explained by example using an arthropod specimen.

Initial studies were performed on the darkling beetle, Eleodes obscura sulcipennis (Tenebrionidae) (Figure 2.5). It was chosen for its availability, durability, leg visibility, relatively large size and its flight inability. This beetle is commonly found in semiarid and desert areas of the U.S. and has a body length of about 30 mm. Each of its six legs have five segments which are connected by pivot joints as described at the beginning of this chapter. The individual ball and sockets of these joints are herein referred to as articulations. Three of the beetle's four pivot joints provide most of its leg motion. The joint connecting trochanter and femur was observed to allow little to no motion between the two leg segments so was initially assumed to be immobile thus the coxa-trochanter joint will be referred to as the coxa-femur joint. The tarsus (or foot) is, in a robotic sense, an end effector and does not contribute to the beetle's overall leg movement. Hence the leg of a darkling beetle can be regarded as an RRR manipulator.

As with the Sheth and Uicker model, a joint in the A-model is defined as a relationship between two coordinate frames, each fixed to one of two adjoining leg segments as shown in Figure 2.6. The joint i is defined by a transformation from coordinate frame uvw_i, fixed to segment i-1, to coordinate frame xyz_i, fixed to segment i. Example transformation matrices for three joint types are described

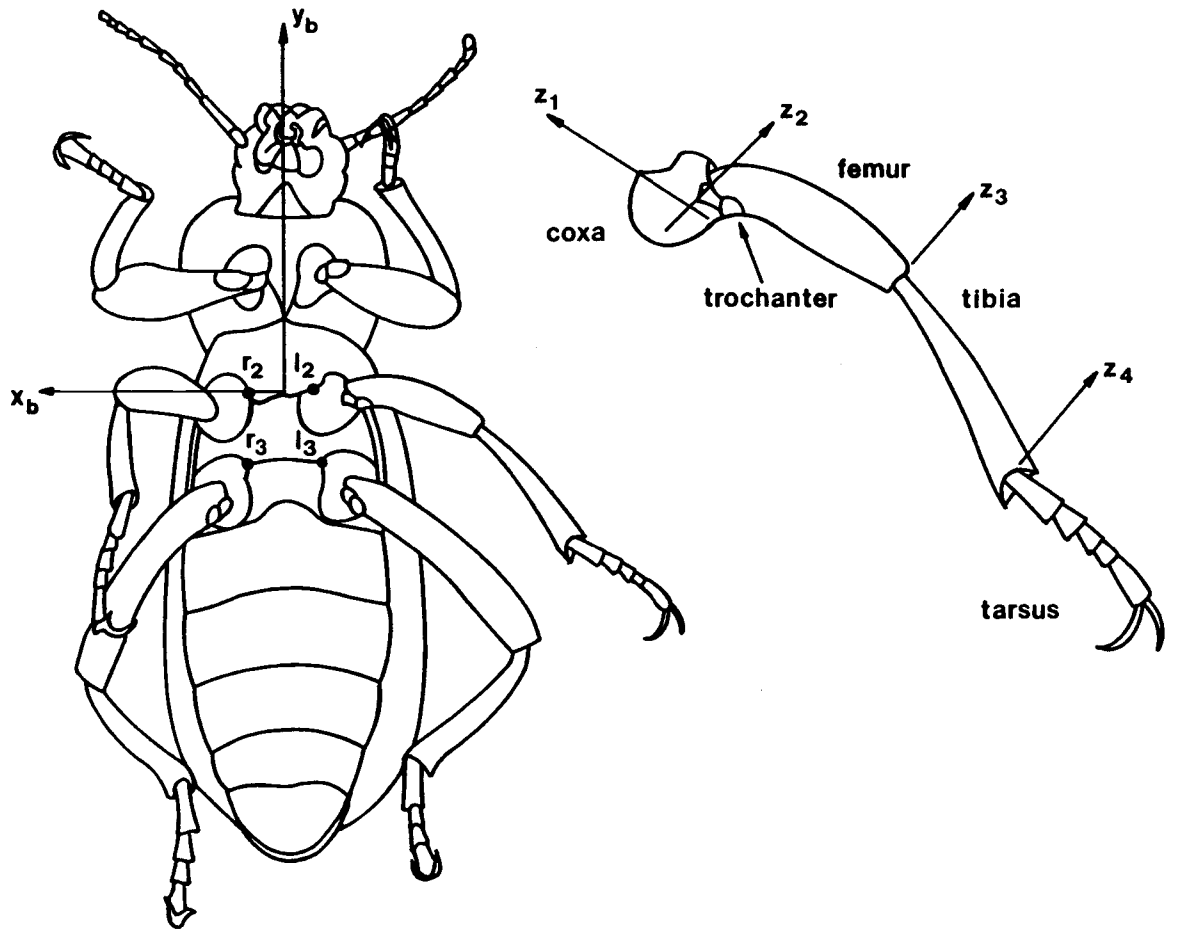

Figure 2.5. Ventral view of a darkling beetle showing the body coordinate system, segment names and joint axes of the left middle leg.

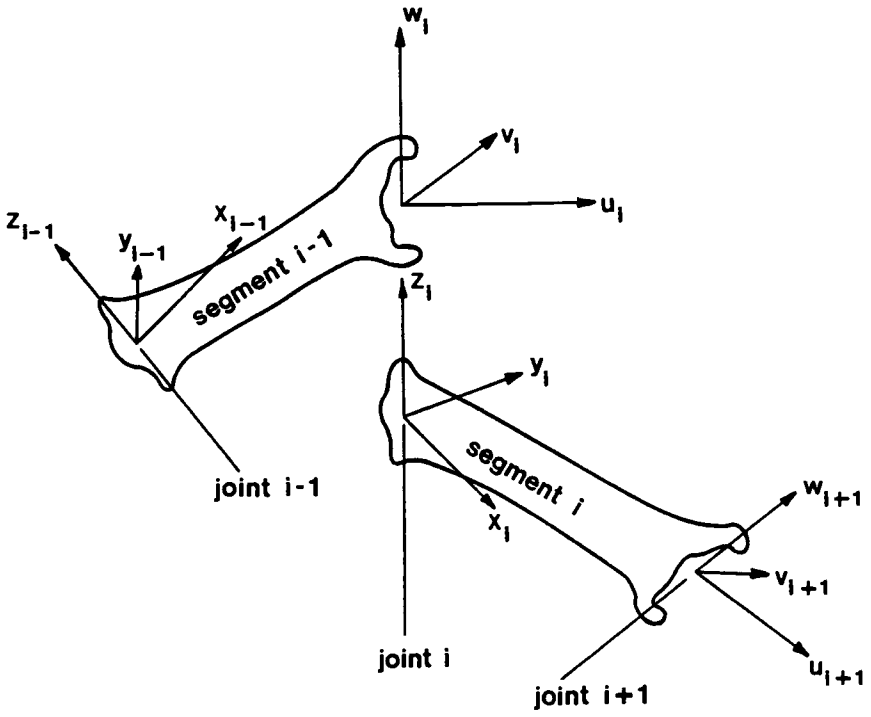

Figure 2.6. Joint frames of A-model fixed in their respective leg segments.

later. When joint i variables are zero, the two coordinate frames coincide. These are the basic conditions for all types of pairs. The revolute pair is described below first since it is the predominant arthropod joint and provides the simplest illustration of the A-model.

The origins of frames uvw_i and xyz_i are coincident and positioned on the joint axis half way between the joint's articulations. Axis w_i and axis z_i both lie along joint i axis. The distance between the origins of frames xyz_i and uvw_{i+1} is the length of the leg segment i.

Positioning a joint-frame origin mid way between joint articulations is reasonable only when both articulations can be found without dissection of the arthropod. Some of the joints have only one visible articulation such as the coxa-femur joint on the darkling beetle. In this case the origin should be placed on the joint axis on the surface of the cuticle of the visible articulation. The origin is positioned here to retain as close a relationship to the physical joint as practical.

Matrix $\mathbf{S}_i$ is the homogeneous transformation from frame xyz_i to frame uvw_{i+1} and is formulated using four parameters as follows (Figure 2.7). To move frame xyz_i to frame uvw_{i+1}:

1. rotate about y by τ_i so x contains the origin of frame uvw_{i+1}.
2. translate along x by s_i to origin of frame uvw_{i+1}.

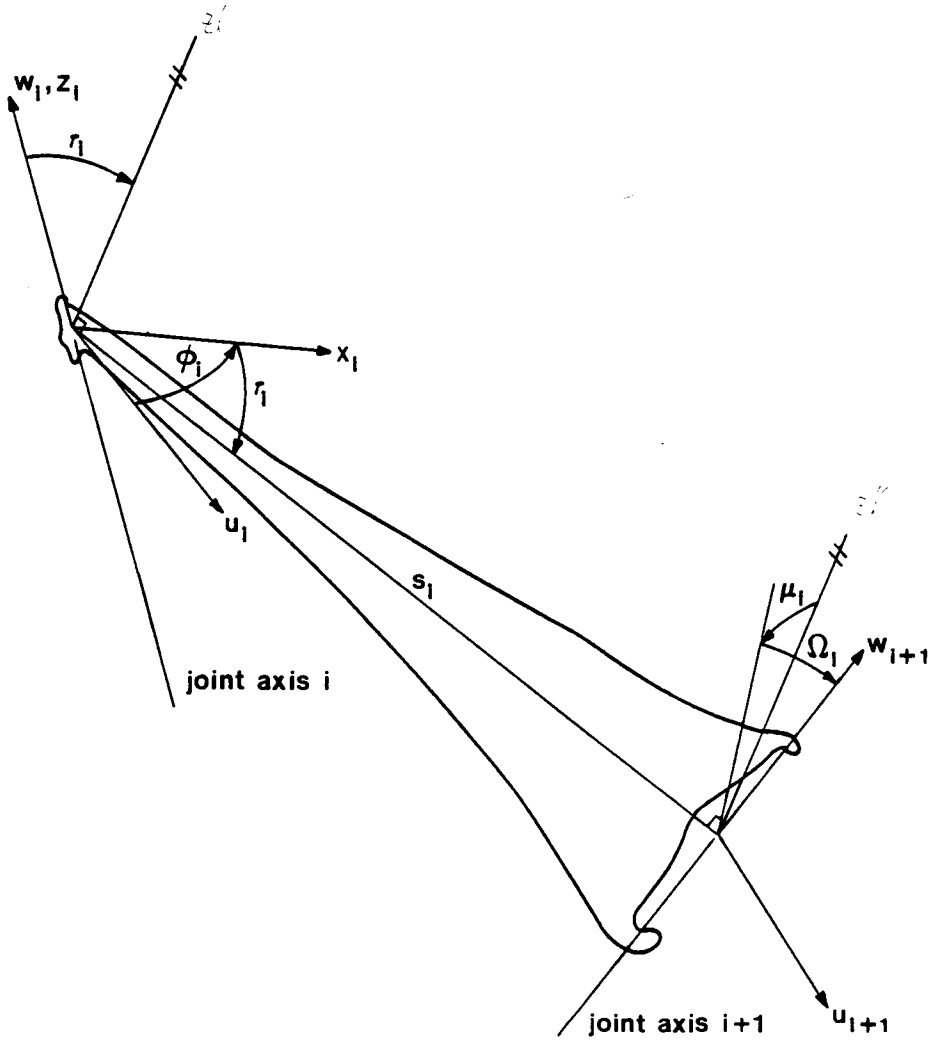

Figure 2.7. Four fixed parameters of shape matrix **S** and variable parameter of revolute pair matrix **Φ**.

3. rotate about x by μ_i so z is in plane containing x and w_{i+1}.

4. rotate about y by Ω_i so z lies along w_{i+1}.

This is mathematically expressed by

$$\mathbf{s}_i = \mathrm{Rot}(y,\tau_i)\ \mathrm{Trans}(s_i,0,0)\ \mathrm{Rot}(x,\mu_i)\ \mathrm{Rot}(y,\Omega_i) \qquad (2.2)$$

Expanding this equation yields

$$\mathbf{s}_i = \begin{bmatrix} c\tau_i c\Omega_i - s\tau_i c\mu_i s\Omega_i & s\tau_i s\mu_i & c\tau_i s\Omega_i + s\tau_i c\mu_i c\Omega_i & s_i c\tau_i \\ s\mu_i s\Omega_i & c\mu_i & -s\mu_i c\Omega_i & 0 \\ -s\tau_i c\Omega_i - c\tau_i c\mu_i s\Omega_i & c\tau_i s\mu_i & -s\tau_i s\Omega_i + c\tau_i c\mu_i c\Omega_i & -s_i s\tau_i \\ 0 & 0 & 0 & 1 \end{bmatrix} \qquad (2.3)$$

There are two special conditions for this matrix. First, if z_i passes through the origin of frame uvw_{i+1} then the orientation of x_i is arbitrary. How it is chosen is described in the measurement procedure of the next chapter. Second, if w_{i+1} passes through the origin of frame xyz_i then μ_i is arbitrarily set to zero.

The coordinate frame fixed to the arthropod body serves as the base frame and does not follow the orientation criteria above. Origin of body frame, b, is at the midpoint of the line segment connecting proximal articulations of the

second pair of legs (marked r_2 and l_2 in Figure 2.5). The x_b axis lies along this line segment, positive toward the right of the animal. The y_b axis intersects the line connecting proximal articulations of the third pair of legs (marked r_3 and l_3), positive toward the head. The z_b axis completes a right hand coordinate system with its positive direction upward when the beetle stands. Rotating body frame about z_b by θ_0 orients it with frame xyz_0 (Figure 2.8). Since θ_0 is a fixed parameter it is included in the transformation matrix **B** which, from body frame to frame uvw_1, is expressed by

$$\mathbf{B} = \text{Rot}(z,\theta_0)\ \text{Rot}(y,\tau_0)\ \text{Trans}(s_0,0,0)\ \text{Rot}(x,\mu_0)\ \text{Rot}(y,\Omega_0) \tag{2.4}$$

Pair matrix Φ_i is the transformation from frame uvw_i to frame xyz_i. For the case of a revolute pair, the motion is described by a counter-clockwise rotation of ϕ_i about w_i from u_i to x_i. This motion is mathematically expressed by

$$\Phi_i(\phi_i) = \begin{bmatrix} c\phi_i & -s\phi_i & 0 & 0 \\ s\phi_i & c\phi_i & 0 & 0 \\ 0 & 0 & 1 & 0 \\ 0 & 0 & 0 & 1 \end{bmatrix} \tag{2.5}$$

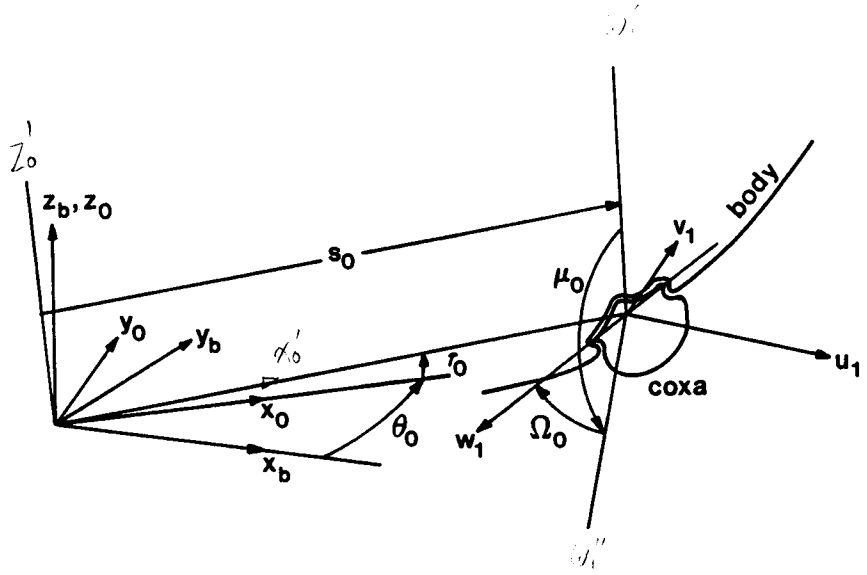

Figure 2.8. Five parameters of B matrix.

A prismatic pair, with its displacement along w_i from frame uvw_i to xyz_i termed d_i, is expressed by

$$\Phi_i(d_i) = \begin{bmatrix} 1 & 0 & 0 & 0 \\ 0 & 1 & 0 & 0 \\ 0 & 0 & 1 & d_i \\ 0 & 0 & 0 & 1 \end{bmatrix} \tag{2.6}$$

A more complex pair such as a spherical pair can be represented by a combination of three revolute pairs with orthogonal rotation axes (Figure 2.9). Again following the example of Sheth and Uicker, the relationship between the axes of each revolute pair has a shape. Using the parameters of the shape matrix and a revolute pair **R** with z axis rotation, the symbolic D-H notation of the spherical pair is written

$$\mathbf{R}(\phi_i) \begin{vmatrix} \tau_{ii}' \\ s_{ii}' \\ \mu_{ii}' \\ \Omega_{ii}' \end{vmatrix} \mathbf{R}(\phi_i') \begin{vmatrix} \tau_i'_i'' \\ s_i'_i'' \\ \mu_i'_i'' \\ \Omega_i'_i'' \end{vmatrix} \mathbf{R}(\phi_i'') \tag{2.7}$$

where the two columns of parameters are representations of matrix 2.3 and **R** is a rotation matrix similar to 2.5. So

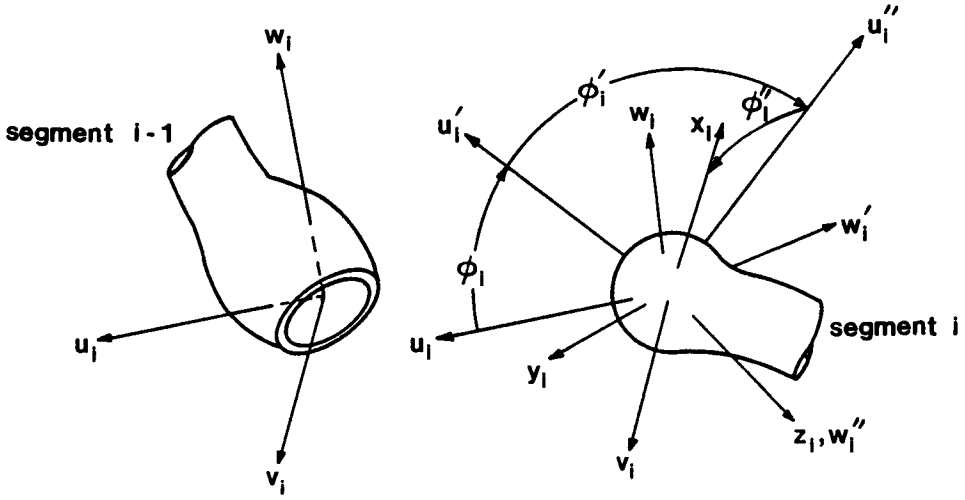

Figure 2.9. Spherical pair.

the axes are orthogonal and all intersect at one point, μ is 90° and the parameters τ, s and Ω are zero in both columns. The spherical pair matrix can then be expressed by expanding equation 2.7.

$$\Phi(\phi_i,\phi_i',\phi_i'') = \begin{bmatrix} c\phi_i c\phi_i' c\phi_i''+s\phi_i s\phi_i'' & -c\phi_i c\phi_i' s\phi_i''+s\phi_i c\phi_i'' & c\phi_i s\phi_i' & 0 \\ s\phi_i c\phi_i' c\phi_i''-c\phi_i s\phi_i'' & -s\phi_i c\phi_i' s\phi_i''-c\phi_i c\phi_i'' & s\phi_i s\phi_i' & 0 \\ s\phi_i' c\phi_i'' & -s\phi_i' s\phi_i'' & -c\phi_i' & 0 \\ 0 & 0 & 0 & 1 \end{bmatrix} \tag{2.8}$$

These examples show the A-model's ability to adapt to various joint types. The model also meets the requirements of physical resemblance by the nature of its description. All parameters are defined with rotations and translations taking place directly on the physical leg or linkage. In contrast, the D-H model uses the common perpendicular so the segment (physical link) length can't be determined from the D-H parameters for a mechanism of general geometry such as

an arthropod leg.

The shape matrix meets criteria of proportionality in all parameters with two exceptions. This is when axis z_i passes through or is close to passing through the origin of frame uvw_{i+1} and when axis w_{i+1} passes through or is close to passing through the origin of frame xyz_i. When z_i passes through origin i+1, the direction of x_i is defined arbitrarily (see section on computing A-model parameters, 3.3). When z_i is close to this intersection, μ_i can have a value of -180° to 180° depending on the geometry of segment i. When w_{i+1} passes through origin of frame xyz_i, μ_i is zero and when it is close to intersecting, again μ_i can have a value of -180° to 180° depending on the geometry of segment i. The exception to proportionality does not cause a problem in determining direction of x_i or identifying parameter μ_i because parameter computation is done analytically, as is seen in the next chapter. Parameter μ_i does, however, loose physical significance in these joint axis configurations and hence in these situations its value is not considered important in describing a leg's physical characteristics. This condition is signaled by parameters τ_i and Ω_i when either of their values are equal or close to 90°.

As a result of meeting the leg modeling criteria, the A-model has a mathematical limitation. It is relatively difficult to manipulate its transformation matrix. This is

seen in the inverse kinematic solution in Appendix B. The problem lies in the shape matrix where three rotations and one translation are used to complete the transform from a link frame to the succeeding one. This causes expressions for rotation elements of the matrix to be long in comparison to those of the D-H model where only one fixed parameter is a rotation. However, the measurement procedure used in this study allows other models, such as the D-H, to be determined (Fichter, Albright and Fichter, 1988) . For revolute or prismatic joints, the D-H model could be used for its manipulation advantages and the A-model for its comparison advantages. The procedure for measuring and computing A-model parameters is the subject of the next chapter.

3. Determining A-model Parameters

3.1. Overview

The apparatus and procedure used for determining the A-model parameters and joint range-of-motion of arthropod legs is the subject of this chapter. The equipment described below was used by Fichter, Albright and Fichter (1988) to determine S and D-H model parameters of these legs. Their measurement and parameter evaluation approach, which closely resembles the approach used by Stone, is adapted here to characteristics unique to the A-model. The procedure used in this research differs from most of those cited in the previous chapter in one important way. Instead of making several measurements of the free end of a manipulator then determining its kinematic parameters numerically, individual measurements of each joint are made from which the model parameters are determined analytically.

For an arthropod leg with hinge type joints, the kinematic geometry between successive joint frames is described by the A-model using five parameters, four fixed and one variable. Expressing this geometry as a transformation from frame xyz_i to frame xyz_{i+1} with matrix ${}^{i}U_{i+1}$ we have

$$ {}^{i}U_{i+1} = S_i \, \Phi_{i+1} \qquad (3.1) $$

where **S** and **Φ** are defined by matrix transformations 2.3 and 2.5 respectively. Using the parameter determination approach of Fichter, Albright and Fichter (1988), the values of matrix ${}^{i}U_{i+1}$ would be determined by measuring the position and orientation of both frames xyz_i and xyz_{i+1} with respect to a common reference frame and then relating the frames to each other through this common frame. From the calculated ${}^{i}U_{i+1}$ matrix, the parameters of shape matrix $\mathbf{S}_i$ and pair matrix $\mathbf{\Phi}_{i+1}$ would then be extracted. However, the individual measurement of these joint frames pose a difficulty for the A-model. A constraint which dictates the origin of frame xyz_{i+1} lie in the xz_i-plane requires a priori knowledge of the relationship between the two frames before the orientation of frame xyz_i can be measured. This problem is overcome by introducing a third joint-axis coordinate frame used solely for measurement purposes. As shown in Figure 3.1, the orientation of the frame xyz_i', herein termed joint frame i', is defined by parameters ϕ_i' and θ_i relative to frames uvw_i and xyz_i respectively. Joint displacement ϕ_i is related to these parameters by

$$\phi_i = \phi_i' + \theta_i \tag{3.2}$$

Orientation of x_i' is arbitrary and is defined during the measurement of joint axis i. What follows is a description of the equipment and procedure used in measuring each joint

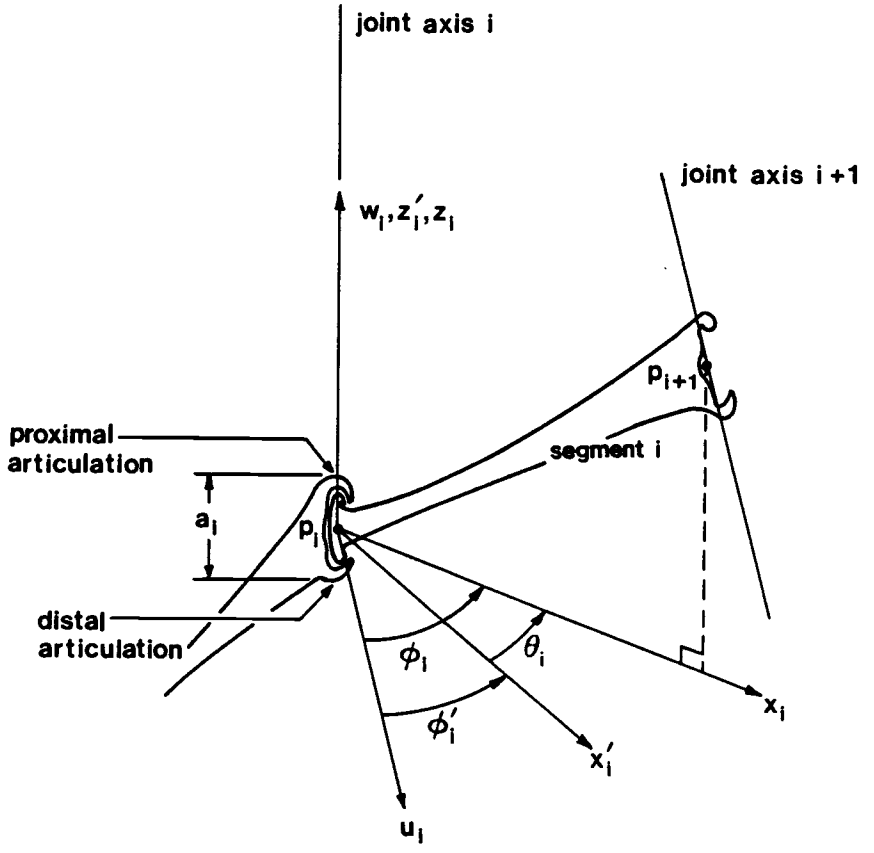

Figure 3.1. Joint frame xyz_i' relative to frames uvw_i and xyz_i. Position of proximal and distal joint articulations shown along joint axis.

frame i′ with respect to a reference frame and the mathematical manipulations used for extracting the A-model parameters from these measurements.

3.2. Apparatus and Procedure

The measuring apparatus (Figure 3.2) consists of a dissecting microscope rigidly mounted above a positioning device. The positioner provides translational movement along three linear orthogonal slides and rotational movement about the axes of two orthogonal turntables. This allows determination of orientation of a leg segment's joint axis and position of a point on that axis relative to a reference frame.

Four coordinate frames of the positioner are defined for the purposes of measuring joint frame i′. The global reference frame, frame g, is parallel to the three linear slides of the positioner (Figure 3.3). Its origin coincides with the intersection of the two turntable axes when the readings from all three slides are zero. Microscope frame m is fixed in frame g with its z_m-axis, also the optical axis, parallel to z_g. Axes x_m and y_m lie in the microscope focal plane with x_m parallel to x_g. The origin of frame m is marked in the focal plane by a cross-hair reticle in the microscope.

The positioner frame p, also parallel to the three slides, translates relative to frame g. Its origin is fixed

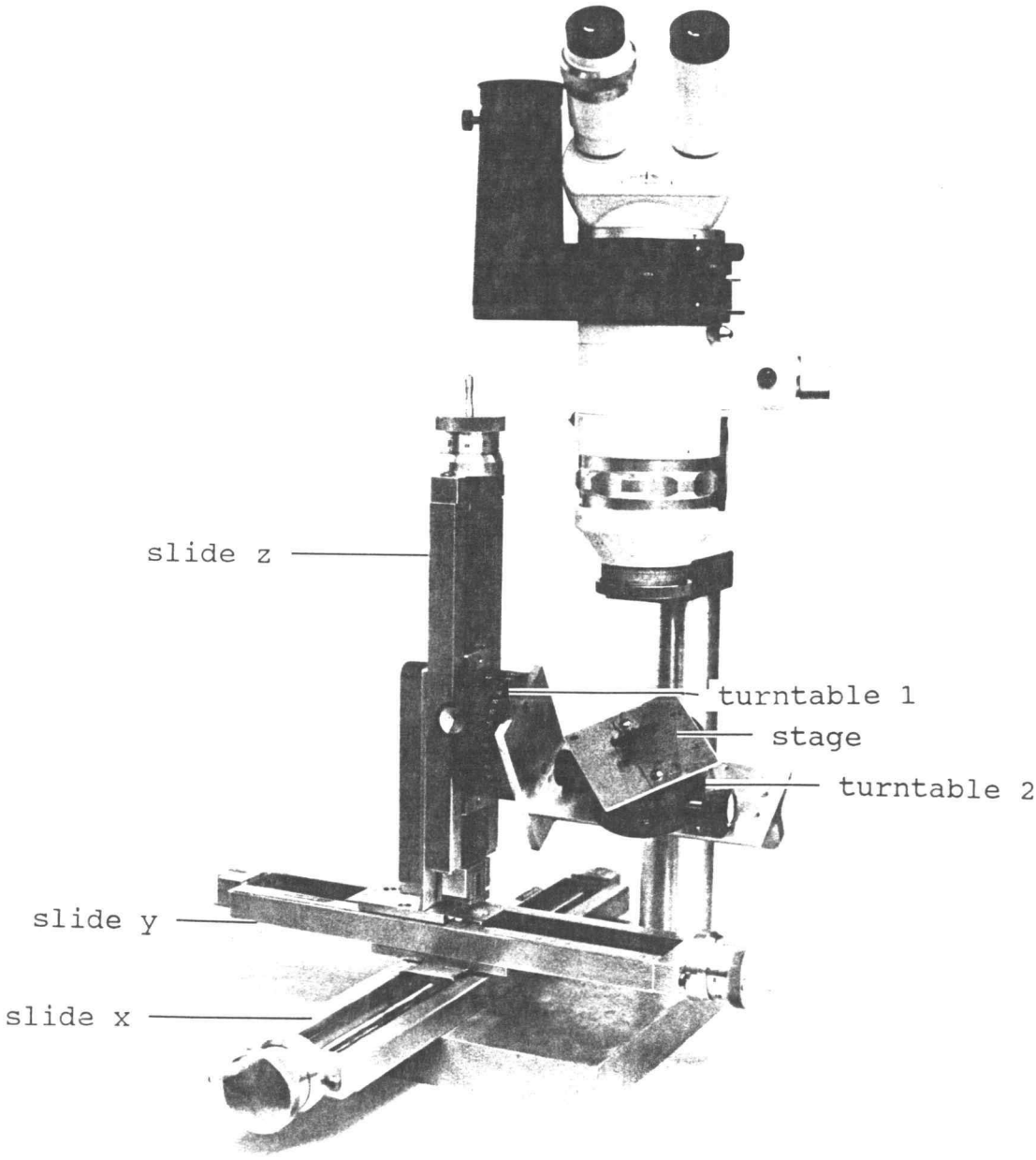

Figure 3.2. Dissecting microscope and 5-axis positioner.

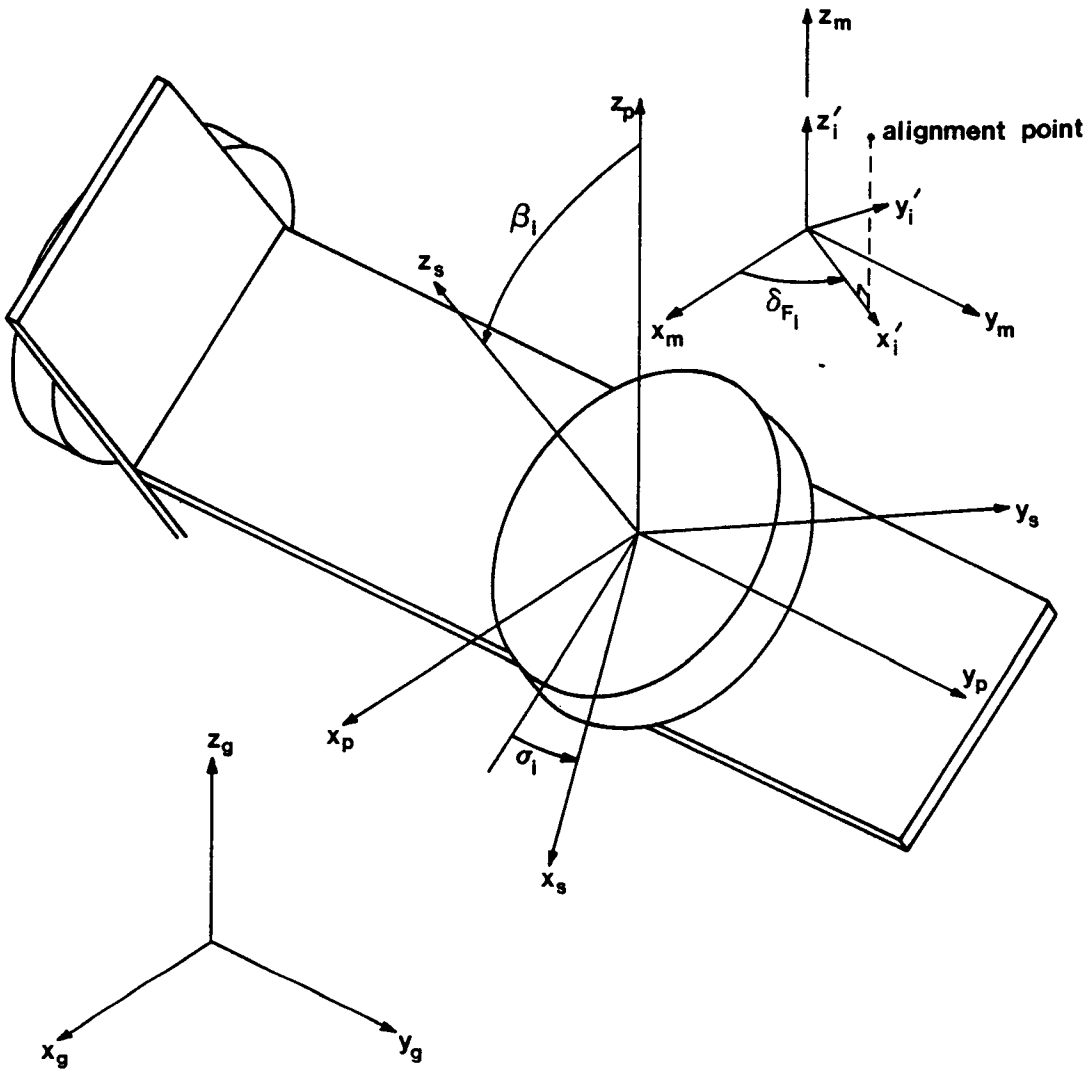

Figure 3.3. Positioner coordinate frames used in defining the transformation of each joint frame.

to the intersection of the turntable axes. The axis of turntable 2 is the z_s-axis of the stage frame s. When the σ-angle of the turntable 2 is set to zero and the β-angle of turntable 1 adjusted so z_s is aligned with z_p, frame s is coincident to frame p. These are the turntable positions from which all orientation measurements are to be referenced. From this reference orientation, the frames of s, p and m can be positioned coincident to each other by adjusting the linear slides so the origins of frames s and p coincide with the cross-hair. This marks the position of frame m's origin, x_r, y_r, z_r, relative to frame g.

The subject to be measured is secured to an aluminum plate mounted to the stage as seen in Figure 3.2. With the turntables in their reference orientation, the proximal articulation positions of the left and right mesocoxae and metacoxae are determined to establish the body coordinate frame as described in section 2.4 of chapter 2. Joint measurements begin with body/coxa joint and progress outward to the tarsus. After all measurements of an individual joint are complete, the joint is immobilized (glued) before proceeding to measure the next one.

Measurements are taken by adjusting the turntables until joint axis i is aligned with the optical axis then adjusting the slides so the point lying where joint axis i pierces the cuticle nearest the proximal articulation (Figure 3.1) is at the cross-hair. The actual position of

the origin of joint frame i′ is at point p_i (i.e. joint position i) lying mid way between the proximal and distal articulations. The distance between the articulations is obtained by a 90° rotation of turntable 1 aligning the joint axis parallel to x_p. From this position, the distance between the proximal and distal articulations, defined as a_i, can be measured in the direction of slide x. For joints having only one visible articulation, the origin of joint frame i′ is considered coincident to a point lying on the joint axis and the visible articulation (see A-model description in chapter 2.4). Distance a_i is considered zero for these joints.

Aligning the joint axis of rotation with the optical axis of the microscope is an iterative process. Alignment is confirmed if a point on the far end of the leg segment remains in the focal plane when the segment is rotated. This point, termed alignment point, can be a distinguishing mark or small contrasting object (e.g. bit of wax) attached to the far end of the leg segment. Once alignment is achieved, slide and turntable positions x_i, y_i, z_i, β_i and σ_i are recorded. These measurements establish the position and orientation of z_i'. To determine joint range-of-motion, the locations of the alignment point are measured when the leg segment is positioned at its extreme clockwise and counter-clockwise positions. These correspond to positions x_{Li}, y_{Li}, z_{Li} and x_{Hi}, y_{Hi}, z_{Hi} respectively. Finally, the joint is

glued and the fixed position of the alignment point x_{Fi}, y_{Fi}, z_{Fi} is measured. The projection of this fixed position onto the xy_m-plane defines the orientation of x_i (Figure 3.3).

The joint frame i′ on joint axis i is to be described in reference to the stage frame s. The required transformation from reference frame s to joint frame i′ is the product of four transformations.

$$ {}^{s}T_{i}' = {}^{s}T_{p} \; {}^{p}T_{g} \; {}^{g}T_{m} \; {}^{m}T_{i}' \qquad (3.3) $$

These measured joint coordinate frames are manipulated into A-model parameters as described below.

3.3. Computing A-model Parameters

Found in this section are the derivation of transformation matrix ${}^{i}U_{i+1}'$ defining frame i+1′ relative to i′ in terms of measured parameters, the formulation of matrix ${}^{i}U_{i+1}'$ in terms of A-model parameters, and the method for extracting A-model parameters from ${}^{i}U_{i+1}'$.

Each coordinate transformation in equation 3.3 above is derived as follows. The transformation from microscope coordinate frame m to joint frame i′ is a rotation about the z_m-axis.

$$ {}^{m}T_{i}' = \mathrm{Rot}(z, \delta_{Fi}) \qquad (3.4) $$

where

$$\delta_{Fi} = \text{atan2}\ (y_{Fi} - y_i,\ x_{Fi} - x_i) \qquad (3.5)$$

The function atan2 computes the arctangent in one of four quadrants from -180° to 180° by examining the signs of the numerator and denominator, y and x. The transformation from global frame g to microscope frame m is a fixed translation as described in section 3.2 and is written here as

$$^{g}T_{m} = \text{Trans}(x_r,\ y_r,\ z_r) \qquad (3.6)$$

From recorded positions of the origin of joint frame i', the transformation from global frame g to positioner frame p is a translation.

$$^{g}T_{p} = \text{Trans}(x_i,\ y_i,\ z_i+a_i/2) \qquad (3.7)$$

Measurement parameter a_i is the distance along the joint axis between proximal and distal joint articulations. The transformation of 3.7 is inverted to obtain the required one.

$$^{p}T_{g} = \text{Trans}(-x_i,\ -y_i,\ -(z_i+a_i/2)) \qquad (3.8)$$

From recorded angles, transformation from positioner frame p to stage frame s is:

$$ {}^{p}T_{s} = \text{Rot}(y, \beta_i)\ \text{Rot}(z, \sigma_i) \qquad (3.9) $$

This transformation is also inverted to obtain the required one.

$$ {}^{s}T_{p} = \text{Rot}(z, -\sigma_i)\ \text{Rot}(y, -\beta_i) \qquad (3.10) $$

Equations 3.4, 3.6, 3.8 and 3.10 are substituted into equation 3.3 to give the transformation from reference frame s to joint frame i .

The transformation ${}^{i}U_{i+1}'$ is determined from two successive joint frame matrix transformations relative to the reference frame.

$$ {}^{i}U_{i+1}' = {}^{s}T_{i}'^{-1}\ \ {}^{s}T_{i+1}' \qquad (3.11) $$

The transformation matrix ${}^{i}U_{i+1}'$ is written as

$$ {}^{i}U_{i+1}' = \begin{bmatrix} nx & ox & cx & px \\ ny & oy & cy & py \\ nz & oz & cz & pz \\ 0 & 0 & 0 & 1 \end{bmatrix} \qquad (3.12) $$

where the individual elements are known. As seen in Figure 3.4, the transformation ${}^{i}U_{i+1}'$ can also be defined in terms of the new parameters θ_i and ϕ_{i+1}' and fixed A-model parameters τ_i, s_i, μi and Ω_i. The transformation matrix is defined as

$$
\begin{aligned}
{}^{i}U_{i+1}' = {} & \mathrm{Rot}(z, \theta_i)\ \mathrm{Rot}(y, \tau_i)\ \mathrm{Trans}(s_i, 0, 0) \\
& \mathrm{Rot}(x, \mu_i)\ \mathrm{Rot}(y, \Omega_i)\ \mathrm{Rot}(z, \phi_{i+1}')
\end{aligned}
\qquad (3.13)
$$

By equating matrix transformations 3.12 and 3.13 the values of the unknown parameters can be determined. The solution, described by Paul [1981], is accomplished by a sequential premultiplication of individual transforms to isolate each parameter. Premultiplying equation 3.13 by $\mathrm{Rot}^{-1}(z, \theta_i)$ and expanding yields equation 3.14.

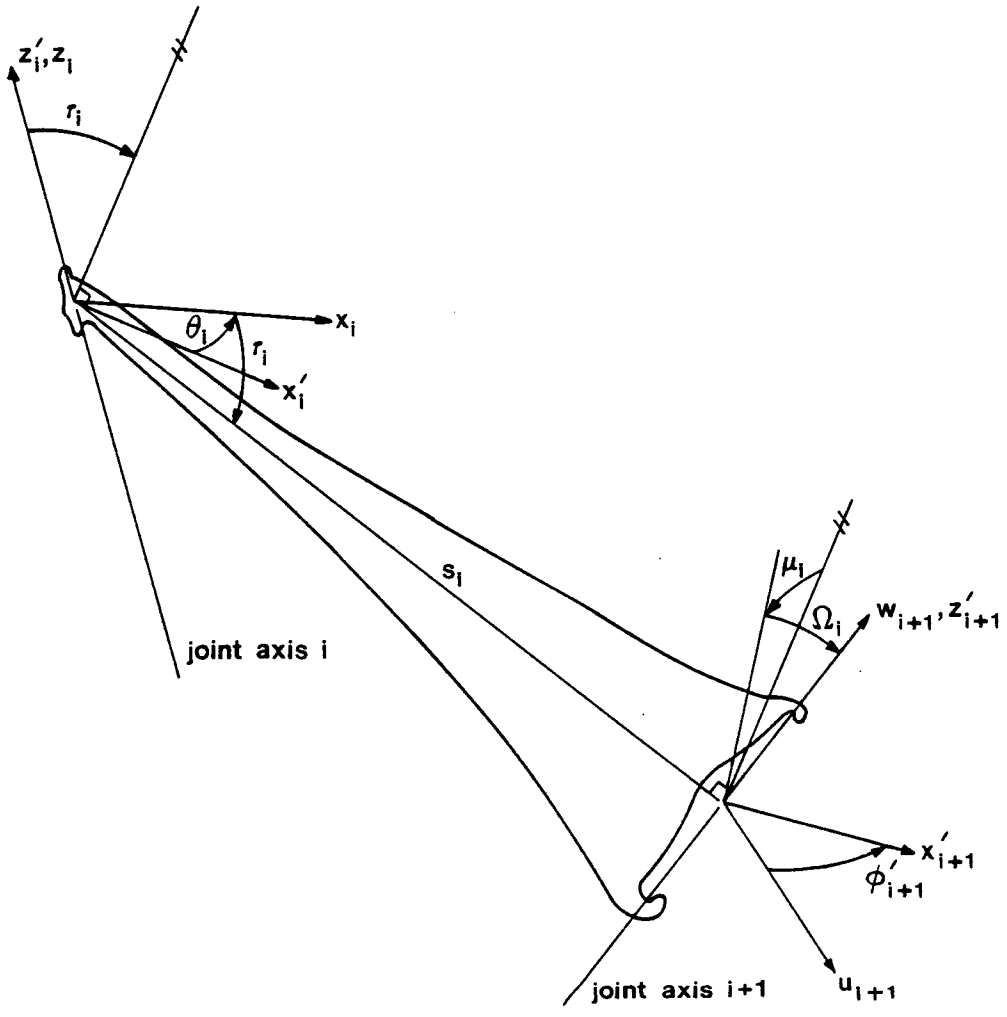

Figure 3.4. Four fixed parameters of A-model and two additional parameters used to transform frame xyz_i' to frame xyz_{i+1}'.

$$\begin{bmatrix} \cos\theta_i & \sin\theta_i & 0 & 0 \\ -\sin\theta_i & \cos\theta_i & 0 & 0 \\ 0 & 0 & 1 & 0 \\ 0 & 0 & 0 & 1 \end{bmatrix} {}^{i}\mathbf{U}_{i+1}' =$$

$$\begin{bmatrix} \cos\tau_i\ e11 + \sin\tau_i\ e31 & \cos\tau_i\ e12 + \sin\tau_i\ e32 \\ e21 & e22 \\ -\sin\tau_i\ e11 + \cos\tau_i\ e31 & -\sin\tau_i\ e12 + \cos\tau_i\ e32 \\ 0 & 0 \end{bmatrix}$$

$$\begin{bmatrix} \cos\tau_i\ e13 + \sin\tau_i\ e33 & \cos\tau_i\ s_i \\ e22 & 0 \\ -\sin\tau_i\ e13 + \cos\tau_i\ e33 & -\sin\tau_i\ s_i \\ 0 & 1 \end{bmatrix} \qquad (3.14)$$

where

$e11 = \cos\Omega_i \cos\phi_{i+1}'$

$e21 = \cos\mu_i \sin\phi_{i+1}' + \sin\mu_i \sin\Omega_i \cos\phi_{i+1}'$

$e31 = \sin\mu_i \sin\phi_{i+1}' - \cos\mu_i \sin\Omega_i \cos\phi_{i+1}'$

$e12 = -\cos\Omega_i \sin\phi_{i+1}'$

$e22 = \cos\mu_i \cos\phi_{i+1}' - \sin\mu_i \sin\Omega_i \sin\phi_{i+1}'$

$e32 = \sin\mu_i \cos\phi_{i+1}' + \cos\mu_i \sin\Omega_i \sin\phi_{i+1}'$

$e13 = \sin\Omega_i$

$e23 = -\sin\mu_i \cos\Omega_i$

$e33 = \cos\mu_i \cos\Omega_i$

An expression for θ_i is obtained by equating the (2,4) elements in equation 3.14 arriving at

$$-px \sin\theta_i + py \cos\theta_i = 0 \tag{3.15}$$

from which two solutions are obtained

$$\theta_i = \text{atan2}\ (py,\ px) \qquad \text{and}$$
$$\theta_i = \text{atan2}\ (-py,\ -px). \tag{3.16}$$

The solutions of 3.16 differ by 180°. If both px and py are zero, joint-axis i passes through the origin of joint frame i+1 (i.e. joint position i+1) and θ_i is arbitrarily set to zero. Hence,

$$\theta_i = 0 \tag{3.17}$$

when px = py = 0. Parameter s_i is found from equating elements (1,4), (2,4) and (3,4) to get

$$\cos\theta_i\ px + \sin\theta_i\ py = \cos\tau_i\ s_i \tag{3.18}$$
$$-\sin\theta_i\ px + \cos\theta_i\ py = 0 \tag{3.19}$$
$$pz = -\sin\tau_i\ s_i. \tag{3.20}$$

Squaring equations 3.18 - 3.20 then adding yields

$$s_i^2 = px^2 + py^2 + pz^2. \qquad (3.21)$$

Parameter s_i is always a positive solution.

Parameter τ_i is found from equations 3.18 and 3.20. Its unique solution is

$$\tau_i = \text{atan2}\ (-pz,\ \cos\theta_i\ px + \sin\theta_i\ py) \qquad (3.22)$$

The A-model specifies that $-90^\circ \le \tau_i \le 90^\circ$ and so equation 3.16 is chosen to satisfy this constraint. If px, py and pz are zero then τ_i is zero.

Premultiplying equation 3.14 by $\text{Trans}^{-1}(s_i, 0, 0)\text{Rot}^{-1}(y, -\tau_i)$ results in

$$\begin{bmatrix} \cos\tau_i\cos\theta_i & \cos\tau_i\sin\theta_i & -\sin\tau_i & -s_i \\ -\sin\theta_i & \cos\theta_i & 0 & 0 \\ \sin\tau_i\cos\theta_i & \sin\tau_i\sin\theta_i & \cos\tau_i & 0 \\ 0 & 0 & 0 & 1 \end{bmatrix} {}^{i}U_{i+1}' =$$

$$\begin{bmatrix} e11 & e12 & e13 & 0 \\ e21 & e22 & e23 & 0 \\ e31 & e32 & e33 & 0 \\ 0 & 0 & 0 & 1 \end{bmatrix} \qquad (3.23)$$

The last three parameters can all be extracted from matrix equation 3.23 and expressed in unique solutions. Equating elements (2,3) and (3,3) then dividing results in the solution

$$\mu_i = \text{atan2}\ (s\theta_i\ cx - c\theta i\ cy,\ s\tau_i\ (c\theta_i\ cx + s\theta_i\ cy) + c\tau_i\ cz) \tag{3.24}$$

where s and c represent the sine and cosine respectively. If joint axis i+1 passes through joint i ($c\Omega_i = 0$) then equation 3.24 becomes indeterminate and $\mu_i = 0$.

Parameter Ω_i is found by equating elements (2,3) and (3,3) then multiply these equations by $-\sin\mu_i$ and $\cos\mu_i$ respectively. Dividing the result of their sums into the equation obtained from equating element (1,3) yields

$$\Omega_i = \text{atan2}\ [(c\tau_i(c\theta_i\ cx + s\theta_i\ cy) - s\tau_i\ cz) \cdot (s\mu_i(s\theta_i\ cx - c\theta_i\ cy) + c\mu_i(s\tau_i(c\theta_i\ cx + s\theta_i\ cy) + c\tau_i\ cz))] \tag{3.25}$$

Finally, equate elements (1,1) and (1,2) then divide to obtain the solution

$$\phi_{i+1}' = \text{atan2}\ (c\tau_i(c\theta_i\ nx + s\theta_i\ ny) - s\tau_i\ nz,\ -s\theta_i\ nx + c\theta_i\ ny) \tag{3.26}$$

The joint range-of-motion is found from the position measurements of the alignment point when the leg segment was at its extremes. These are expressed by

$$\delta_{Li} = \text{atan2}\ (y_{Li} - y_i,\ x_{Li} - x_i) \tag{3.27}$$

and

$$\delta_{Hi} = \text{atan2}\ (y_{Hi} - y_i,\ x_{Hi} - x_i) \tag{3.28}$$

where δ_{Li} and δ_{Hi} represent the extreme clockwise and counter-clockwise positions of joint frame i relative to frame m. Expressing the fixed joint displacement from equation 3.2 as

$$\phi_{Fi} = \phi_i' + \theta_i \tag{3.29}$$

and referring to equation 3.5, the low and high joint displacements are

$$\phi_{Li} = \phi_{Fi} + (\delta_{Li} - \delta_{Fi}) \tag{3.30}$$

and

$$\phi_{Hi} = \phi_{Fi} + (\delta_{Hi} - \delta_{Fi}) \tag{3.31}$$

When i is zero, ϕ_i', δ_{Li}, δ_{Hi} and δ_{Fi} are also zero.

This completes the derivation of A-model parameters from measured parameters. The results of extracting the parameters from the measurements made on a right middle leg

of a darkling beetle are found in Table 3.1. Since the actual parameter values for the leg of this animal are not known, the errors can not be assessed directly. An estimate of their accuracy, however, can be obtained from knowledge of measuring errors inherent in the positioner. These errors and how they are reflected in foot position accuracy is the subject of the next two chapters.

TABLE 3.1

A-model parameters for the right middle leg of a darkling beetle.

Leg Segment	range-of-motion (ϕ_{Li} to ϕ_{Hi}) (deg)	τ_i (deg)	segment length s_i (mm)	μ_i (deg)	Ω_i (deg)
body	-3.4	-29.3	2.59	-173.9	-61.5
coxa	-65.1 to 50.0	-19.7	1.68	112.7	25.1
femur	-109.3 to 0.7	-12.7	8.53	-6.2	3.2
tibia	30.8 to 170.8	-0.2	7.48	-0.0	0.2

Because the measurement procedure is used to determine the transform between successive joint frames, described by matrix ${}^{i}U_{i+1}'$, a number of different models can be determined from this relationship. This has advantages when one model is best suited for characterizing physical aspects and another best suited for analytical analysis. This is the case with the A-model and the D-H model.

4. POSITIONER MEASUREMENT ACCURACY AND CONSTRUCTION

4.1. Overview

The positioner's measurement accuracy and construction is important for reliable determination of kinematic parameters. Measurement accuracy is categorized into two types, position and orientation. Errors in these two measurement types are functions of the measurement procedure and positioner inaccuracies, but to different extents. In position measurement, the procedure is relatively straight forward and errors lie mainly with the equipment. These errors are quantified by measuring known distances and evaluating the differences between actual and measured quantities. Errors in position measurement are the same for each joint. Orientation-measurement errors, however, differ from joint to joint. This is due to the procedure involved in aligning a joint axis. Errors in orientation measurements are quantified by investigating the relationship between the procedural and equipment errors.

Once leg measurements have been made, they are manipulated into model parameters according to the configuration of the positioner's axes. Because transformations used in the previous chapter were formulated assuming orthogonal positioner axes, any deviation from this assumption will introduce errors in the determination of model parameters.

Discussed in this chapter are the errors in determining position and orientation of a joint axis, and the positioner construction discrepancies requiring a correction to transformation matrices.

4.2. Errors in Position Measurement

In evaluating the errors of joint-axis position measurement, it is assumed the joint position, as described in chapter 2, can be precisely seen through the microscope and that all errors lie with positioner equipment. The position measurement procedure involves aligning a point at the reticle cross-hairs and within the focal plane by adjusting slides x, y and z. There are two aspects of position measurement to consider when evaluating its errors. One is the accuracy in which a point can be aligned at the origin of frame m (see Figure 3.3) and the other is the accuracy of position-measurement readings relative to frame g. Alignment and relative measurement accuracies differ for each slide.

When aligning a point, interpolation between the 0.01 mm slide scale marks is possible to the nearest 0.005 mm. The lash between a lead screw and slide is greater than 0.010 mm but is eliminated by always approaching the alignment position using a clockwise rotation of the lead screw. When aligning a point with the cross-hairs in the x direction, misalignment can be detected within half a scale

division and thus the alignment error of slide x is ±0.005 mm. The alignment error of slide y is somewhat greater due to compliance in the positioner. Exact alignment error could not be measured but it was observed when moving the positioner to be between ±0.005 and ±0.010 mm. Positioner compliance is discussed later.

Horizontal alignments using slides x and y are made with greater accuracy than vertical alignments using slide z. This is due to the apparent thickness of the microscope focal plane. Apparent focal plane thickness was determined experimentally by repeated alignment of a smooth horizontal surface with the focal plane. Alignment was done in the z direction by always approaching the focal plane from below with a clockwise leadscrew rotation. Figure 4.1 shows the deviation of 120 aligned positions from the average aligned position. All but four points lie within a range of 0.04 mm which is assumed to be the apparent focal plane thickness. The distribution of alignment measurements appear random and the actual surface is assumed to lie somewhere within this range.

Errors in measuring distances involve not only alignment errors but also errors in a point's position read from positioner scales. Reasons for this are as follows. A measured point (i.e. aligned at origin of frame m) is related to frame p through frame g. From the translation portion of equation 3.3, this relationship is written as

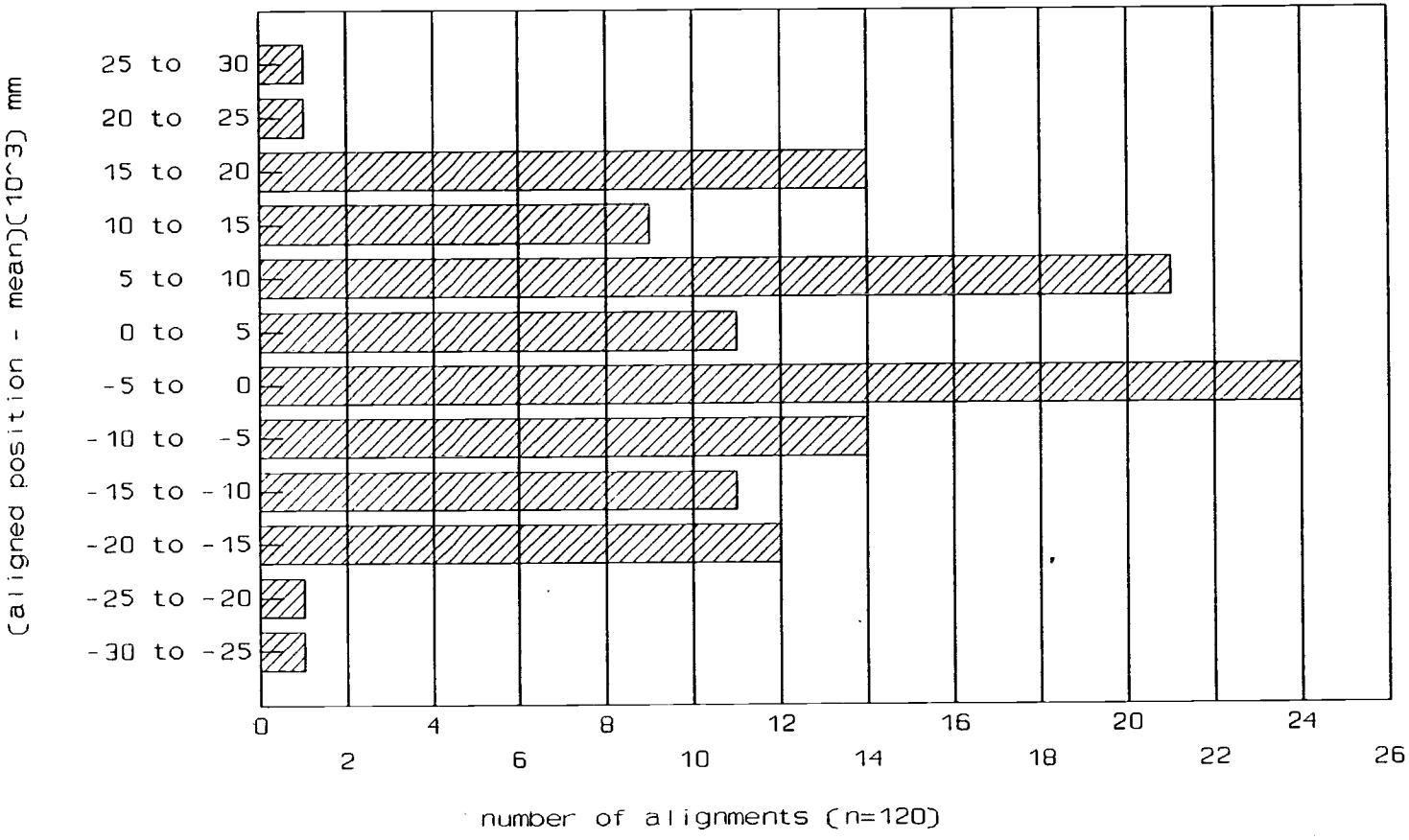

Figure 4.1. Precision in aligning surface into focal plane using slide z.

$$ {}^{p}T_{m} = {}^{p}T_{g}\ {}^{g}T_{m} \qquad (4.1) $$

Coordinates of the measured point are contained in the last column of the expanded transformation matrix. Using equations 3.6 and 3.8, this becomes

$$ {}^{p}T_{m} = \begin{bmatrix} 1 & 0 & 0 & -x_i + x_r \\ 0 & 1 & 0 & -y_i + y_r \\ 0 & 0 & 1 & -(z_i+a_i/2) + z_r \\ 0 & 0 & 0 & 1 \end{bmatrix} \qquad (4.2) $$

where x_i, y_i, $(z_i+a_i/2)$ are positioner readings of a point on joint axis i aligned at the reticle cross-hairs. Positioner readings x_r, y_r, z_r locate the origin of frame p aligned at the reticle cross-hairs. Errors in measuring the origin of joint i and frame p depend on their location within frame g. As slides are adjusted to align a point, compliance and small deviations in the positioner cause shifting in the stage to which a measured point is fixed. Because the stage extends out from each of the slides, small slide deviations causing rotational movement in other slides are magnified at the point of measurement (i.e. reticle cross-hairs).

Compliance is defined as any movement between parts of the positioner assembly other than movement in the positioner's 5 axes needed for measurement. The most

notable compliance occurs as a rotation about slide x. As an aid in explaining how this occurs, a cross section of slide x and its relationship to other slides is illustrated in Figure 4.2. Moments placed about the axis of slide x vary as adjustments are made to slide y, moving the center of mass of slide z assembly in the y direction. When these moments change, small movements are visible between the dovetail slide and dovetail base surfaces of slide x. The "Nylatron GS" pads between the surfaces, used to reduce adjustment friction in direction of the screw, are compliant enough to allow small rotations about the screw. A negative moment (or negative rotation) about the slide x axis causes a positive y shift of the point being aligned. Once the point is aligned, the reading from slide y is less than that had no shift occurred (Figure 4.3). Shift in y is expressed as

$$y_s = y_c - y_i \tag{4.3}$$

where y_c is the measurement assuming no compliance in the positioner and y_i is the actual measurement reflecting positioner deviations. Shifts in x and z are expressed in a similar manner.

Other causes of shifts are manufacturing errors. Referring to slide x, there can be a departure from straightness upward (z-direction) designated as bow error.

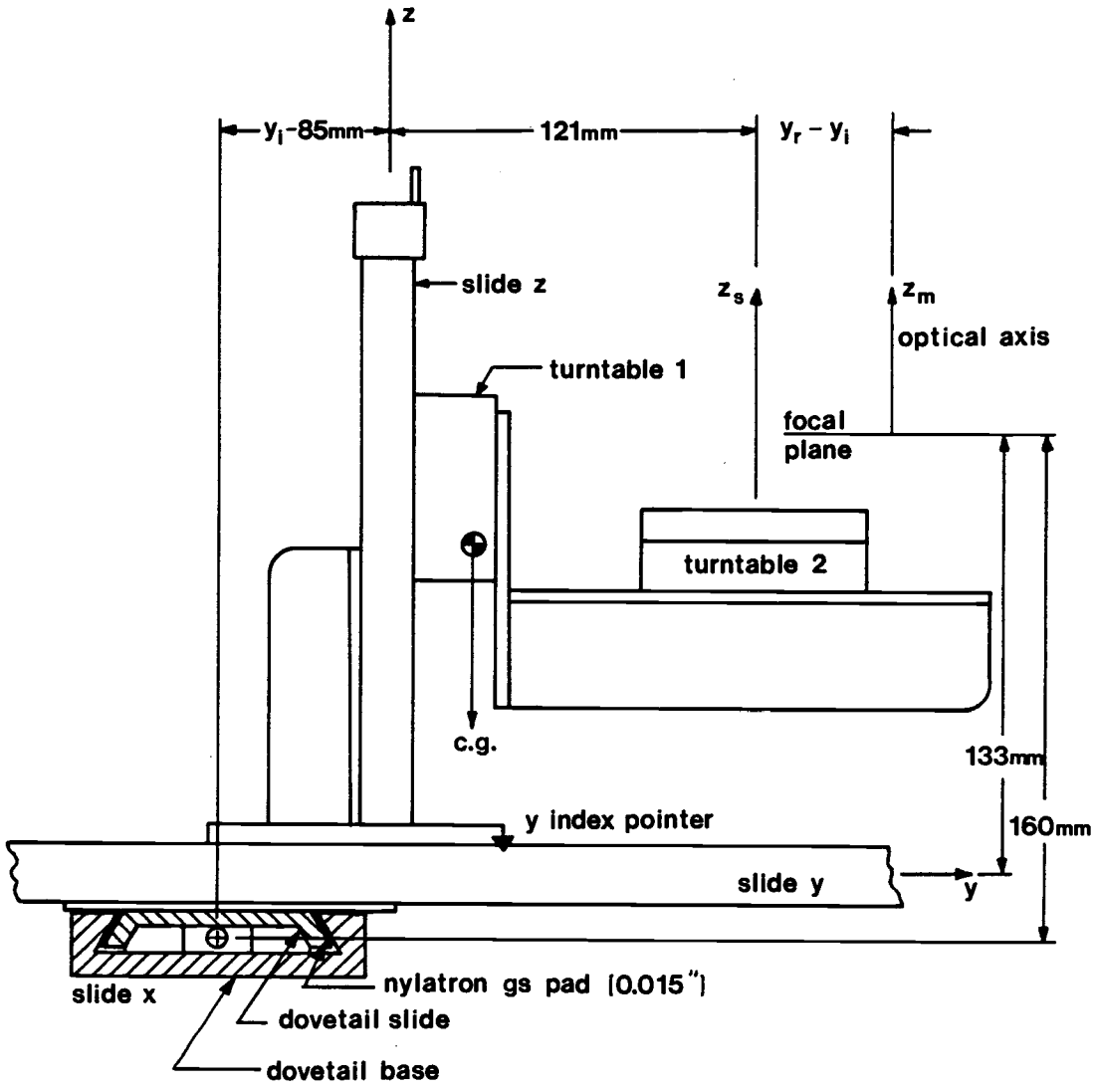

Figure 4.2. View of positioner assembly from -x direction.

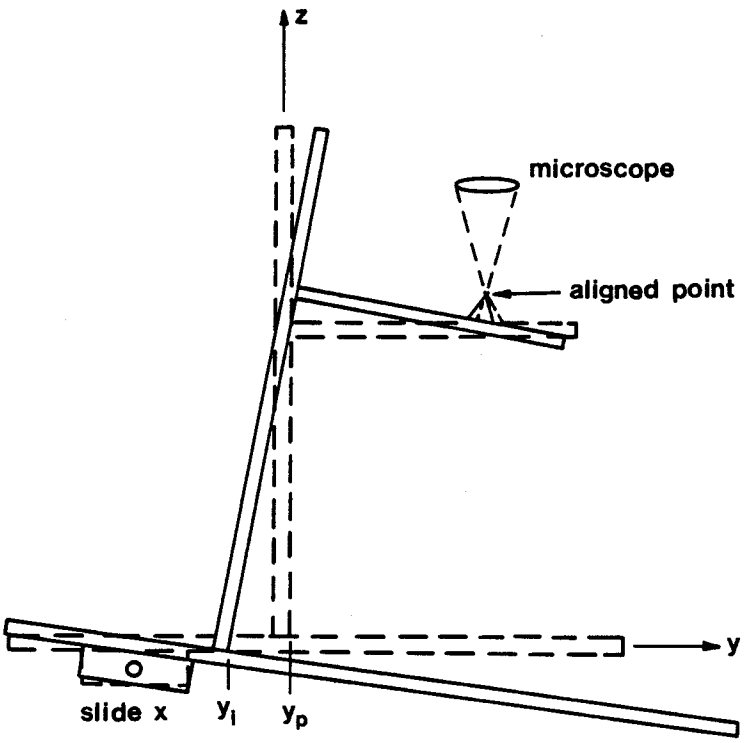

Figure 4.3. Illustration of positioner compliance about slide x causing position shift in direction y.

A horizontal deviation from straightness (y-direction) is termed **run-out**. Finally, there can be a **twist** in the x-direction. The manufacturer's upper limits of these deviations are; bow, 0.002" per foot; run-out, 0.001" per foot; and twist, 1 milliradian per foot.

The individual shifting effects of positioner compliance, bow, run-out and twist could not be measured because equipment accurate enough to measure such small deviations was not available. Instead, the shift attributed to each slide was calibrated against slide position to approximate the aggregate effect of these deviations. For slide x, a one inch gage block (25.4 mm) accurate to ±0.00004 in. at 68°F was mounted to the stage with its calibrated surface vertical and adjusted parallel to slide y. Parallelism was confirmed when a cross-hair traverse along the gage block edge did not deviate from that edge. Once adjusted, the known gage block dimension was measured by adjusting slide x so a cross-hair aligned with one side then the other. The difference in the two alignment positions and actual block length were then compared to determine shift in the x direction. This measurement was performed for several positions along slide x over a distance of 70 mm measured at the extreme ends of the gage block. This distance chosen as the anticipated range needed for future arthropod leg measurements. Slide y was calibrated using the same procedure.

Because of the microscope's vertical alignment inaccuracy, a dial gage accurate to 0.0001 inch was used to calibrate slide z. A gage block of arbitrary dimension was placed on the stage with its calibrated surface horizontal. The surface was then positioned against the dial gage by adjusting slide z. After recording this position, the calibrated surface of the 1" gage block was placed on top of that of the other block and its opposite surface was positioned against the dial gage as above. The difference between the two positions was compared to the known gage block length to determine shift. Slide z had a more limited range of motion than slides x and y so the gage block could be measured at only one position.

The data obtained from calibrating the slides were fit to curves expressing shift as a function of slide position. These curves are as follows.

$$x_s(x) = 0.219 - 6.26(10^{-3})\ x + 5.79(10^{-5})\ x^2 - 1.73(10^{-7})\ x^3 \qquad (4.4)$$

$$y_s(y) = -0.131 + 3.28(10^{-3})\ y - 3.79(10^{-6})\ y^2 \qquad (4.5)$$

The third and second order curve fits for slides x and y represent the best fit of data collected. Slide x included data from positions 127 mm to 173 mm and slide y included data from positions 57 mm to 103 mm. Positions

were measured from the center of the gage block at its extreme positions during calibration. A total of 5 positions were measured with 4 measurements at each position. Since the greater percentage of errors in slide z measurements were less than the apparent focal plane thickness of the microscope, a calibration curve was not realistic.

Calibration equations 4.4 - 4.5 were then used to correct all x and y position measurements. Using a subscript c to indicate a corrected measurement, corrections for each direction are expressed as

$$x_{ci} = x_i + x_s(x_i) \tag{4.6}$$

$$y_{ci} = y_i + y_s(y_i) \tag{4.7}$$

$$x_{cr} = x_r + x_s(x_r) \tag{4.8}$$

$$y_{cr} = y_r + y_s(y_r) \tag{4.9}$$

where x_i, y_i, x_r and y_r are actual (uncorrected) position measurements read from each slide. Equations 4.6 - 4.9 are essentially a rearrangement of equation 4.3 and approximate a measurement assuming no positioner compliance slides.

Several gage block measurements were made with the positioner then corrected using the above equations. The statistical results of these corrected measurements were used to define the error in the positioner's ability to make relative measurements. Table 4.1 shows these results.

The 95% confidence interval is the range in which 95% of all errors fall and is the confidence level chosen for this study. For a normal distribution, this interval is equivalent to twice the standard deviation multiplied by 1.96.

TABLE 4.1.

Corrected position measurement accuracy estimate of 1.000" (25.40 mm) gage block. Numbers in parenthesis indicate number of measurements.

	distance (mm)		
	$x_c(80)$	$y_c(77)$	z(60)
mean	25.400	25.400	25.406
mean error	+0.000	-0.000	+0.006
standard dev.	0.0046	0.0082	*
error: maximum	+0.012	+0.024	+0.045
minimum	-0.011	-0.022	-0.020
95% confidence interval	0.018	0.032	0.100

* Explained in text.

Graphically illustrating this data, Figure 4.4 show the errors in slides x and y to approximate a normal distribution which justifies use of standard deviation. Distribution of errors in slide z, however, are nearly random as shown in Figure 4.5. The 95% confidence interval for this slide was calculated by eliminating 5% of data (3 points) at the extremes then multiplying the range between remaining maximum and minimum data values by 2.

This completes the positioning error estimation.

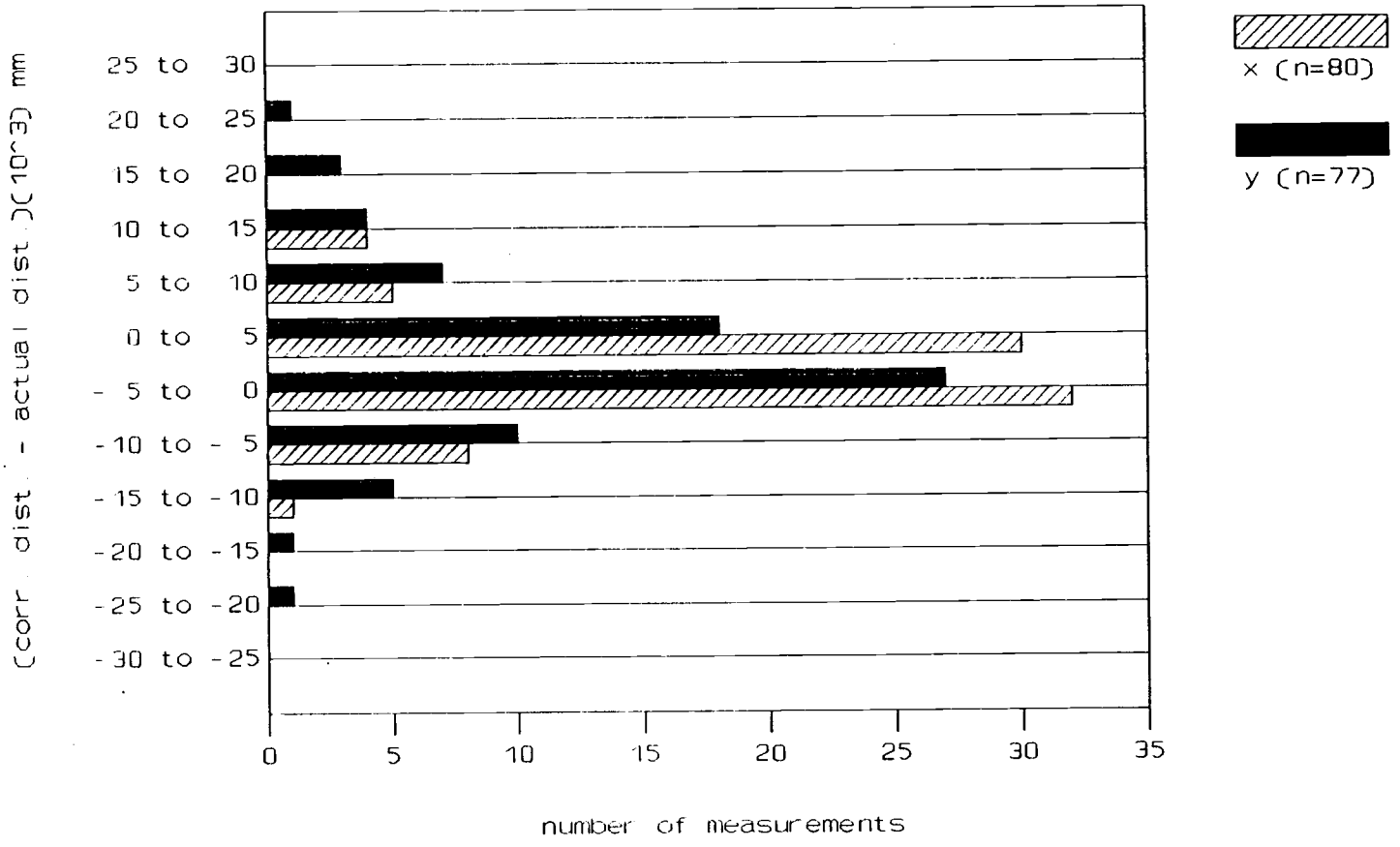

Figure 4.4. Distribution of corrected slide measurements x and y minus actual gage-block distance.

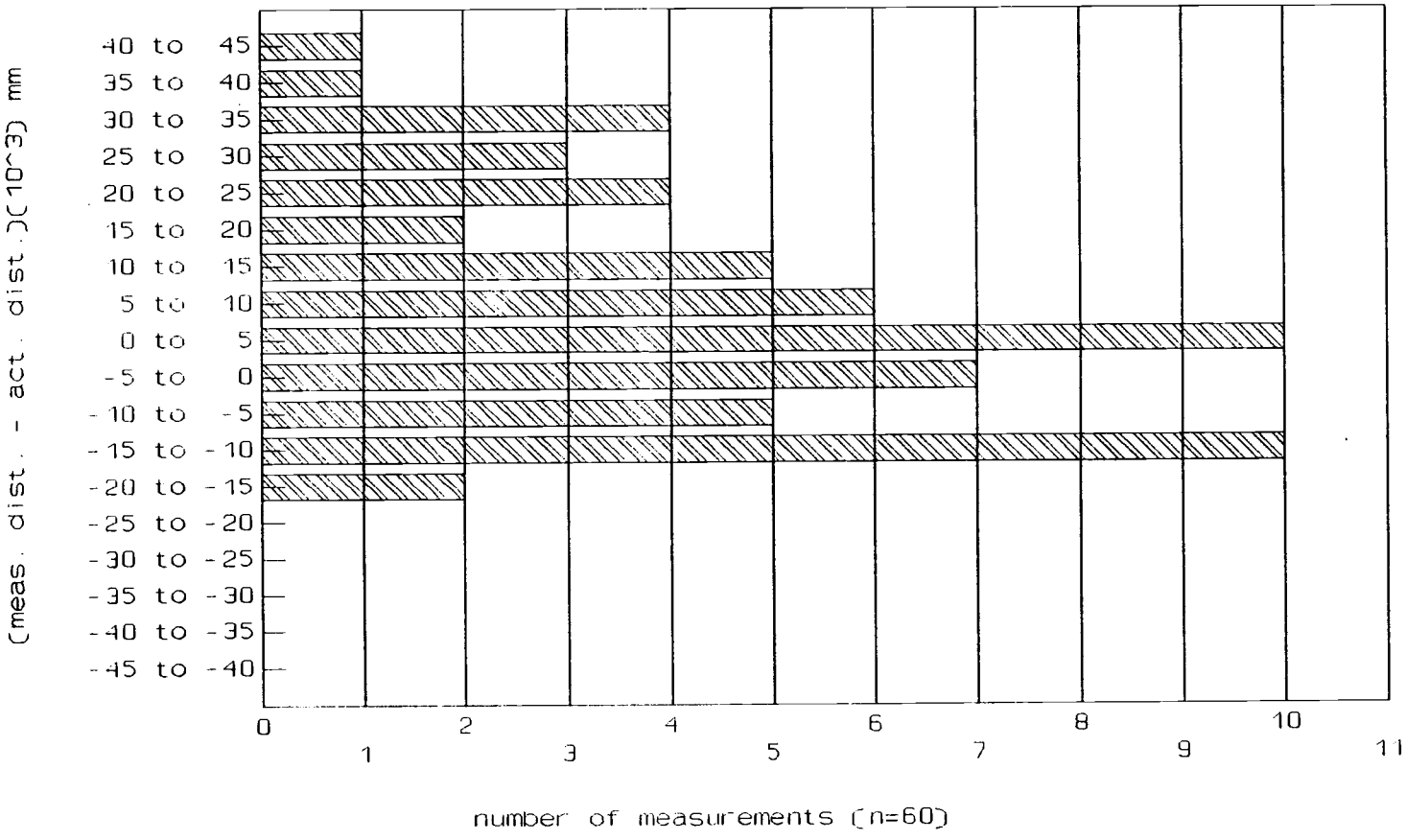

Figure 4.5. Distribution of slide z measurements minus actual gage-block distance.

4.3. Errors in Orientation Measurement

In evaluating the errors of joint-axis orientation measurements, it is assumed that all joints are perfect revolutes having no compliance, even though preliminary investigations indicate that this assumption is not correct. Because of the lack of information about the true kinematics of individual arthropod joints, the assumption of perfect joints is considered reasonable for an initial error analysis with the understanding that these errors are, at least, partly due to joint imperfection.

Errors in measuring joint-axis orientation depend on the procedure used to determine its alignment and the length of the segment attached to the joint. As discussed in chapter 3, orientation of joint axis z_i is measured by aligning it with the microscope optical axis, axis z_m. This alignment is made by first picking a point on the far end of the free leg segment i. The perpendicular distance from this point (alignment point) to the joint axis is termed the "effective alignment length". Axis z_i is considered aligned to z_m when the alignment point remains in the focal plane for all positions of segment i. Errors encountered in measuring this alignment are attributed to the thickness of the focal plane, z_t; the effective alignment length of the leg segment, L; and the range of motion of the leg segment, R. From these three parameters, two cases of orientation error are defined.

A case 1 error occurs when the alignment point coincides with a focal extreme at the midpoint of the leg segment's range of motion and coincides with the opposite focal extreme at its motion limits (Figure 4.6). The orientation angle error, ϵ_a, is expressed by

$$\epsilon_a = \sin^{-1}\left[\frac{z_t}{L\ (1 - \cos\ R/2)}\right] \tag{4.10}$$

A case 2 error occurs when the alignment point is midway between the focal extremes at the midpoint of the leg segment's range of motion and never crosses the focal extremes through its full range of motion. When $R \leq 180^\circ$, the alignment point coincides with the focal extremes 90° in either direction of its midposition. Hence, the orientation angle error, ϵ_b, is expressed by

$$\epsilon_b = \begin{cases} \sin^{-1}\left[\dfrac{z_t}{2\ L\ \sin\ R/2}\right] & \text{for } 0^\circ \leq R \leq 180^\circ \\ \sin^{-1}\left[\dfrac{z_t}{2\ L}\right] & \text{for } 180^\circ \leq R \leq 360^\circ \end{cases} \tag{4.11}$$

These two cases represent the worst and best of a continuum of extreme errors in measuring orientation of a joint axis. The reason for distinguishing between the two

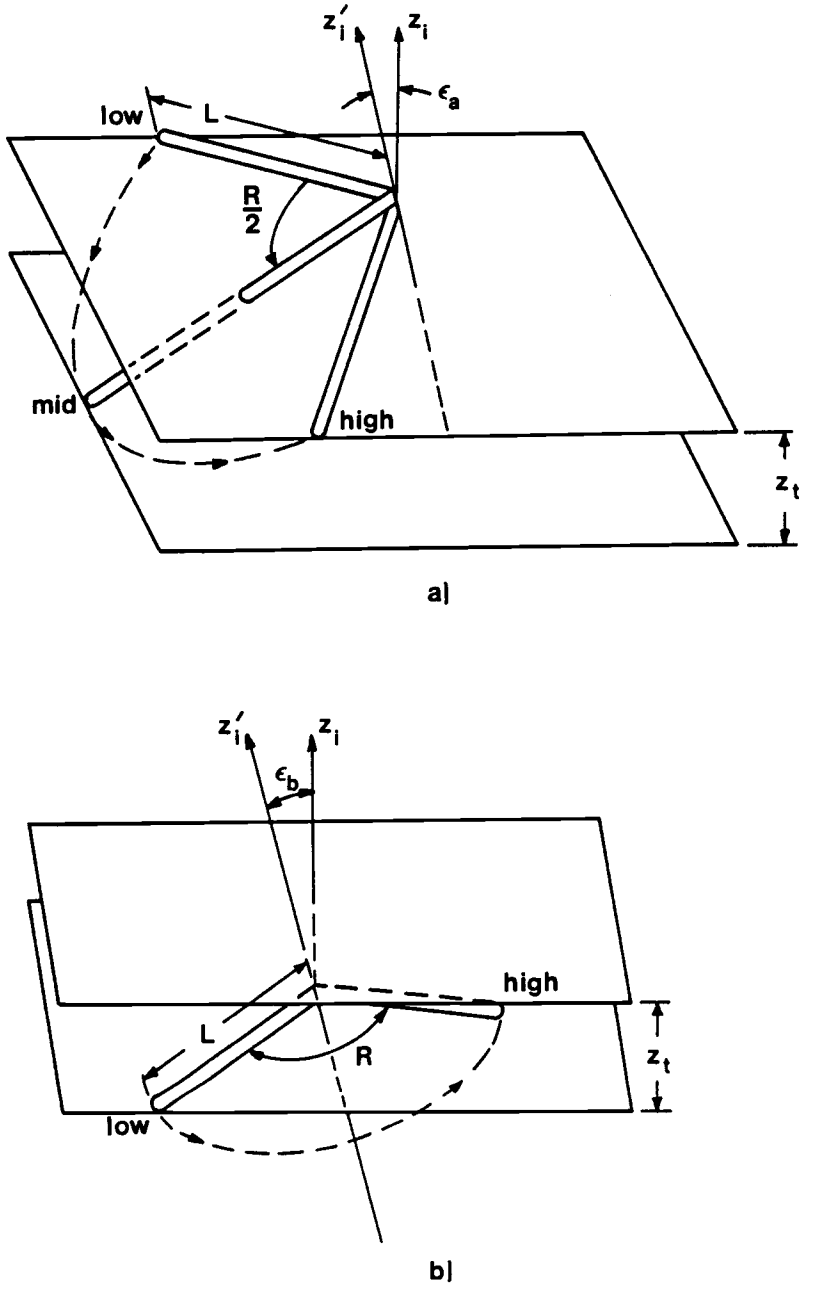

Figure 4.6. Orientation measurement error: a) case 1, b) case 2.

is discussed in chapter 5.

To check if it was reasonable to define errors in this manner, an experimental test was performed by mounting a small hinge to the stage and setting its axis in an arbitrary orientation. Using the alignment procedure described above, the joint axis was repeatedly aligned with the optical axis. Results of 17 axis alignments are shown in table 4.2 below. If orientation error definitions are reasonable, then the maximum experimental orientation error should not exceed the error calculated in case 1 (i.e. the worst case). Using a hinge equivalent alignment length of 5.88 mm, an apparent focal thickness of 0.04 mm and the average range-of-motion results, error for case 1 is calculated as $\epsilon_a = 0.43^\circ$. The results in table 4.2 show the deviations in the axis to be within this error.

How position and orientation measurement errors are reflected in model parameters and foot position is the subject of chapter 5. For now, the discussion of positioner characteristics is completed by an evaluation of its construction.

4.4. Positioner Construction

The positioner was assembled from 3 linear slides with lead screws and digital readouts and two turntables with vernier scales (Velmex Corporation). Each linear slide has a resolution of 0.01 mm and are stated by the manufacturer

Table 4.2

Orientation alignment precision estimate of a hinge with 5.88 mm effective alignment length.

	turntable measurements		range-of-motion	axis unit direction in frame s			joint-axis orient. error
	β (deg)	σ (deg)	R (deg)	x	y	z	ϵ^* (deg)
mean	62.0	120.4	168.5	0.4473	0.7612	0.4696	0.23
standard dev.	0.09	0.27	0.44	0.0038	0.0018	0.0014	0.118
maximum	62.1	120.9	169.1	n/a	n/a	n/a	0.42
minimum	61.8	120.0	167.6	n/a	n/a	n/a	0.04

* Error is defined as the difference between individual and mean axis unit vectors.

to be accurate to 0.10 mm/meter. The resolution of each turntable is 0.1 degrees with no manufacturer's statement of accuracy. Mounted rigidly above the positioner is a Wild dissecting microscope with a high magnification of 156x. The positioner was constructed on a 2 inch machined aluminum base one axis at a time. Each axis was shimmed for proper alignment with the microscope. Horizontal slides x and y were adjusted parallel to the focal plane and vertical slide z was adjusted by keeping a vertical line on a reticle cross-hair. A similar alignment procedure was used for the turntables.

Computation of A-model parameters as described in the previous chapter is based on four assumptions about the positioner's construction;

1. x, y and z slides are orthogonal,
2. turntable 1 rotation axis is parallel to y slide,
3. turntable 2 rotation axis is parallel to z slide at stage reference orientation (i.e. plane xy_s parallel to plane xy_p),
4. axes of turntables 1 and 2 intersect.

Given these assumptions, equation 3.3 accurately expresses the transformation from stage reference frame s to joint frame i'. This transformation, upon substitution of equation 4.1 into 3.3, is

$$ {}^{s}T_{i'} = {}^{s}T_{p} \; {}^{p}T_{m} \; {}^{m}T_{i'} \qquad (4.12) $$

where

$$^{m}T_i = \mathrm{Rot}(z,\delta_{Fi}) \qquad (3.4)$$

$$^{p}T_m = \mathrm{Trans}(x_r-x_i, y_r-y_i, z_r-(z_i+a_i/2)) \qquad (4.13)$$

$$^{s}T_p = \mathrm{Rot}(z,-\sigma_i)\ \mathrm{Rot}(y,-\beta_i) \qquad (3.10)$$

After the positioner construction was complete, various precision experiments were performed to estimate the actual position and orientation of all five axes. Discrepancies between experimental results and the above assumptions required certain corrections be made to z slide measurements. The slide and turntable discrepancies are discussed separately below.

4.4.1. Error in Slides

Angles between the three slides were measured against known dimensions of an aluminum block, referred to as test block. Two adjacent sides of the test block subtended an angle of 89.989 degrees ± 0.006 degrees. The test block was measured against a granite honed gage block with a right angle accurate to 0.001" over a 6" length. Using the microscope and a reticle cross-hair, differences could be observed between the angle subtended by slides x and y and the right angle of the test block. The test block was mounted to turntable 2 and adjusted until one side aligned with the x slide. Alignment was confirmed when a cross-hair remained on the test block edge while traversing the x

slide. A cross-hair was then aligned on the test block's adjacent edge and a traverse was made in the y direction. Differences in test-block edge and cross-hair positions in x were recorded for a specific y traverse distance.

To measure the angle between slides y and z, the test block was rotated 90° about the turntable 1 axis so the calibrated surfaces of the test block were approximately horizontal and vertical. The block's horizontal side was aligned to slide y by measuring deflections during a traverse using a 0.0001" resolution dial gage. Adjustments were made to turntable 2 until a minimum change in dial gage deflection was observed. A traverse was made of the adjacent side and dial gage deflection changes were noted.

The angle between the x and z slides was measured using the same method as for the y and z angle except the test block was mounted directly to turntable 1. Table 4.3 shows the results of the slide orientation test. The 89.91 degree angle between slides x and z affects the relative translation measurements found in the ${}^{P}T_{m}$ matrix. These measurements are defined by ${}^{P}x_i$, ${}^{P}y_i$ and ${}^{P}z_i$ and expressed as

$$ {}^{P}x_i = x_{cr} - x_{ci} \tag{4.14} $$

$$ {}^{P}y_i = y_{cr} - y_{ci} \tag{4.15} $$

$$ {}^{P}z_i = z_r - (z_i + a_i/2) \tag{4.16} $$

where x_{ci}, y_{ci}, x_{cr} and y_{cr} are defined by 4.6 - 4.9. When a

Table 4.3

Orthogonality test of slides x, y and z.

slides (aligned/measured)	traverse in positive direction of measured slide (mm)	deviation from block in direction of aligned slide (mm)	subtended angle (deg)
x/y	25.00	0.00 ±0.03	90.00 ±0.07
y/z	30.00	0.00 ±0.02	90.00 ±0.05
z/x	25.00	-0.04 ±0.03	89.91 ±0.07

point is brought into the focal plane along slide z, the measured value of ${}^{P}x_i$ differs from the measurement that would have been observed assuming slide z orthogonal to x and is corrected by the following.

$$ {}^{P}x_{ci} = {}^{P}x_i + {}^{P}z_i * \cos(89.91^{\circ}) \qquad (4.17) $$

Changes to ${}^{P}z_i$ are unwarranted since they are smaller than can be detected by the positioner for the positioner's full range of motion.

4.4.2. Error in Turntable-Axes

Last to be considered are the rotation axes. Axis orientations and positions of turntables 1 and 2 were measured by locating points which lie along the axes. Reuleaux (1876), in his discussion of Phoronomics (kinematics), showed how the "temporary center" of rotation could be found from knowing locations of two points in a plane before and after some arbitrary rotation about the center. Each rotated point is connected by a line extending from its initial to its final position. The two perpendicular bisectors of these lines intersect at the center of rotation as diagrammed in Figure 4.7. The errors in locating the center point can be minimized by rotating the two points through 180 degrees.

To locate points along turntable-1 axis, the above

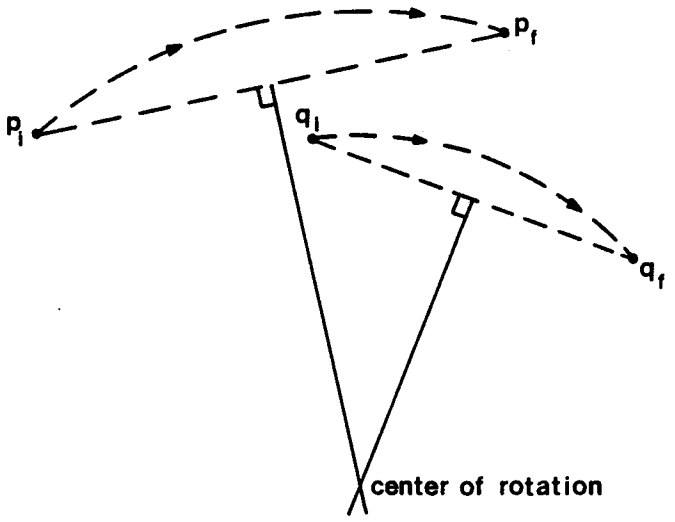

Figure 4.7. Bisection method for finding center of rotation.

process was used with four points lying approximately in a plane perpendicular to the axis. Six pairs of lines were then used to estimate the location of the center of rotation. The average was assumed to be the true value. This method was used at various distances along the axis to identify its orientation and position from $y_i \approx 22$ mm to 104 mm.

Assuming an orthogonal construction of the positioner, the axis of turntable 2 defines the z axis of stage frame s. Its orientation in the x direction is dependent on the position of turntable 1. When turntable 1 is at the reference orientation, turntable-2 axis should be parallel to slide z. The reference orientation is set by adjusting the stage plane parallel to the focal plane, a procedure that is accurate to $\pm 0.03^{\circ}$. This was done by traversing the 3" stage in the x direction and adjusting turntable-1 until the stage was in focus in every position along x. After establishing the reference orientation, the axis of turntable-2 was measured in the same manner as 1 from $z_i \approx$ 4 mm to 65 mm. Knowing the positions and orientations of both axes, their approximate common perpendicular was calculated to be 0.16 ±0.02 mm in the positive x_s direction from axis-2 to axis-1 (Figure 4.8). Error of ±0.02 mm reflects the maximum deviation in x direction data. Orientation results of turntable axis measurements are presented in Table 4.4. Values are given with respect to

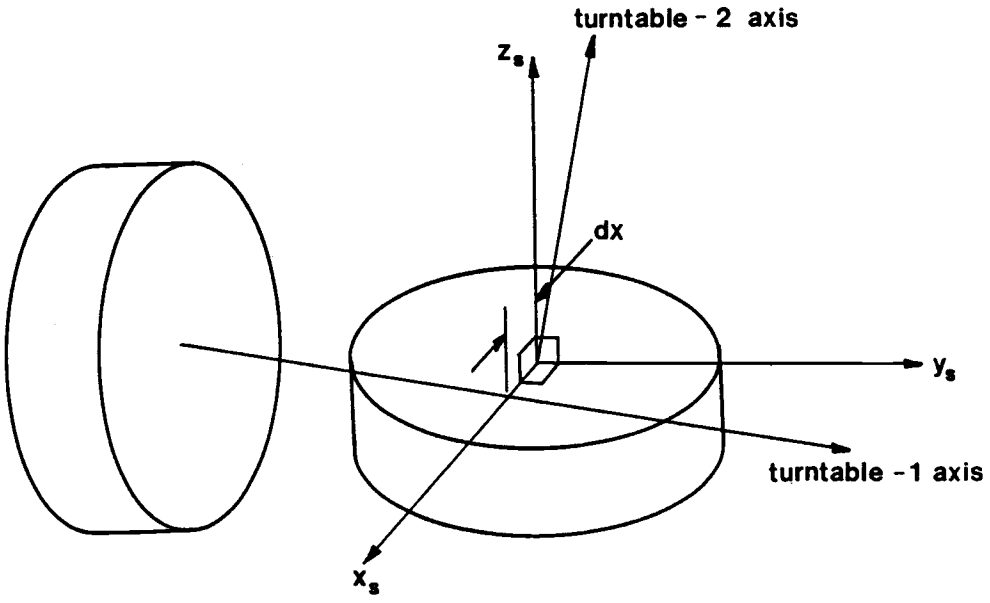

Figure 4.8. Turntable axes 1 and 2 shown with respect to orthogonal frame s.

orthogonal frame s in its reference orientation.

TABLE 4.4

Estimated orientation of turntable axes.

	direction cosines in orthogonal frame s		
turntable	u_x	u_y	u_z
1	-0.0014 ±0.0005*	1.0000	-0.0010 ±0.0005*
2	0.0000 ±0.0005*	0.0000 ±0.0005*	1.0000

* Errors equal to the largest direction deviations in data.

To account for displacement and orientation discrepancies between actual and assumed turntable axes, the matrix ${}^{s}\mathbf{T}_{p}$ is redefined as follows.

$$ {}^{s}\mathbf{T}_{p} = {}^{p}\mathbf{T}_{s}^{-1} \tag{4.18} $$

where

$$ {}^{p}\mathbf{T}_{s} = \text{Trans}(dx,0,0)\ \text{Rot}(\mathbf{u},\beta_i)\ \text{Trans}(-dx,0,0)\ \text{Rot}(z,\sigma_i) \tag{4.19} $$

Translation dx is the common perpendicular distance between the turntable axes (0.16 ±0.02mm). Rotation matrix $\text{Rot}(\mathbf{u},\beta_i)$ is a rotation about an axis whose direction is defined by the vector **u** and whose transformation, as presented by Paul (1981), is expressed by

$$\mathrm{Rot}(\mathbf{u},\beta_i) = \begin{bmatrix} u_x u_x v\beta_i + c\beta_i & u_x u_y v\beta_i - u_z s\beta_i & u_x u_z v\beta_i + u_y s\beta_i & 0 \\ u_y u_x v\beta_i + u_z s\beta_i & u_y u_y v\beta_i + c\beta_i & u_y u_z v\beta_i - u_x s\beta_i & 0 \\ u_z u_x v\beta_i - u_y s\beta_i & u_z u_y v\beta_i + u_x s\beta_i & u_z u_z v\beta_i + c\beta_i & 0 \\ 0 & 0 & 0 & 1 \end{bmatrix} \tag{4.20}$$

where v is the versine defined by $v\beta_i = 1 - \cos\beta_i$ and s and c are the sine and cosine. The values of u_x, u_y and u_z are direction cosines of turntable 1 as defined in Table 4.4. Substituting 1 for u_y and neglecting second order terms $u_x u_z$, u_x^2 and u_z^2 equation 4.20 becomes

$$\mathrm{Rot}(\mathbf{u},\beta_i) = \begin{bmatrix} c\beta_i & u_x v\beta_i - u_z s\beta_i & s\beta_i & 0 \\ u_x v\beta_i + u_z s\beta_i & 1 & u_z v\beta_i - u_x s\beta_i & 0 \\ -s\beta_i & u_z v\beta_i + u_x s\beta_i & c\beta_i & 0 \\ 0 & 0 & 0 & 1 \end{bmatrix} \tag{4.21}$$

The required inverse of equation 4.19 is written

$$ {}^{s}\mathbf{T}_{p} = \mathrm{Rot}(z,-\sigma_i)\ \mathrm{Trans}(dx,0,0)\ \mathrm{Rot}(u,-\beta_i)\ \mathrm{Trans}(-dx,0,0) \tag{4.25} $$

Expanded, 4.25 becomes

$$ {}^{s}\mathbf{T}_{p} = \begin{bmatrix} c\beta_i c\sigma_i + (u_x v\beta_i - u_z s\beta_i)s\sigma_i & (u_x v\beta_i + u_z s\beta_i)c\sigma_i + s\sigma_i & -s\beta_i c\sigma_i + (u_z v\beta_i + u_x s\beta_i)s\sigma_i & dx[v\beta_i c\sigma_i - (u_x v\beta_i - u_z s\beta_i)s\sigma_i] \\ -c\beta_i s\sigma_i + (u_x v\beta_i - u_z s\beta_i)c\sigma_i & -(u_x v\beta_i + u_z s\beta_i)s\sigma_i + c\sigma_i & s\beta_i s\sigma_i + (u_z v\beta_i + u_x s\beta_i)c\sigma_i & -dx[v\beta_i s\sigma_i + (u_x v\beta_i - u_z s\beta_i)c\sigma_i] \\ s\beta_i & (u_z v\beta_i - u_x s\beta_i) & c\beta_i & -dx(s\beta_i) \\ 0 & 0 & 0 & 1 \end{bmatrix} \tag{4.23} $$

4.5. Summary of Transformation Matrix Corrections

As discussed in chapter 3, all joint axis measurements must be transformed in reference to frame s in order to compute A-model parameters. This transformation is expressed in equation 3.3 as

$$ {}^{s}T_{i'} = {}^{s}T_{p} \quad {}^{p}T_{g} \quad {}^{g}T_{m} \quad {}^{m}T_{i'} \tag{3.3} $$

Transformation matrix ${}^{s}T_{p}$ as defined by equation 3.10 assumes that turntable axes intersect and align with orthogonal positioner slides. Because this is not the case, ${}^{s}T_{p}$ is instead defined by transformation 4.25 above which more accurately reflects orientations and positions of actual turntable axes.

Transformation matrices ${}^{p}T_{g}$ and ${}^{g}T_{m}$, containing only translations, are combined to form matrix ${}^{p}T_{m}$. Equation 3.3 is rewritten as

$$ {}^{s}T_{i'} = {}^{s}T_{p} \quad {}^{p}T_{m} \quad {}^{m}T_{i'} \tag{4.12} $$

The translation elements of matrix ${}^{p}T_{m}$ are corrected to account for errors inherent in positioner slides and construction. Formulation of this matrix is

$$ {}^{p}T_{m} = \mathrm{Trans}({}^{p}x_{ci}, \; {}^{p}y_{i}, \; {}^{p}z_{i}) \tag{4.24} $$

where

$$^{P}x_{ci} = {}^{P}x_i + {}^{P}z_i * \cos(89.91^{\circ}) \quad (4.17)$$

$$^{P}x_i = x_{cr} - x_{ci} \quad (4.14)$$

$$^{P}y_i = y_{cr} - y_{ci} \quad (4.15)$$

$$^{P}z_i = z_r - (z_i + a_i/2) \quad (4.16)$$

and further where

$$x_{ci} = x_i + x_s(x_i) \quad (4.6)$$

$$y_{ci} = y_i + y_s(y_i) \quad (4.7)$$

$$x_{cr} = x_r + x_s(x_r) \quad (4.8)$$

$$y_{cr} = y_r + y_s(y_r) \quad (4.9)$$

and finally where

$$x_s(x) = 0.219 - 6.26(10^{-3})\, x + 5.79(10^{-5})\, x^2 - 1.73(10^{-7})\, x^3 \quad (4.4)$$

$$y_s(y) = -0.131 + 3.28(10^{-3})\, y - 3.79(10^{-6})\, y^2 \quad (4.5)$$

Coordinates x and y in equations 4.4 and 4.5 are values read directly from positioner slides.

There still remain position and orientation measurement errors which can not be corrected for. Position errors are those listed in table 4.1 and orientation errors are defined by cases 1 and 2 in equations 4.10 and 4.11 respectively. How these errors effect leg model parameters and foot positioning is the subject of the next chapter.

5. ERRORS IN THE KINEMATIC MODEL: EVALUATION APPROACH

5.1. Overview

Accuracy of measured A-model parameters are evaluated by how well the measured model predicts true kinematics of the leg. In an analogous situation, researchers evaluate robot calibration methods by comparing predicted position of their calibrated model to actual position of the robot for a given set of joint displacements.

As an example, Judd and Knasinski (1987) evaluated their robot calibration procedure by running experiments on a Automatix Aid 900 robot. They positioned the robot with a known set of joint angles and measured actual position of the robot tool plate. The same joint angles were used in their calibrated robot model to determine a predicted tool-plate position which was then compared with its measured position. The error between the two was a measure of their calibration accuracy. Whitney, Lozinski and Rouke (1984) used the approach of comparing actual to predicted positions to test their calibration method on a Puma 560 robot. Also using the Puma 560, Stone (1987) tested his signature identification technique by measuring errors between actual and predicted positions while controlling the robot in one, two and three-dimensional grid touching tasks.

Obviously an arthropod leg's position can not be controlled in the same way a robot arm can and hence the

comparative technique used by the above mentioned researchers can not be used to evaluate the accuracy of the measured A-model. However, by quantifying errors which are inherent in the leg measurement equipment and technique, as was done in the previous chapter, measurement errors can be translated into foot (tarsus) position errors. This is accomplished by first determining A-model parameters which reflect measurement errors then using these parameters to determine foot position. Positions of the foot determined from the A-model containing errors can then be compared to those assuming no errors. Since error for each leg measurement is described by a range of values, the above approach results in an error volume defined about some "actual" foot position. Actual is defined here as the position obtained from a specified set of joint displacements and the actual measured A-model parameter values obtained from a leg. The error volume surrounding the actual foot position can be used as an indicator of how good a leg measurement is.

Several approaches were taken to determine the errors in the A-model. One possibility is to calculate model-parameter differentials in terms of measurement-parameter differentials. This method (see Appendix A) was abandoned because of the complexity of the equations, the dependency some measurement parameters had on others and the difficulty in interpreting results.

Error analysis difficulties imposed by complex equations and dependent measurements are avoided in the following solution by representing the position and orientation errors of each joint axis as "dimensional" errors in the kinematic model of the leg. Wang and Roth (1989) also defined dimensional errors in revolute joints in terms of errors in position and orientation. Their concern, however, is with quantifying these errors from knowledge of possible error configurations and forces on the joint.

In this research it is the errors inherent in the measurement device which define position and orientation errors. These errors are used to formulate matrix ${}^{i}\mathbf{E}_{i}'$ which is the transformation from the measured joint axis coordinate frame xyz_i to coordinate frame xyz_i' representing axis position and orientation errors (Figure 5.1). Matrix ${}^{i}\mathbf{E}_{i}'$ is then used to define a matrix relating successive joint error frames as follows.

$$ {}^{i}\mathbf{U}_{i+1}' = {}^{i}\mathbf{E}_{i}'^{-1} \; {}^{i}\mathbf{U}_{i+1} \; {}^{i+1}\mathbf{E}_{i+1}' \tag{5.1} $$

where ${}^{i}\mathbf{U}_{i+1}$ is defined in chapter 3 as

$$ {}^{i}\mathbf{U}_{i+1} = \mathbf{S}_{i} \; \boldsymbol{\theta}_{i+1} \tag{3.1} $$

and relates frame xyz_i to frame xyz_{i+1}. From matrix ${}^{i}\mathbf{U}_{i+1}'$ a new set of A-model parameters are extracted which reflect

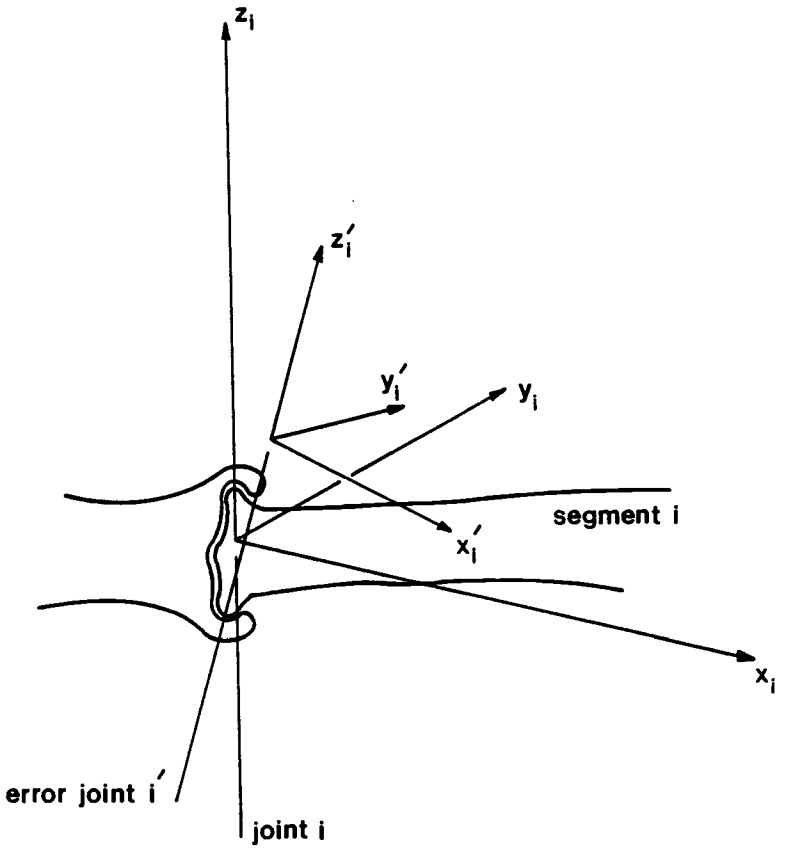

Figure 5.1. Coordinate frame xyz_i' representing dimensional errors in a joint.

errors in measurements of joints i and i+1.

Finally, error in foot position is found by determining a set of joint angles from the inverse kinematics solution of the nonerror A-model for a specified foot position and then using these joint angles with the error A-model in a forward kinematic solution. For each possible combination of measurement errors, there is one foot position error. All combinations result in a volume of error surrounding the foot.

This error evaluation method is presented here in three sections. First is a discussion of how measurement errors are represented in their respective joint frames. Second, a qualitative look is given at how errors effect A-model parameters and foot position. Third, the measured right middle leg of a darkling beetle is used to explain and demonstrate the complete procedure for determining foot position errors.

The method is presented assuming the errors in measuring actual alignment of turntable axes 1 and 2 (see chapter 4) have a negligible effect on parameter errors. This assumption allows a clearer presentation of the error evaluation approach. Implications of such an assumption are discussed at the end of this chapter.

5.2. Representation of Measurement Errors

As in chapter 4, measurement errors are divided into

two categories, those which occur in determining joint position and those which occur in determining joint axis orientation. How these errors appear at each joint axis is the topic of this section.

Position measurements ${}^{p}x_{ci}$, ${}^{p}y_{i}$ and ${}^{p}z_{i}$ define the origin of coordinate frame xyz_i with respect to frame p (see equations 4.20, 4.18, 4.19). For each of the three measurements there are a range of errors Δx, Δy and Δz which are assumed to be distributed equally about ${}^{p}x_{i}$, ${}^{p}y_{i}$ and ${}^{p}z_{i}$ respectively. No subscript is included on these errors because they are assumed the same for each measured joint. When joint i is aligned for measurement, its position is coincident with the origin of microscope frame m. The range of position-measurement errors lie within a rectangular boundary, or "error box", about this origin as shown in Figure 5.2.

Because errors Δx, Δy and Δz have their directions aligned with frame p and orientation of frames p and m are the same, the error box is oriented so the coordinate axes of frame m are normal to the box surfaces. Orientation of frame xyz_i is determined by a rotation of $\delta_{Fi}+\theta_i$ about z_m and thus orientation of the error box to this frame is also known. Errors in determining $\delta_{Fi}+\theta_i$ are too small to have a significant effect on orientation of the error box and resulting parameter errors and hence are ignored. The length of each of the three box dimensions is defined by the

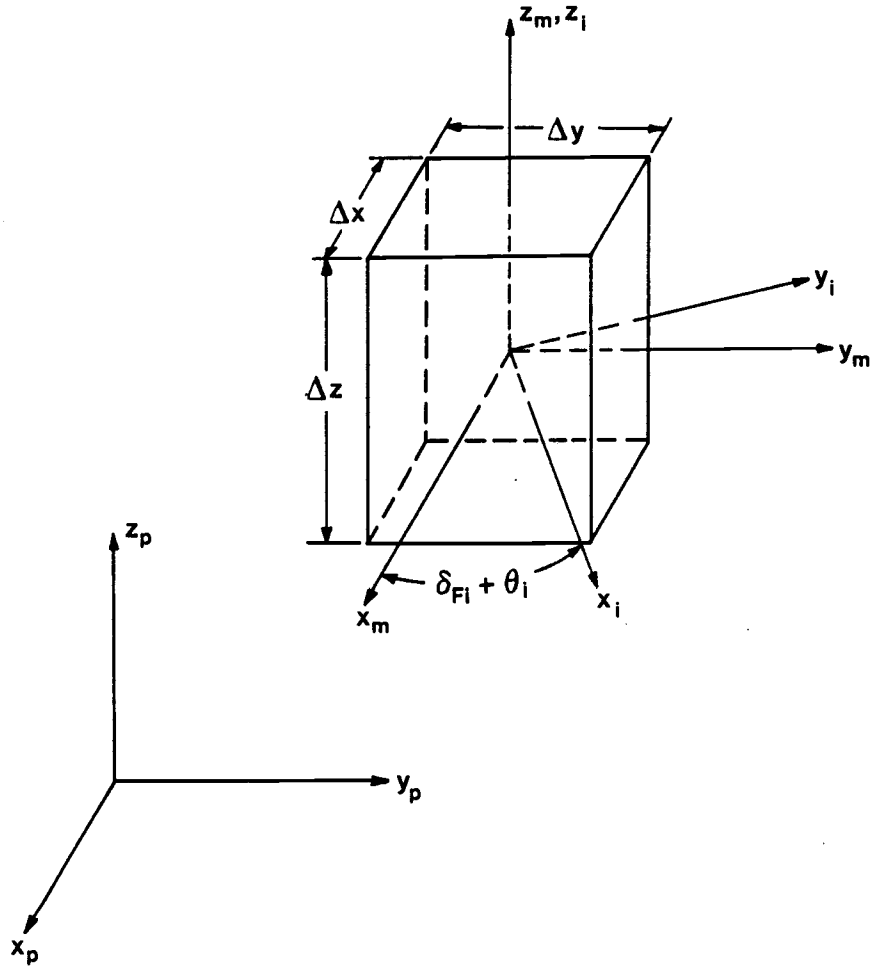

Figure 5.2. Boundary of position measurement errors represented by an error box about frame xyz_i.

error confidence interval (see Table 4.1).

When evaluating model parameters of leg segment i, errors in measuring both joint axes i and i+1 must be considered, as in equation 5.1. Because joint axes i and i+1 are ordinarily skew to one another, their associated error boxes will also have a skew relationship as depicted in Figure 5.3.

The geometric representation of orientation errors is based on their evaluation as discussed in chapter 4. From cases 1 and 2, four joint axis orientation error extremes are defined, two for each case. The two cases represent maximum and minimum extremes in formation of an orientation error boundary. Projections of these axis extremes onto the xy_m-plane lie 90° apart. This is seen by examining the difference between the two cases. The error axis in case 1 is directed toward or away from the mid position of the leg segment. In case 2, the error axis is directed perpendicular to the leg segment's mid position. Between the four axes exist an infinite number of other axis orientation errors which collectively generate a ruled surface. The resulting shape of these errors on joint i is best described by an elliptical cone or "error cone" whose vertex lies within the error box of joint i and whose axis is z_i.

As with the error box, geometry of an error cone on joint i can be described with respect to frame xyz_i. The major axis, x_e, of a section of the cone perpendicular to

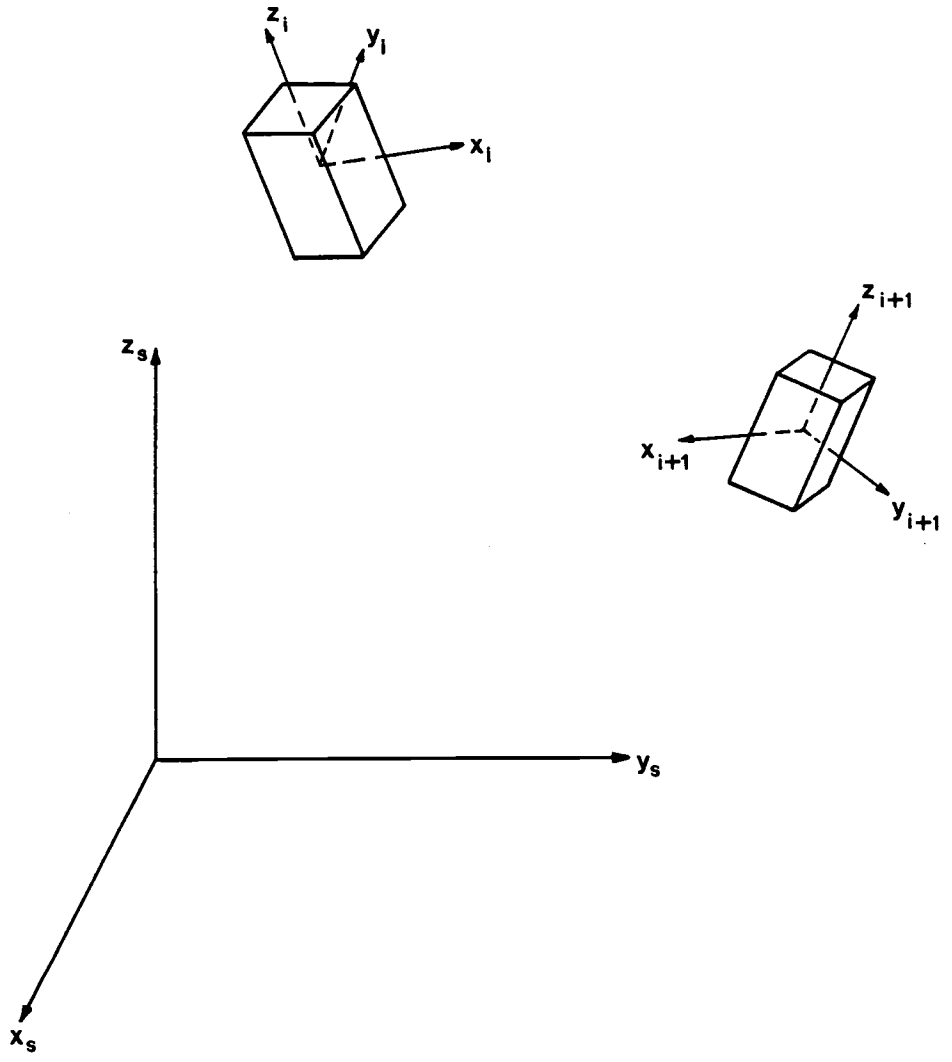

Figure 5.3. Error boxes i and i+1 with respect to frame s.

its axis is defined by projecting the mid position of segment i in case 1 onto the xy_m-plane (Figure 5.4). Orientation of the ellipse with respect to frame i is related through angle δ_e which is expressed by

$$\delta_e = (\delta_{Li} + \delta_{Hi})/2 - (\delta_{fi} + \theta_i) \tag{5.2}$$

If the ellipse in Figure 5.4 is positioned along z_i one unit from the vertex, then half the major axis distance is equal to the tangent of orientation error ϵ_a and half the minor axis distance is the tangent of ϵ_b. The location of any point x_i, y_i on this ellipse relative to frame xyz_i is then described by

$$x_i = \cos\delta_e \tan(\epsilon_a) \cos(\Gamma - \delta_e) - \sin\delta_e \tan(\epsilon_b) \sin(\Gamma - \delta_e) \tag{5.3}$$

$$y_i = \sin\delta_e \tan(\epsilon_a) \cos(\Gamma - \delta_e) + \cos\delta_e \tan(\epsilon_b) \sin(\Gamma - \delta_e) \tag{5.4}$$

When a leg segment's range of motion is 360°, orientation errors a and b are equal and the error cone becomes circular.

Finally, the angle between a generator of the error cone and the measured joint axis, defined by angle ϵ_i, is expressed by

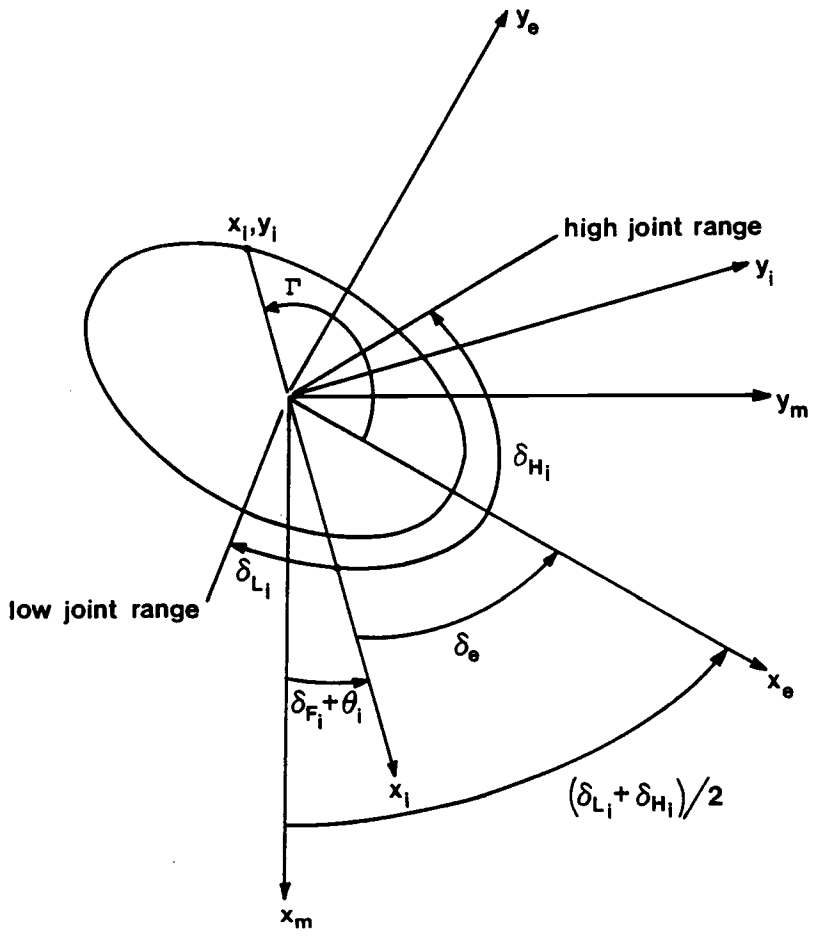

Figure 5.4. Cross-section of error cone i parallel to xy_m-plane.

$$\epsilon_i = \text{atan2}\ ((x_i^2 + y_i^2)^{1/2},\ 1) \qquad (5.5)$$

As with the error boxes, error cones of both frames i and i+1 influence parameters of segment i. Again, these two cones are skew to one another as depicted in Figure 5.5.

To complete a representation of dimensional errors in the kinematic model, the errors in determining the base coordinate frame fixed to the body (i.e. frame b) must be considered. As described in section 2.4 of chapter 2, frame b is defined by the proximal articulation positions of the middle and rear coxa segments. Errors in these positions are bounded by error boxes as shown in Figure 5.6. For purposes of explanation, it is assumed that x, y and z dimensions of the error boxes are aligned with actual x_b, y_b and z_b axes of the body frame. Position errors of the frame b origin are bounded by an error box of same size and orientation as those at the articulations. The orientation error boundary of z_b-axis is defined by an error cone where errors ϵ_a and ϵ_b are expressed by

$$\epsilon_a = \text{atan2}(\Delta z,\ Ly) \qquad (5.6)$$

and

$$\epsilon_b = \text{atan2}(\Delta z,\ Lx) \qquad (5.7)$$

Length Ly is the distance from the line connecting mesocoxa articulations to the line connecting metacoxa articulations along y_b. Length Lx is the distance between the mesocoxa

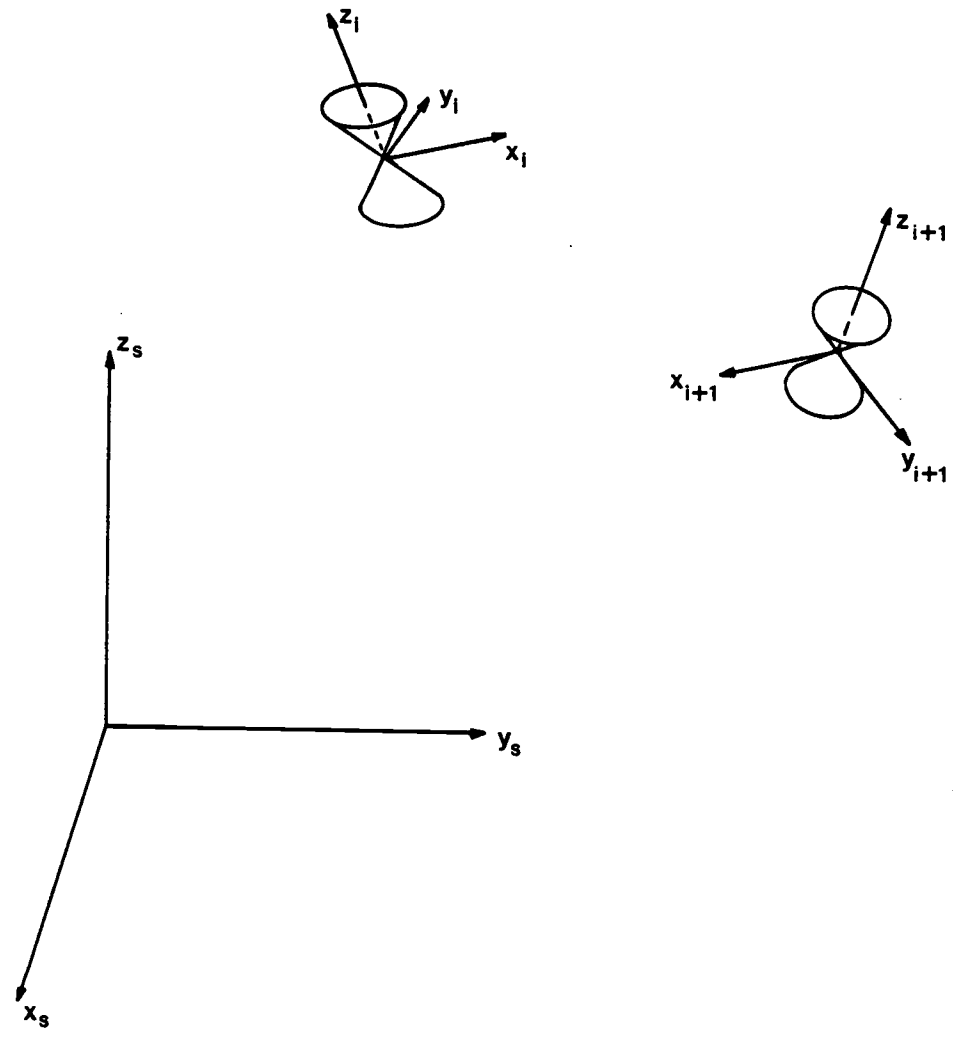

Figure 5.5. Error cones i and i+1 with respect to frame s.

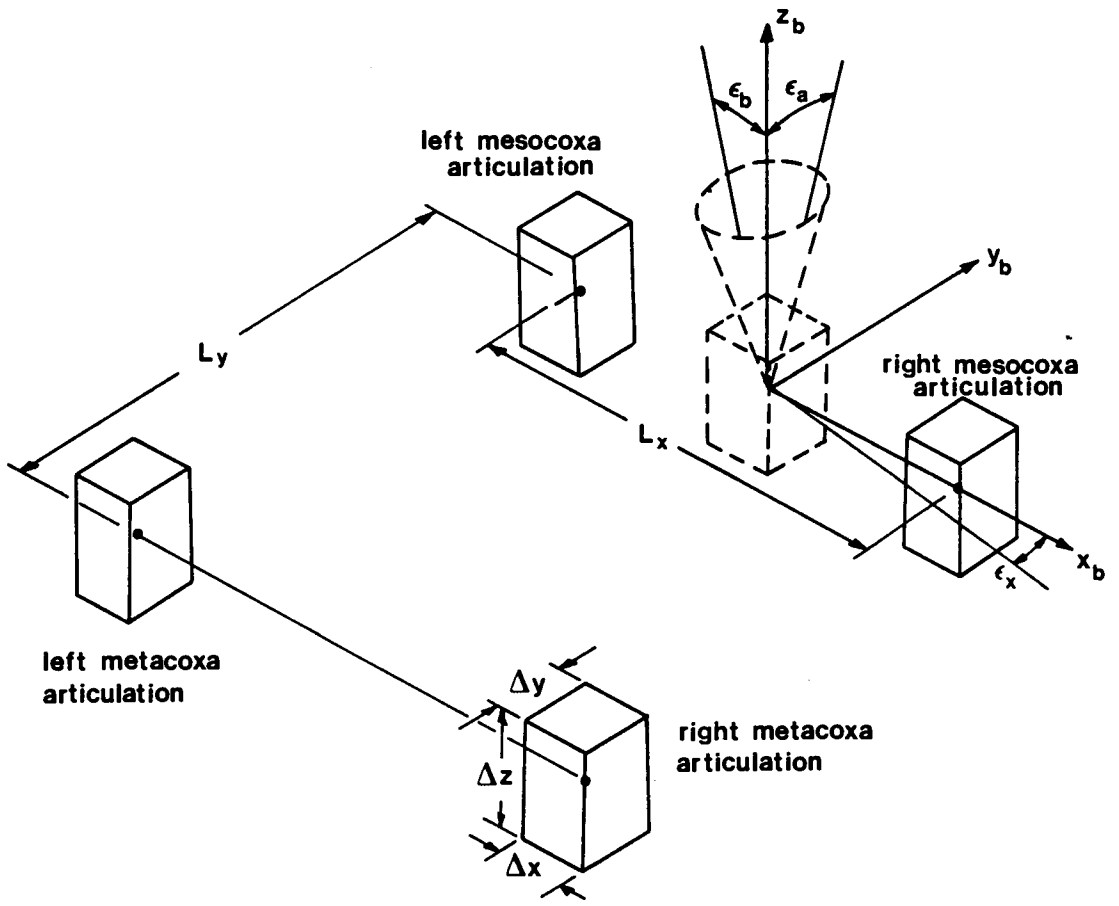

Figure 5.6. Body frame b and error boxes around proximal articulations of four rear coxa segments.

articulations along x_b. Orientation error angle ϵ_a is about x_b-axis and ϵ_b is about y_b-axis.

An additional orientation error occurring in the body frame but not the joint frames is that of x_b-axis. This error is a rotation about z_b and expressed by

$$\epsilon_x = \text{atan2}(\Delta y,\ Lx) \tag{5.8}$$

5.3. Qualitative Error Effect on A-model Parameters

With a knowledge of how measurement errors are represented at each joint axis and the body frame, the effect of the error boxes and error cones on A-model parameters can be illustrated qualitatively as in this section. The intention here is to give a physical understanding of the effect of errors on A-model parameters.

Parameter τ_i

Parameter τ_i is the rotation about y_i required to align coordinate axis x_i with line p_i-p_{i+1} (see Figure 3.4). By projecting images of error boxes i and i+1 into the xz_i-plane, the change in τ_i, $\Delta\tau_i$, can be illustrated. Figure 5.7 shows the position on the boxes for which error in τ_i is maximum. This error is dependent on size of the error boxes, orientation with respect to each other and distance between them (i.e. the segment length). As s_i decreases, error in τ_i increases. This is also seen in the

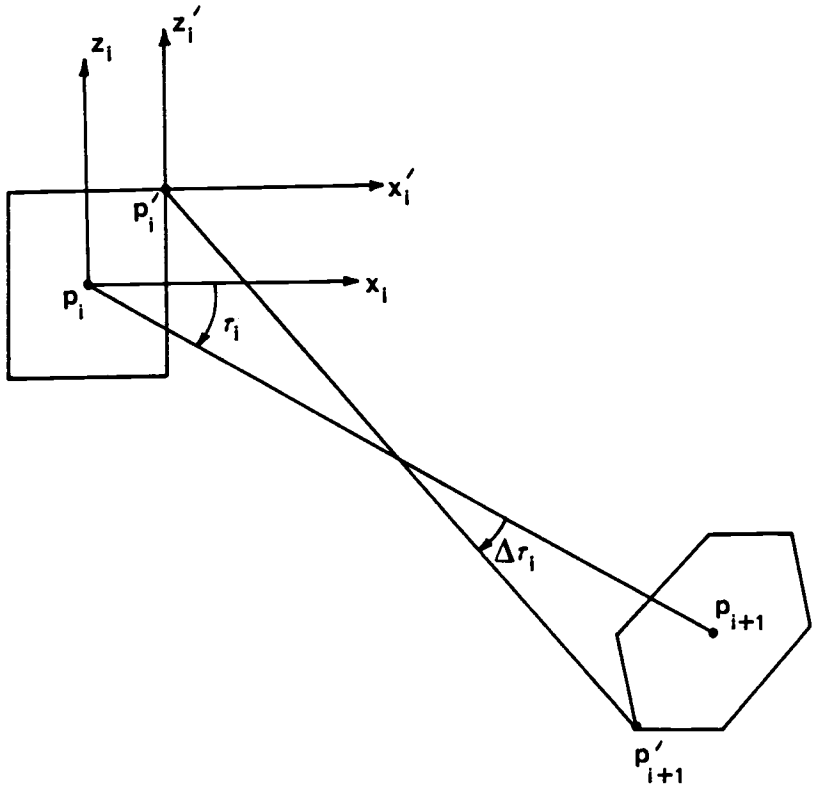

Figure 5.7. Projections of error boxes i and i+1 onto xz_i-plane showing error in parameter τ_i.

differential of τ_i expressed by equation A.5 in Appendix A.

Only error cone i has an effect on τ_i. The error is shown by passing a plane through cone i parallel to a plane containing x_i and z_i, as in Figure 5.8. Error in parameter τ_i is influenced by the error cone size and orientation with respect to frame i. This influence is the same for all s_i.

Parameter s_i

Error in segment length s_i is influenced only by the size of error boxes i and i+1 and their orientation to each other (Figure 5.9). In general, greatest error occurs between the closest or furthest two corners of error boxes i and i+1. Since s_i is only a measure of distance between joints i and i+1 in frame s, errors in s_i are not a result of axis orientation errors (see equation A.6).

Parameter μ_i

Parameter μ_i is revealed graphically by locating the intersection of plane xz_i and a plane perpendicular to line p_i-p_{i+1} then projecting z_{i+1} on to the plane perpendicular to line p_i-p_{i+1}. The error is illustrated by projecting the outline of error cones i and i+1 onto this same plane (Figure 5.10). As orientation of axes z_i or z_{i+1} approaches alignment with line p_i-p_{i+1}, the angle between the error cone's projected boundary increases and hence possible error in μ_i increases. When either z axis is aligned with line

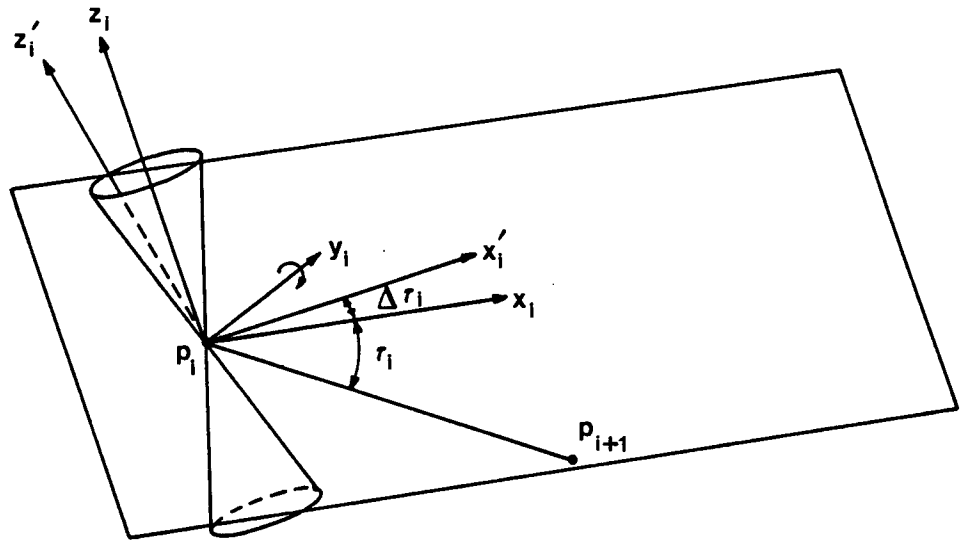

Figure 5.8. Plane xz_i passing through cone i showing error in parameter τ_i.

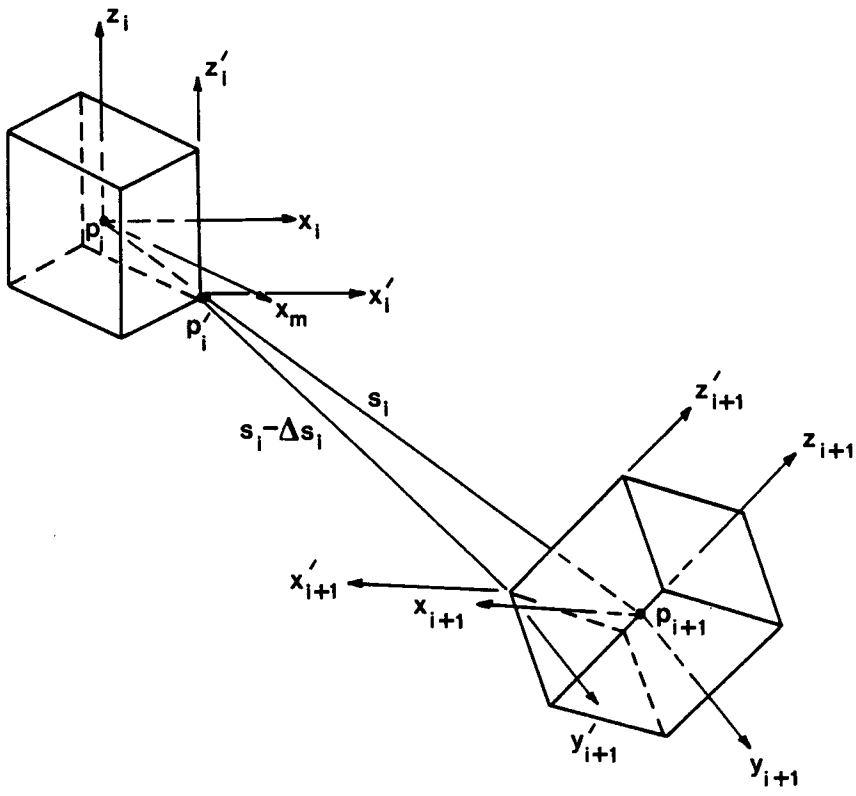

Figure 5.9. Position measurement errors on error boxes i and i+1 showing error in parameter length s_i.

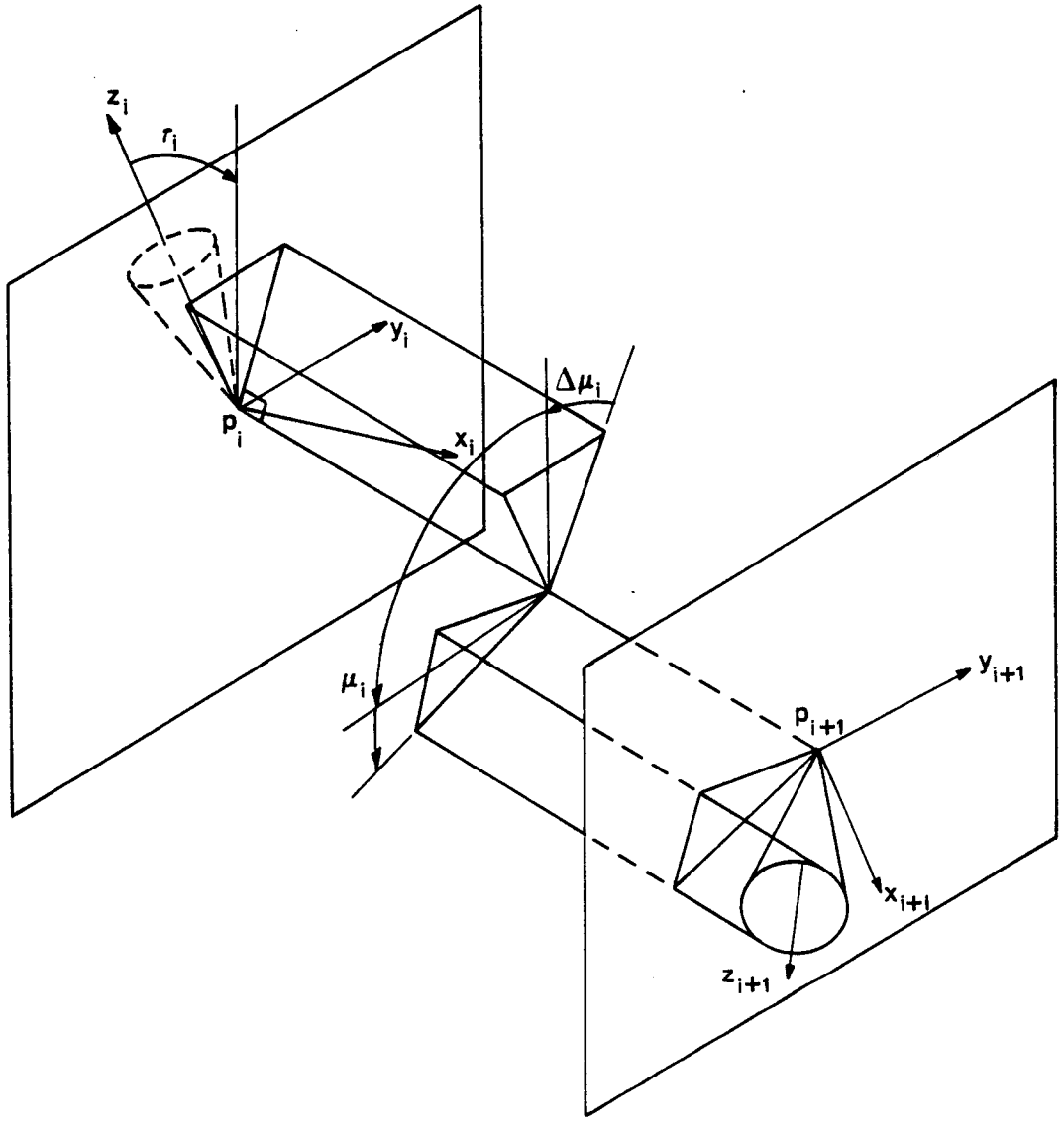

Figure 5.10. Projection of error cones i and i+1 onto plane perpendicular to line p_i-p_{i+1} showing error in parameter μ_i.

p_i-p_{i+1}, parameter μ_i has an arbitrary value and the possible error in μ_i is 2π.

Position error also influences errors in μ_i. Illustrating this error takes two projections. One projection is of the z_i and z_{i+1} axes on to a plane perpendicular to line p_i-p_{i+1} as above. The other is a projection of these axes onto a plane perpendicular to a line extending from two error positions in boxes i and i+1 as in Figure 5.11. The difference between the subtended angles of z_i and z_{i+1} on the two projections is the error in parameter μ_i. As the segment length decreases the influence position measurement errors have on μ_i increases.

Parameter Ω_i

Factors which influence error in parameter Ω_i are similar to those which influence parameter τ_i. Here errors in Ω_i due to positioning errors are illustrated by projecting error boxes i and i+1 onto a plane containing z_{i+1} and point p_i, (Figure 5.12). The Ω_i error resulting from orientation errors are shown by passing a plane through cone i+1 parallel to a plane containing axis z_{i+1} and point p_i, as in Figure 5.13. The same factors that influence error in τ_i also influence Ω_i.

Generally, measurement errors will affect model parameters of the smallest leg segments the most. For the beetle, the smallest segments are nearest the body. As can

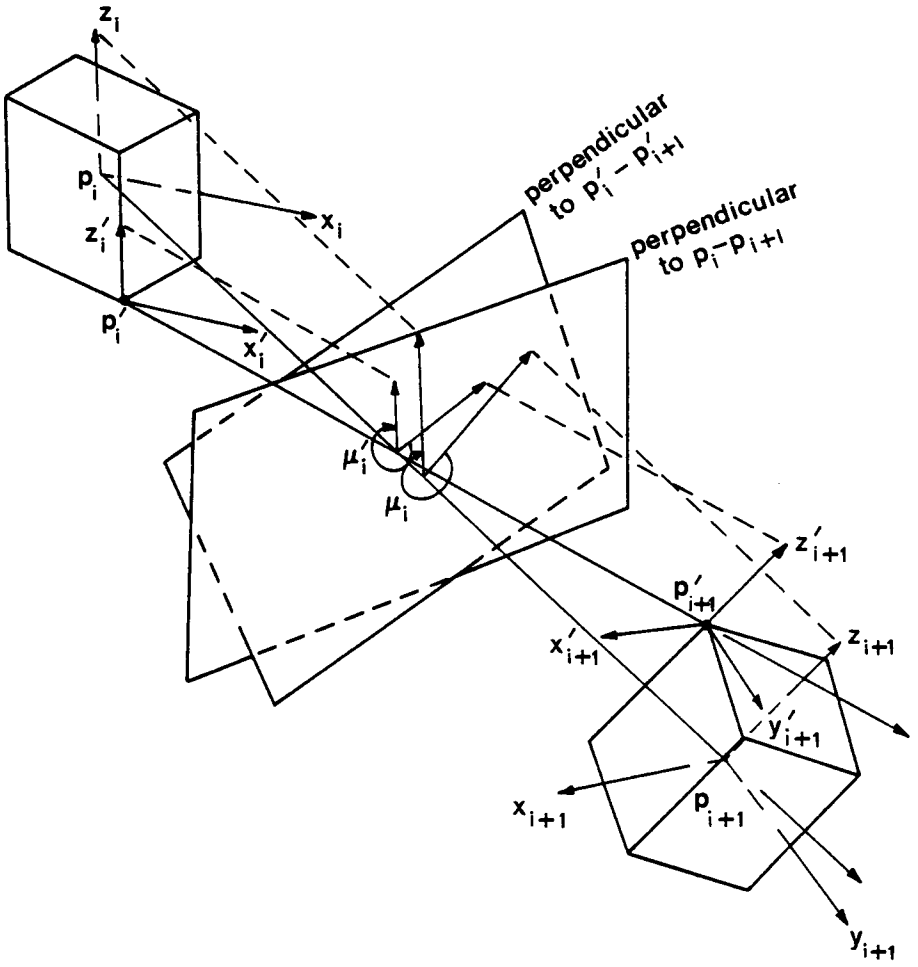

Figure 5.11. Joint axes of measured position and assumed error position projected onto planes perpendicular to lines p_i-p_{i+1} and p_i'-p_{i+1}' to show error in μ_i.

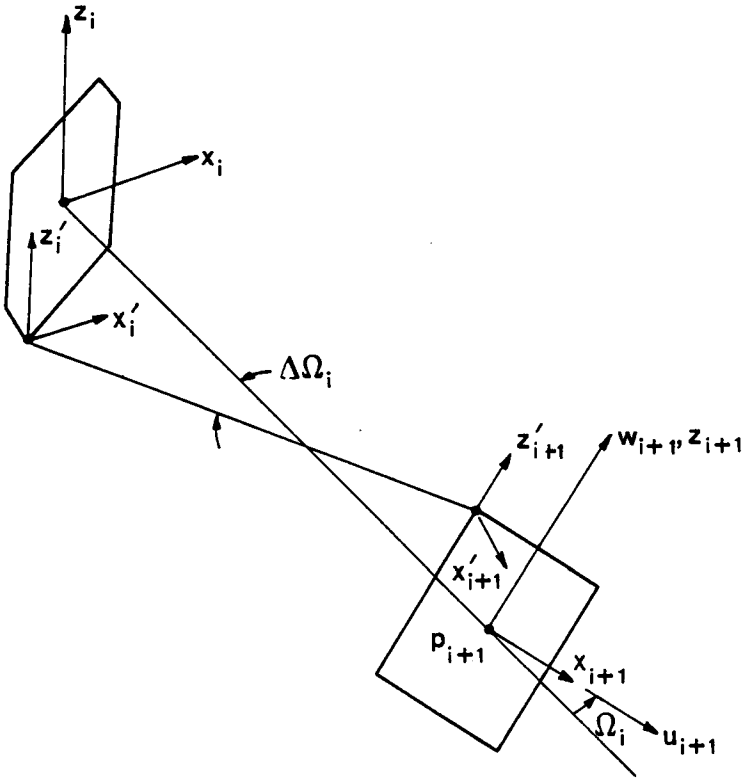

Figure 5.12. Error boxes projected onto plane containing joint axis i+1 and joint i showing error in parameter Ω_i.

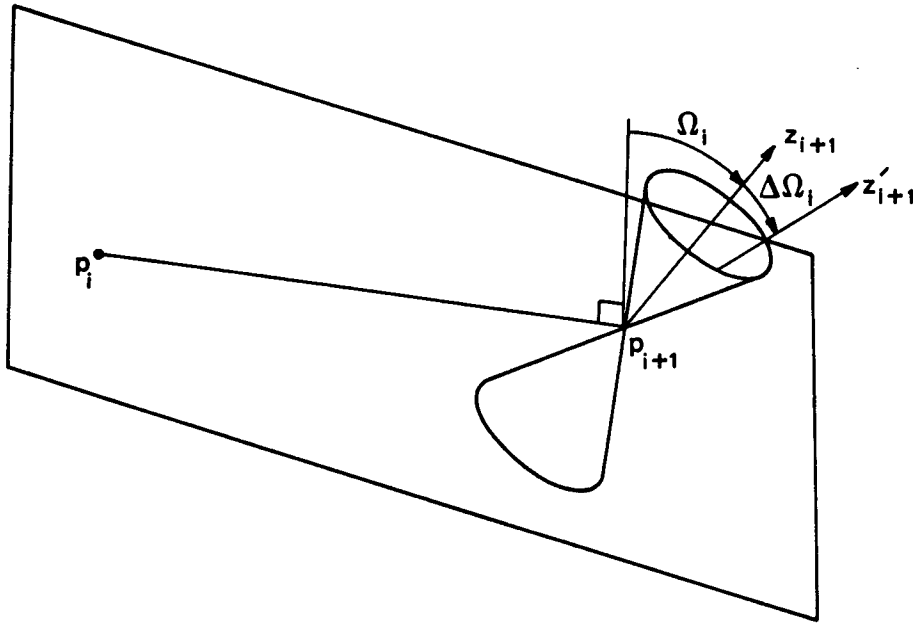

Figure 5.13. Plane containing joint axis i+1 and point p_i, passing through cone i+1 showing error in parameter Ω_i.

be seen in the next two sections, these errors have the greatest impact on foot position errors.

5.4. Qualitative Error Effect on Foot Position

Here a graphical approach is taken to illustrate the influence of position measurement errors on foot position errors. This is demonstrated with a planar linkage of three links drawn with respect to a base frame as in Figure 5.14. All A-model parameters of a planar linkage are zero except length s. Joint 1 is shown in one position and joint 2 in three, a - c. A small rectangular box at joint 1 represents the boundary of measurement error about the actual position of joint 1. Measurement errors at joint 2 are assumed zero to simplify the example. To find errors in foot position due to the error box at joint 1, a line is drawn from the origin of the base to each corner of the box. Each line represents a different direction of u_1 from which joint variable ϕ_1 is measured. The error at each corner results in a change in lengths s_0 and s_1. Using the four error linkages at the box corners and two joint variables, the error box at joint 1 can be translated to an error surrounding the foot. Actual foot position **F** is expressed by

$$\mathbf{F} = \mathbf{B}\ \$_1\ \mathbf{S}_1\ \$_2\ \mathbf{S}_2\ [0,0,0,1]^T \qquad (5.9)$$

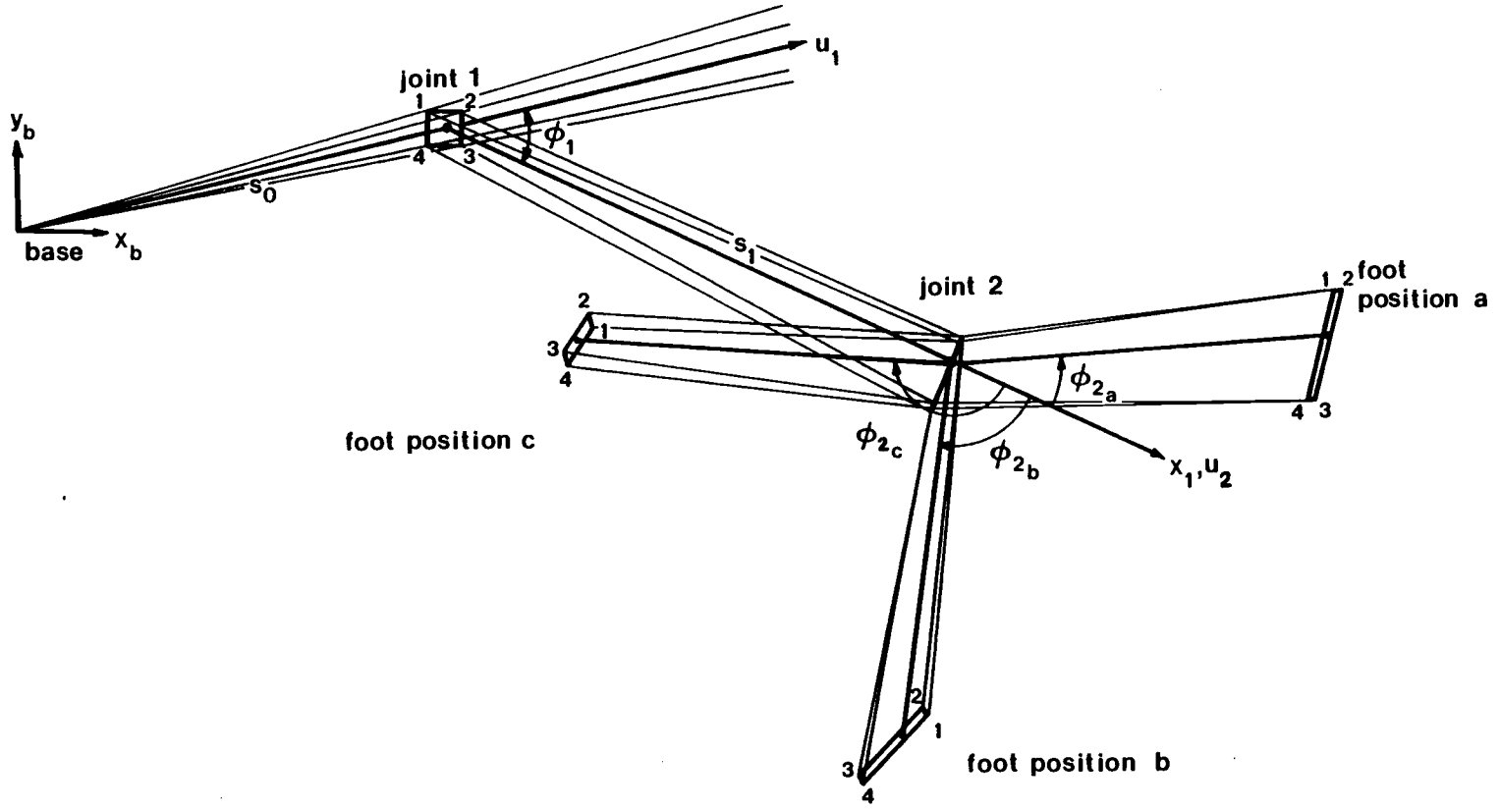

Figure 5.14. Graphic translation of joint position error box to error surrounding foot position.

where **B**, Φ and **S** are defined by equations 2.4, 2.5 and 2.3 respectively. Error in foot position is determined by redefining the shape matrices to reflect dimensional errors of the error box surrounding joint 1. These errors influence the A-model parameters of matrices **B** and $\mathbf{S}_1$. The model parameters containing dimensional errors are computed from matrices ${}^0\mathbf{U}_1'$ and ${}^1\mathbf{U}_2'$ which are expressed by

$$ {}^0\mathbf{U}_1' = {}^0\mathbf{E}_0'^{-1}\ {}^0\mathbf{U}_1\ {}^1\mathbf{E}_1' \tag{5.10} $$

and

$$ {}^1\mathbf{U}_2' = {}^1\mathbf{E}_1'^{-1}\ {}^1\mathbf{U}_2\ {}^2\mathbf{E}_2' \tag{5.11} $$

where ${}^0\mathbf{U}_1 = \mathbf{B}\ \Phi_1$ and ${}^1\mathbf{U}_2 = \mathbf{S}_1\ \Phi_2$. In this example matrices ${}^0\mathbf{E}_0'$ and ${}^2\mathbf{E}_2'$ reflect zero error and are identity matrices. Error matrix ${}^1\mathbf{E}_1'$ reflects translational errors in joint 1 and in expanded form is expressed by

$$ {}^1\mathbf{E}_1' = \begin{bmatrix} 1 & 0 & 0 & \Delta x \\ 0 & 1 & 0 & \Delta y \\ 0 & 0 & 1 & 0 \\ 0 & 0 & 0 & 1 \end{bmatrix} \tag{5.14} $$

The computed model parameters containing error are used to reformulate matrices **B** and $\mathbf{S}_1$ which are then substituted into equation 5.9 to find a new (erroneous) foot position.

Repeating the above procedure four times for each

corner of the error box at joint 1, the error boundary surrounding the actual foot can be drawn. With the dimension of the box very small in comparison to the length of the links, the error boundary approximates a parallelogram. The shape of the parallelogram changes for every foot position. As the foot moves around joint 2 from position a to position b, the error boundary elongates and becomes very thin. After passing the position where $\phi_2 = 0^\circ$, the error boundary reverses direction from a clockwise count of 1-2-3-4 to 1-4-3-2, as shown at position b. The error decreases in size as it approaches joint 1 at position c. This change is expected because small deviations near the base of a linkage are magnified as the free end extends away from the base.

Effects of both error boxes and error cones on foot position are now further examined quantitatively for the measured leg of an arthropod specimen.

5.5 Quantifying Errors in Foot Position

Shape and size of the calculated foot position error volume is dictated by sizes of the error boxes and error cones at each joint axis, overall kinematic geometry of the leg and position of the foot relative to the body reference frame. Investigated in this section are position errors surrounding the foot of the right middle leg of a darkling beetle whose geometry is described by the A-model kinematic

parameters in Table 3.1.

Error in foot position is found in a similar manner as described in the example above. There are three basic steps for defining this error. First, the joint angles are determined for a specified foot position using an inverse kinematic solution of the leg described by the A-model. Second, each corner of an error box and discrete generators of an error cone are used to formulate joint-axis error matrices ${}^{i}E_{i}'$ which are then used to calculate ${}^{i}U_{i+1}'$ matrices. From each ${}^{i}U_{i+1}'$ matrix, a set of A-model parameters are extracted, which essentially reflect specific joint measurement errors of leg segment i. Third, each set of parameters are used in a forward kinematic solution along with the set of original joint angles to find total foot position error. This is accomplished by superposing sets of foot position errors resulting from each leg segment and approximating the final error volume with a rectangular box as depicted in Figure 5.15. Originating from the center of the box (i.e. measured foot position) along x_f, y_f and z_f to the box boundaries are dimensions a, b and c respectively. The orientation of frame xyz_f is dependent on foot position as is shown later.

Details of the first step, the inverse kinematic solution, can be found in Appendix B. Assuming an inverse solution is possible for a given foot position, the remaining two steps are discussed below.

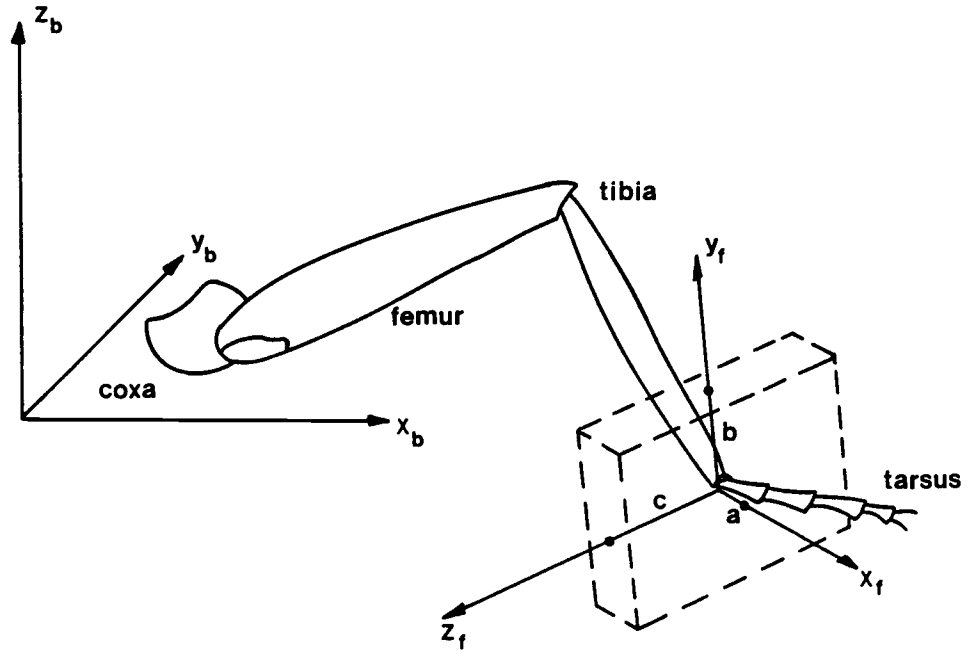

Figure 5.15. Foot position error boundary approximated by rectangular box.

Errors in A-model Parameters

Error volume surrounding a specified foot position reflects the total range of errors in measuring a leg's kinematic geometry. Each point within the error volume is defined by a set of A-model parameters and joint displacements for a given foot position. These parameters are extracted from the U matrices of each segment which have been determined from specific errors in the measurement of each joint axis. A specific error in the position and orientation measurement of joint axis i is represented by frame xyz_i' relative to frame xyz_i in transformation matrix ${}^{i}\mathbf{E}_i'$. To represent a point on the error boundary, rotation and transformation portions of this matrix are formulated from a single error cone axis (i.e. cone generator) and error box corner. Orientation error of a generator on an error cone is determined by a rotation of ϵ_i, as expressed by equation 5.5, about an axis in the xy_i-plane whose direction is given by the unit vector ex + ey where

$$ex = \frac{-\,y_i}{(x_i^{\,2} + y_i^{\,2})^{1/2}} \tag{5.15}$$

and

$$ey = \frac{x_i}{(x_i^{\,2} + y_i^{\,2})^{1/2}} \tag{5.16}$$

and where x_i and y_i are described by (5.3) and (5.4) respectively.

The position of an error box corner relative to frame xyz_i is defined by Δpx, Δpy and Δpz and determined from

$$\begin{bmatrix} \Delta px \\ \Delta py \\ \Delta pz \\ 1 \end{bmatrix} = \begin{bmatrix} \cos(\delta_{Fi}+\theta_i) & \sin(\delta_{Fi}+\theta_i) & 0 & 0 \\ -\sin(\delta_{Fi}+\theta_i) & \cos(\delta_{Fi}+\theta_i) & 0 & 0 \\ 0 & 0 & 1 & 0 \\ 0 & 0 & 0 & 1 \end{bmatrix} \begin{bmatrix} \Delta x/2 \\ \Delta y/2 \\ \Delta z/2 \\ 1 \end{bmatrix} \tag{5.17}$$

From 5.16 and 5.17, matrix ${}^{i}\mathbf{E}_i'$, representing both position and orientation errors, is formulated as

$${}^{i}\mathbf{E}_i' = \begin{bmatrix} ex^2\, v\epsilon_i + c\epsilon_i & ex\ ey\ v\epsilon_i & ey\ s\epsilon_i & \Delta px \\ ex\ ey\ v\epsilon_i & ey^2\, v\epsilon_i + c\epsilon_i & -ex\ s\epsilon_i & \Delta py \\ -ey\ s\epsilon_i & ex\ s\epsilon_i & c\epsilon_i & \Delta pz \\ 0 & 0 & 0 & 1 \end{bmatrix} \tag{5.18}$$

where v, c and s are the versine, cosine and sine respectively. This matrix is formulated in the same manner as that of 4.23.

Using matrix ${}^{i}\mathbf{E}_i'$, A-model parameters and joint displacements, matrix ${}^{i}\mathbf{U}_{i+1}'$ can be determined from equation

5.1. The A-model parameters of segment i extracted from matrix ${}^{i}U_{i+1}$' reflect specific measurement errors of joint axes i and i+1.

Error in foot position

Error in foot position is investigated by first looking at the effects of position and orientation measurement errors of individual joints. In the following example, the error in position measurements of joints 1-3 are all represented by an error box of the same size where Δx=0.02 mm, Δy=0.03 mm and Δz=0.06 mm. Since orientation measurement errors are partially dependent on the length and range-of-motion of each leg segment, the error cones of joint axes 1 - 3 differ. Table 5.1 shows the independent parameters of each error cone and the resulting major and minor orientation errors.

TABLE 5.1.

Measurement parameters contributing to error in joint axis orientation for the darkling beetle right middle leg.

segment (joint axis)	effective alignment length, L (mm)	range-of-motion R (deg)	focal plane thickness z_t (mm)	major error ϵ_a (deg)	minor error ϵ_b (deg)
coxa (1)	1.70	115	0.04	2.91	0.80
femur(2)	8.50	110	0.04	0.63	0.16
tibia(3)	7.50	140	0.04	0.46	0.16

In order to look at the effects that position and orientation measurement errors have on foot position error, an arbitrary foot position relative to the body frame of x = 10, y = 0 and z = -6 was chosen. This position is roughly the location of the beetle's right middle foot with the respect to the body coordinate system when the beetle is standing still.

The orthographic projections in Figure 5.16 depict the error surrounding this foot position considering only position measurement errors (i.e. error box) of the coxa joint. Errors are shown with respect to the body coordinate frame (Figure 2.5). The top view (xy_b) is looking toward the beetle's back with its head in the positive y direction. The front view (xz_b) is looking along the beetle from tail to head. The side view (yz_b) is looking from the foot toward the beetle body along negative x.

When the error box is translated from the coxa to the foot, it becomes skewed and approximately an order of magnitude larger. At this particular position the box is very narrow as seen in the front view. This suggests dimensional errors have little effect on foot position errors in a direction perpendicular to this shape. Graphs in Figure 5.17 show the error surface surrounding the foot due to errors in orientation measurements (i.e. error cone)

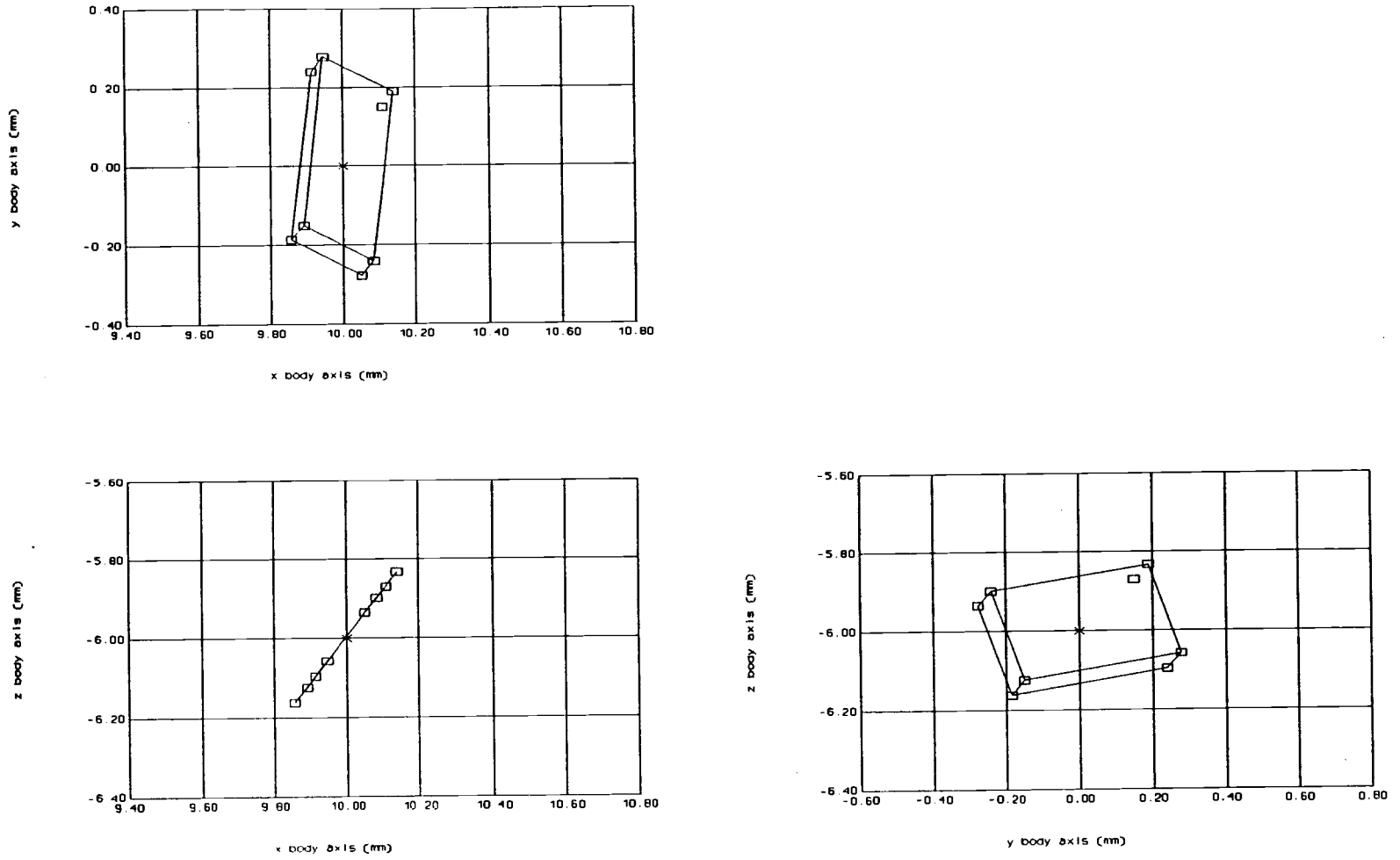

Figure 5.16. Error in foot position due to error box at coxa joint.

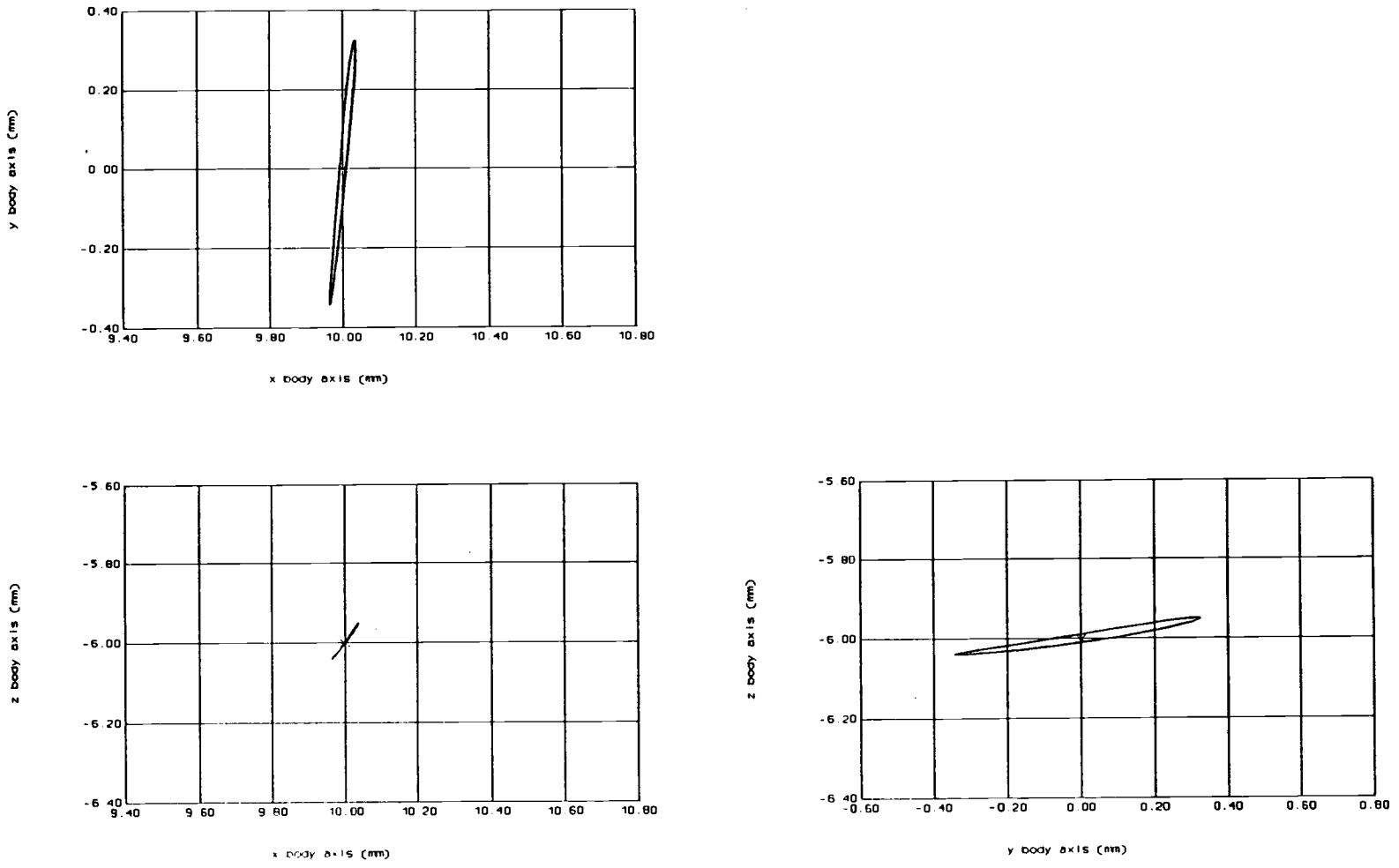

Figure 5.17. Error in foot position due to error cone at coxa joint.

of the coxa.

Effects of positioning and orientation measurement errors of the femur are shown in Figures 5.18 and 5.19 respectively. Since the femur is relatively close to the coxa, error in foot position due to the error box at the femur is similar in size to the error effected by the coxa error box. The error cone at the femur has a much reduced effect on foot position error because its longer effective alignment length allows a more precise joint axis orientation measurement.

The foot position errors reflecting errors in the tibia joint are an order of magnitude less than those of the coxa so their contribution to the error is small as shown in Figures 5.20 and 5.21.

In order to estimate total error surrounding the foot, dimensional errors of the body frame and all joint frames must be combined. This is accomplished by first superposing foot position errors resulting from coxa frame dimensional errors onto those resulting from body frame. Foot position errors resulting from dimensional errors of each succeeding joint are superposed onto those proceeding them till the last joint is reached. Justification for using super-position can be illustrated by combining foot position errors of the coxa and femur. Figure 5.22 shows the combined effect of coxa and femur error boxes only. The 64 empty squares represent 8 corners of the coxa error box

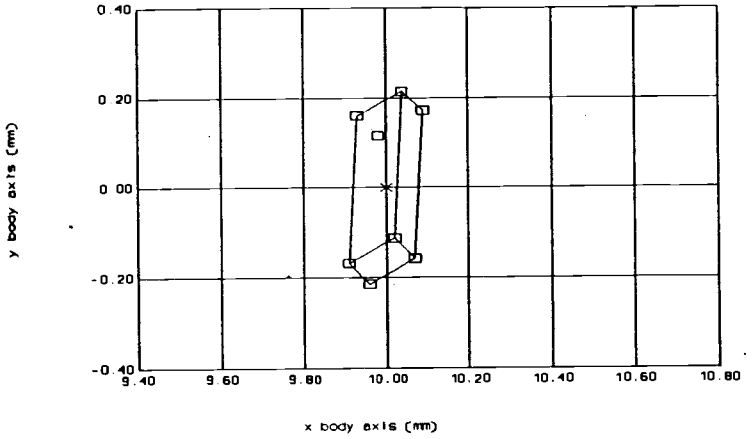

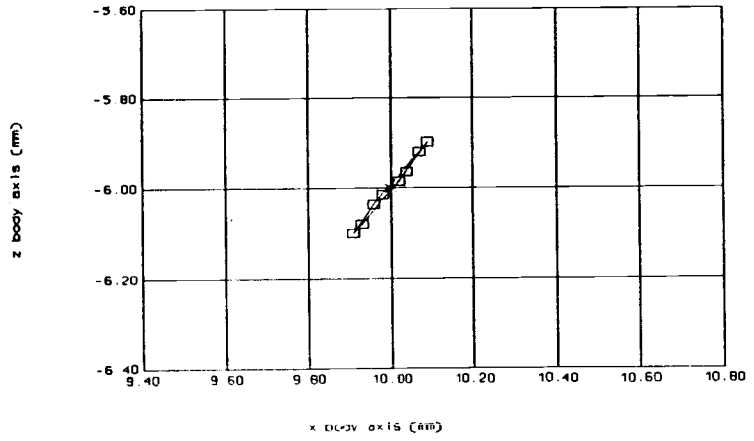

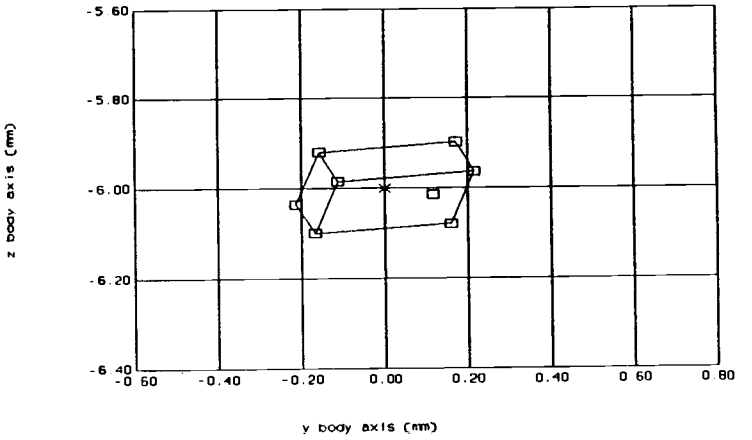

Figure 5.18. Error in foot position due to error box at femur joint.

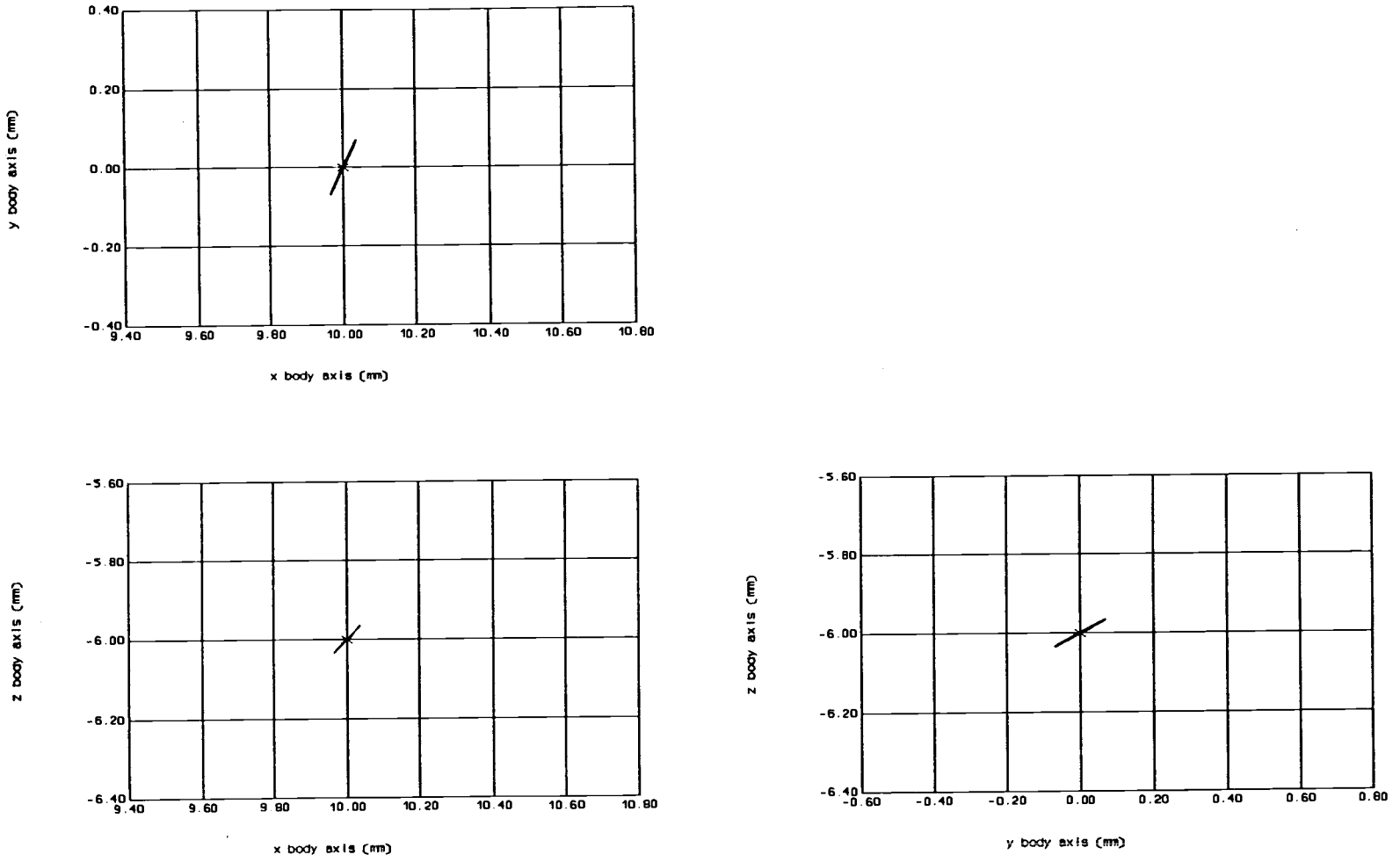

Figure 5.19. Error in foot position due to error cone at femur joint.

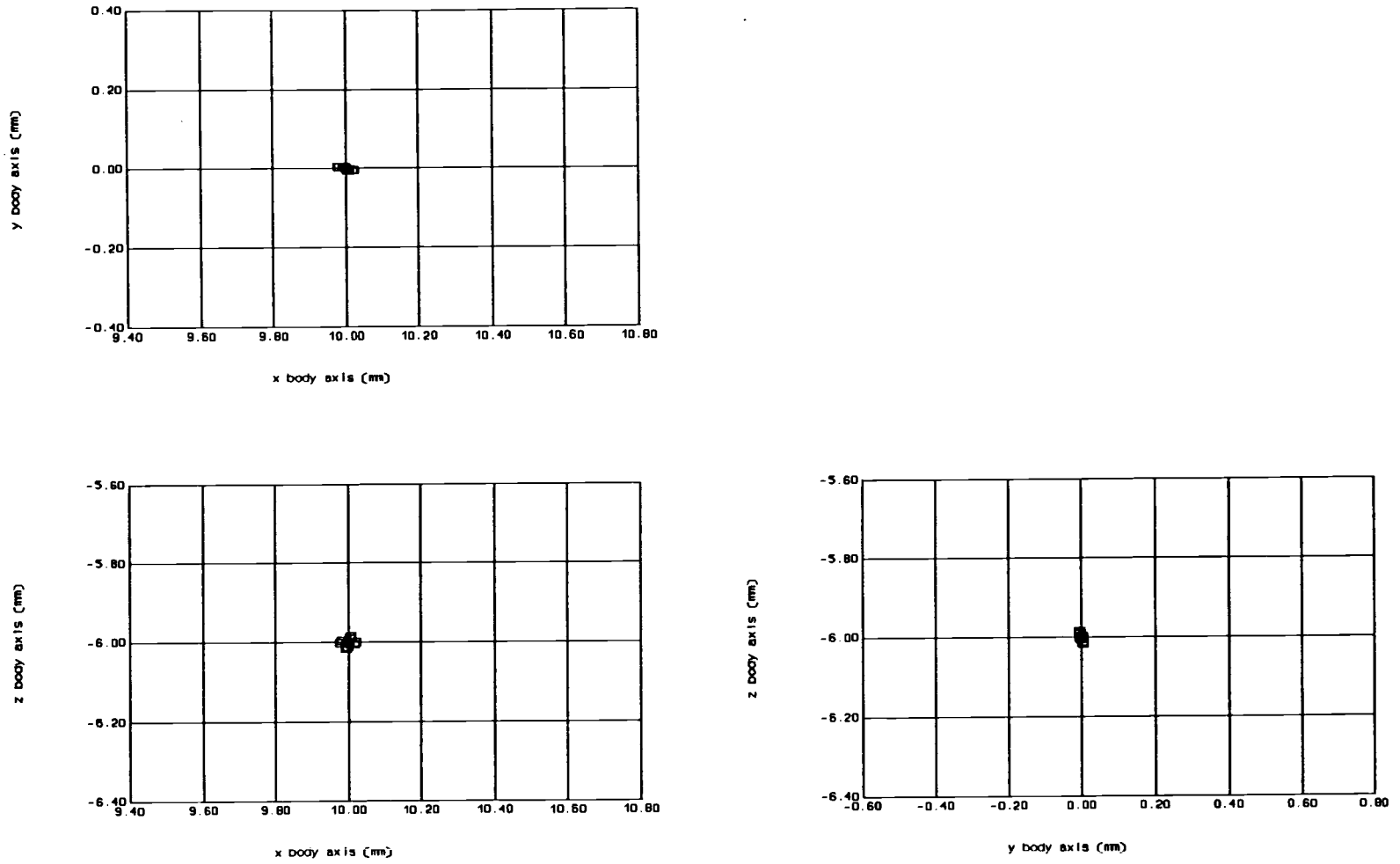

Figure 5.20. Error in foot position due to error box at tibia joint.

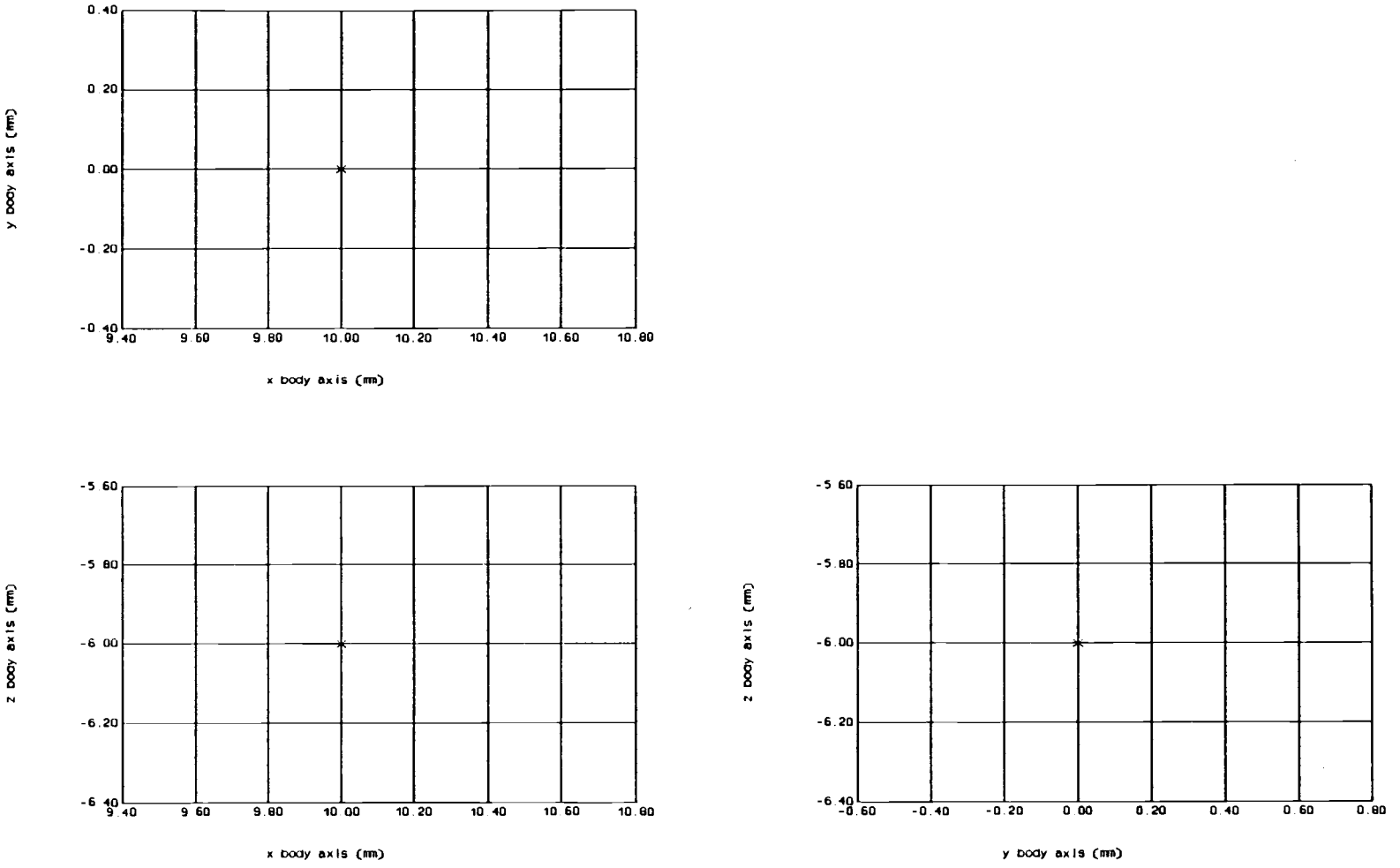

Figure 5.21. Error in foot position due to error cone at tibia joint.

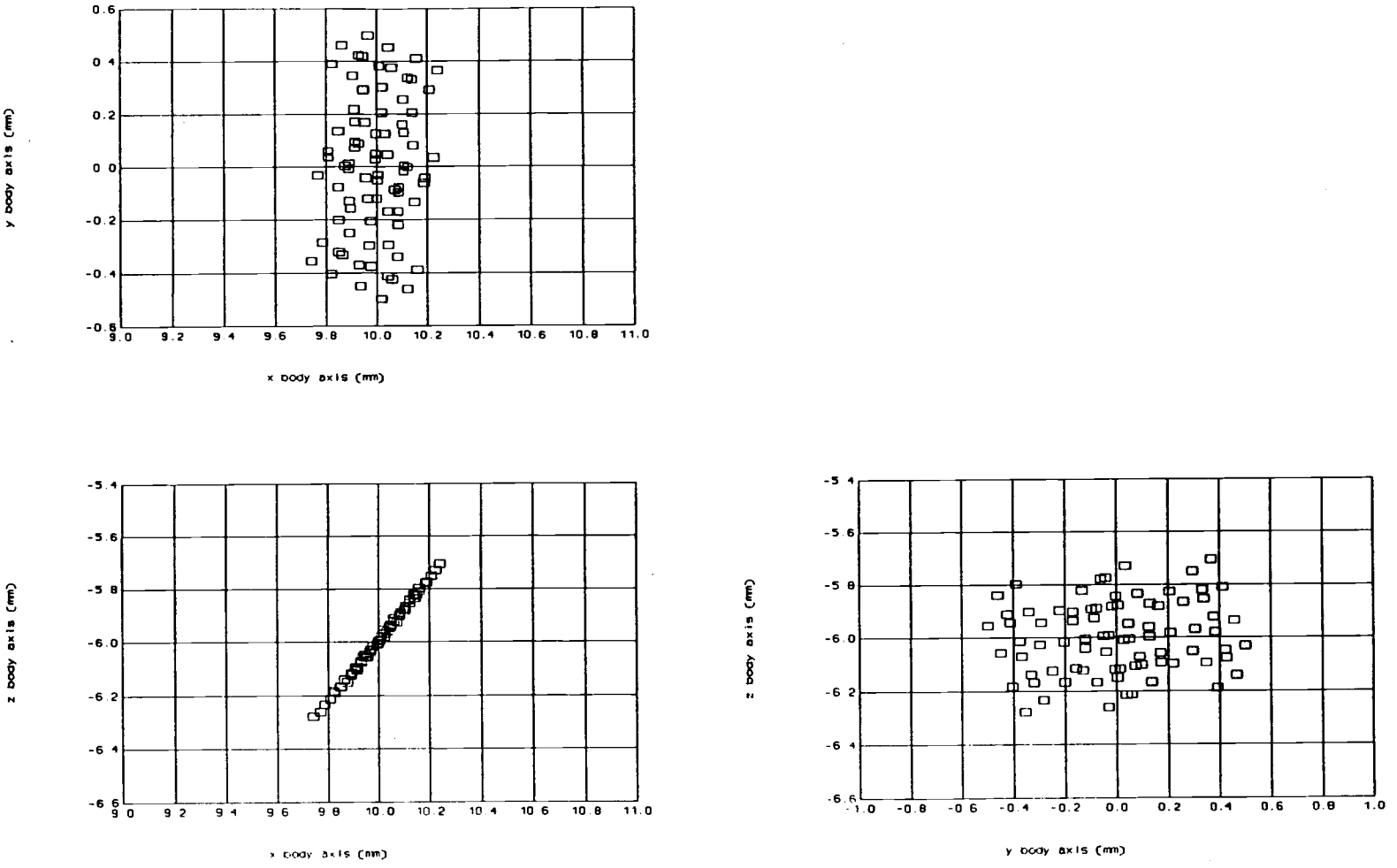

Figure 5.22. 64 error positions generated from the errors boxes of coxa and femur joints.

multiplied by the 8 corners of the femur error box. By selectively eliminating some of the squares, the original error shapes contributed by each error box are revealed (Figure 5.23). The middle box, shown with its corners defined by the filled squares, results from the error box at the coxa and is the shape seen in Figure 5.16. The two other boxes surrounding two opposite corners of the center box result from the error box at the femur and have a shape similar to that seen in Figure 5.18. Since the difference in position of these last two boxes is small, their differences in size are insignificant. This suggests that the total error can be determined by superposing all error effects from each joint.

An analytical procedure of superposition is possible if the error volumes about the foot resulting from errors in each joint are well defined. This is not always the case when combining the position and orientation errors of a single joint frame. Figure 5.24 shows 64 error locations resulting from the combined effects of 8 corners of the femur error box and 8 generators of the femur error cone. The problem lies in determining which of the 64 points define the error boundary and how the boundary can then be mathematically described. This is solved by approximating the error boundary with a box similar to the one illustrated in Figure 5.15. The advantages of such a box shape are that its dimensions and orientation are easily defined.

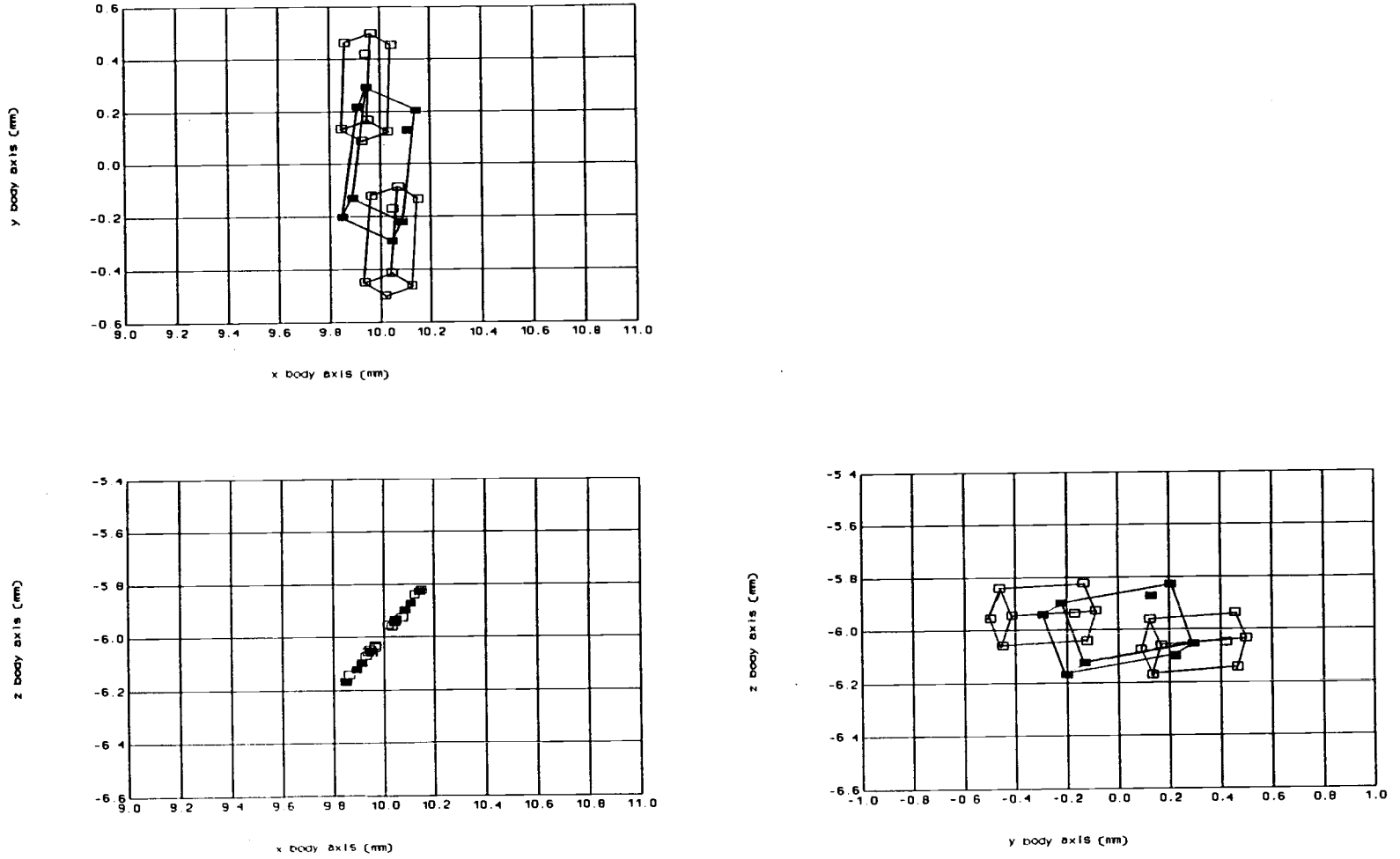

Figure 5.23. Revealed error shapes generated from the coxa and femur error boxes individually.

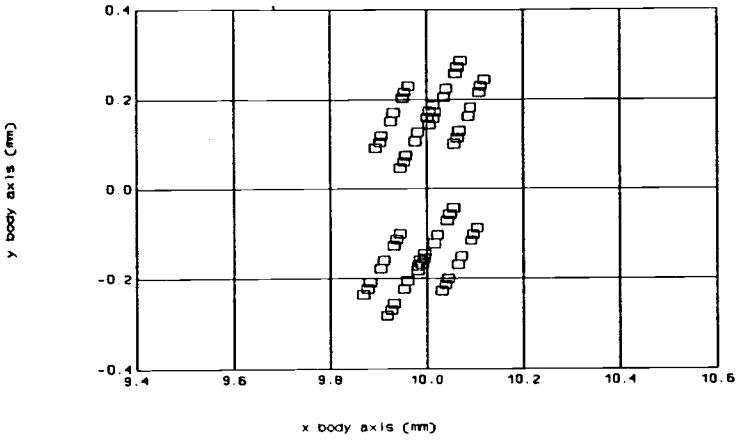

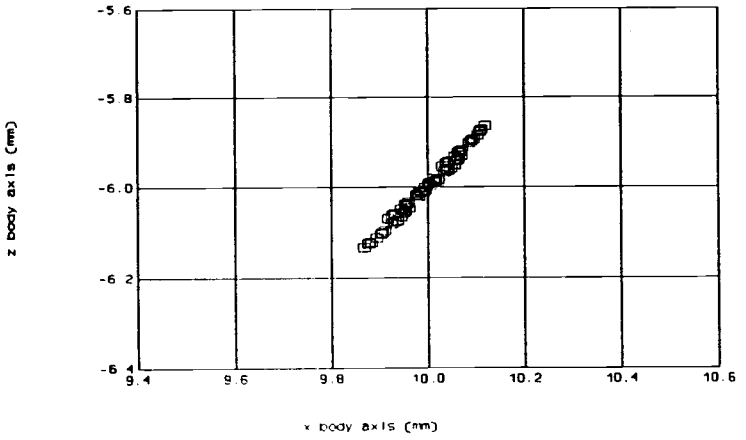

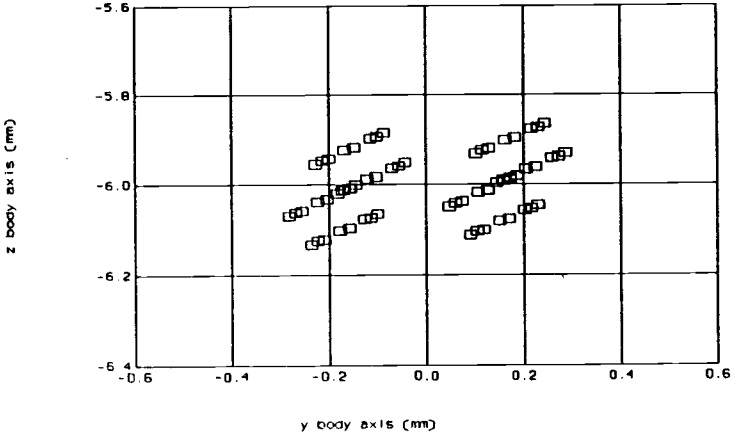

Figure 5.24. 64 error positions generated from the error box and cone of the femur joint.

Using error boundary resulting from the femur joint measurement errors, the approximation procedure involves defining the smallest possible box which will contain all 64 error locations. This is accomplished by considering the 64 points to represent discrete points of unit mass defining an inertial system. Principle axes of this inertial system approximate the directions x_f, y_f and z_f of the error boundary in Figure 5.15. Using these directions, the box dimensions a, b and c can be found.

The procedure for defining the error boundary is as follows. First, the center of mass of the inertial system with respect to the body coordinate frame is located by vector $\mathbf{r}_{cm}$ and is determined by

$$\mathbf{r}_{cm} = \frac{\Sigma\ \mathbf{r}_j}{n} \tag{5.19}$$

Where $\mathbf{r}_j$ is the position of each unit mass j with respect to frame b (Figure 5.25) and n is the total number of unit mass points. The difference between mass center and the actual foot position is negligible. Each unit mass j, relative to a frame translated from frame b to the mass center frame c, is located by vector $\mathbf{p}_j$ where

$$\mathbf{p}_j = \mathbf{r}_j - \mathbf{r}_{cm} \tag{5.20}$$

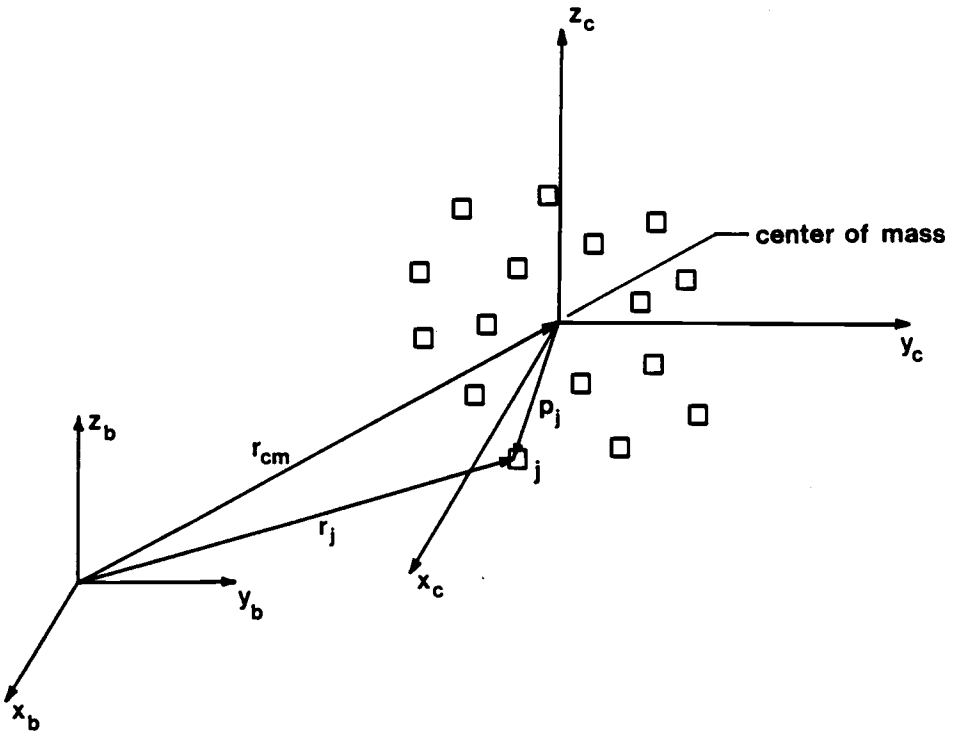

Figure 5.25. Inertial system consisting of unit mass points shown relative to frames b and c.

Vector $\mathbf{p}_j$ is described by a column vector $\mathbf{p}_j = [x_j, y_j, z_j, 0]^T$. The inertial system is described by the inertial matrix **A** with respect to frame c as

$$\mathbf{A} = \begin{bmatrix} I_{xx} & I_{yx} & I_{zx} \\ I_{xy} & I_{yy} & I_{zy} \\ I_{xz} & I_{yz} & I_{zz} \end{bmatrix} \tag{5.21}$$

where

$$I_{xx} = \Sigma\ (y_j^2 + z_j^2)$$

$$I_{yy} = \Sigma\ (z_j^2 + x_j^2)$$

$$I_{zz} = \Sigma\ (x_j^2 + y_j^2)$$

$$I_{xy} = I_{yx} = -\Sigma\ (x_j\ y_j)$$

$$I_{yz} = I_{zy} = -\Sigma\ (y_j\ z_j)$$

$$I_{zx} = I_{xz} = -\Sigma\ (z_j\ x_j)$$

Next, Eigen values and Eigen vectors are determined from matrix **A**. The Eigen vector associated with the largest Eigen value is direction x_f in frame f. This is also the direction of the smallest error boundary dimension, a. Eigen vectors approximating directions y_f and z_f are associated with the middle and smallest Eigen values respectively.

To find the dimensions a, b and c of the error boundary, each unit mass j is defined in terms of frame f. The transformation from frame b to frame f (see Figure 5.15)

is expressed by

$$ {}^{b}\mathbf{T}_f = \begin{bmatrix} x_{fx} & y_{fx} & z_{fx} & F_x \\ x_{fy} & y_{fy} & z_{fy} & F_y \\ x_{fz} & y_{fz} & z_{fz} & F_z \\ 0 & 0 & 0 & 1 \end{bmatrix} \tag{5.22} $$

where the first, second and third columns of the matrix are unit directions of x_f, y_f and z_f respectively. The fourth column is the actual foot position. This transformation is then used to determine $\mathbf{q}_j$, the position of each point j relative to frame f.

$$ \mathbf{q}_j = {}^{b}\mathbf{T}_f^{-1}\ \mathbf{r}_j \tag{5.23} $$

Performing this transformation for all 64 points of the coxa joint errors results in points shown in Figure 5.26. Dimensions a, b and c of the error volume surrounding the actual foot position can be determined from the points $\mathbf{q}_j$ having the largest absolute values in directions x_f, y_f and z_f respectively. Expressing frame f coordinate directions as unit vectors $\mathbf{x}_f$, $\mathbf{y}_f$, and $\mathbf{z}_f$, the error volume dimensions are

$$ a = [\mathrm{abs}(\mathbf{q}_j \cdot \mathbf{x}_f)]_{max} \tag{5.24} $$

$$ b = [\mathrm{abs}(\mathbf{q}_j \cdot \mathbf{y}_f)]_{max} \tag{5.25} $$

$$ c = [\mathrm{abs}(\mathbf{q}_j \cdot \mathbf{z}_f)]_{max} \tag{5.26} $$

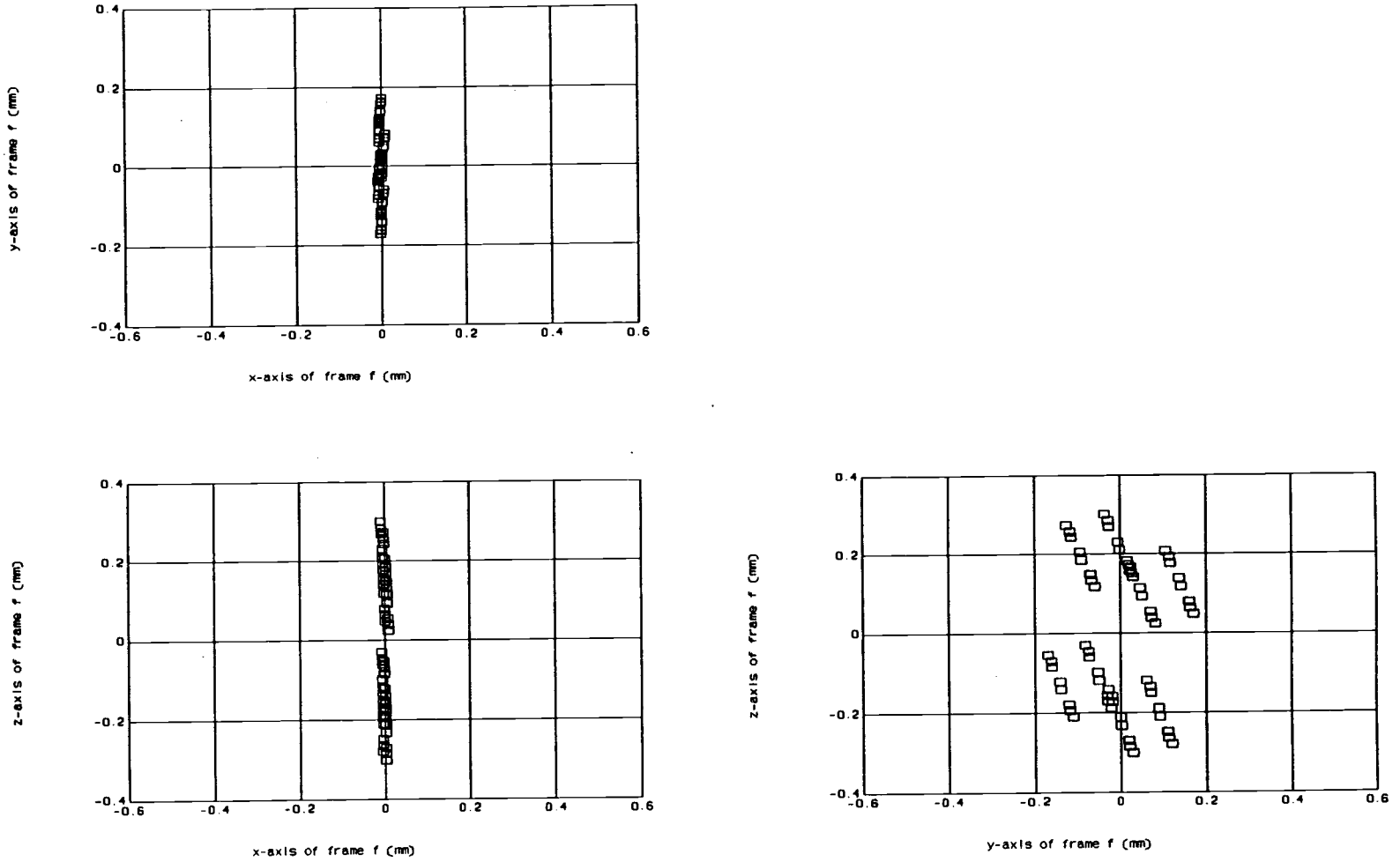

Figure 5.26. Error positions transformed to frame f.

This method results in a good approximation of direction x_f and dimension a. However, directions y_f and z_f can still be improved to find a smaller box containing all 64 points. This is accomplished numerically by rotating all 64 points a small angle about x and then determining a new box size as described above. If the new box is smaller than the old, then another rotation is made in the same direction. When the box size increases in one of these rotations, then a rotation of half the magnitude of the previous is made in the opposite direction. This bisection procedure is continued until the change in rotation becomes very small. Figure 5.27 shows the 64 points after having been subjected to the bisection routine. In this case, the approximated error volume surrounding the actual foot position decreased from 0.00419 cu.mm. to 0.00388 cu. mm., a reduction of 7.4 percent.

Once the smallest box containing all 64 points is found, its 8 corners are transformed back to the body frame as shown in figure 5.28. This method is used to generate an error volume for the dimensional errors of each joint. It is also used to define the error volume resulting from errors in measuring the body frame. Because the body frame has an additional dimensional error (i.e. rotation about z_b) not present in the joints, the method for determining the resulting error volume for it differs.

For the body frame, 64 error points are generated as

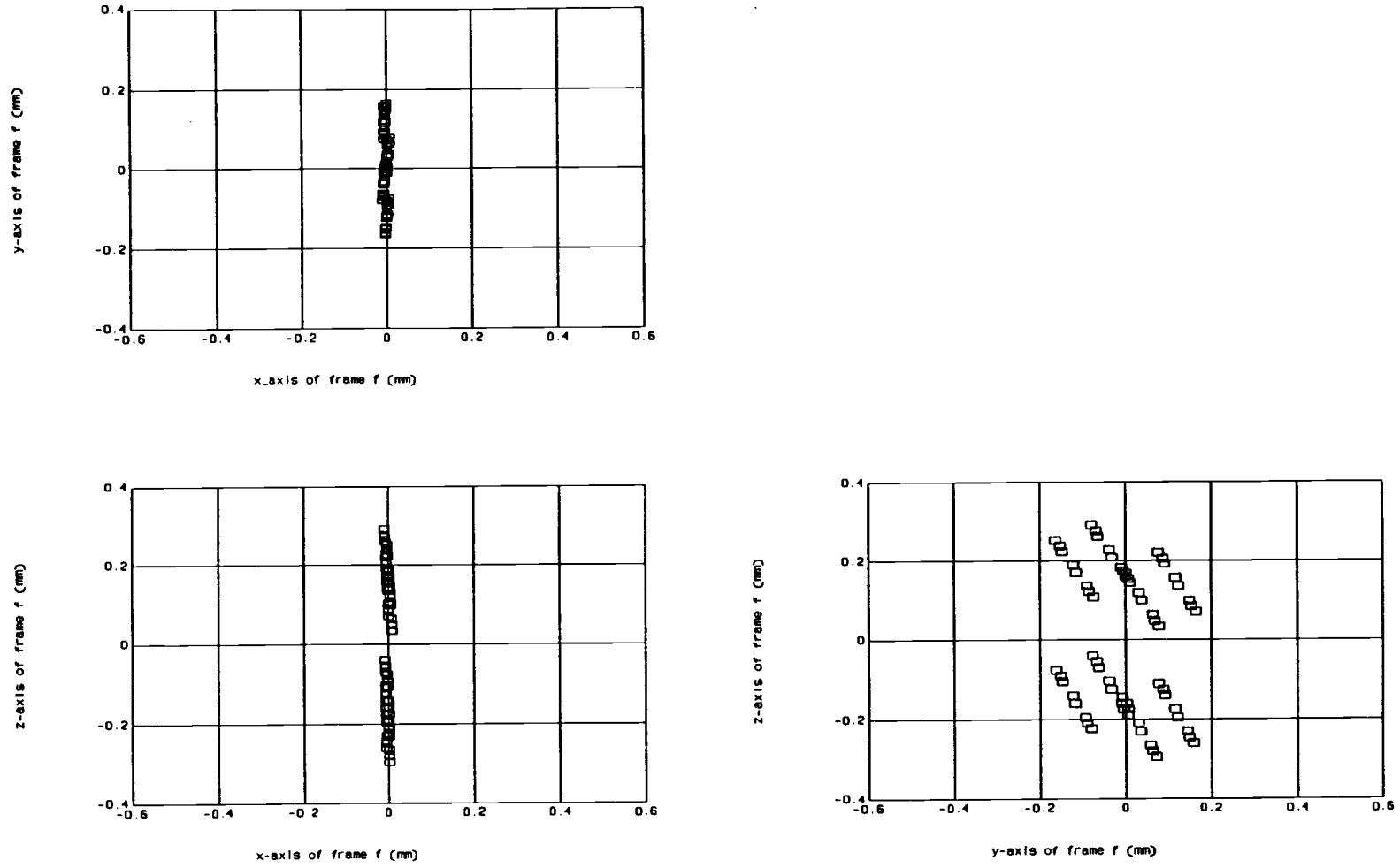

Figure 5.27. Error positions in frame f after reorienting y_f and z_f with bisection numerical routine.

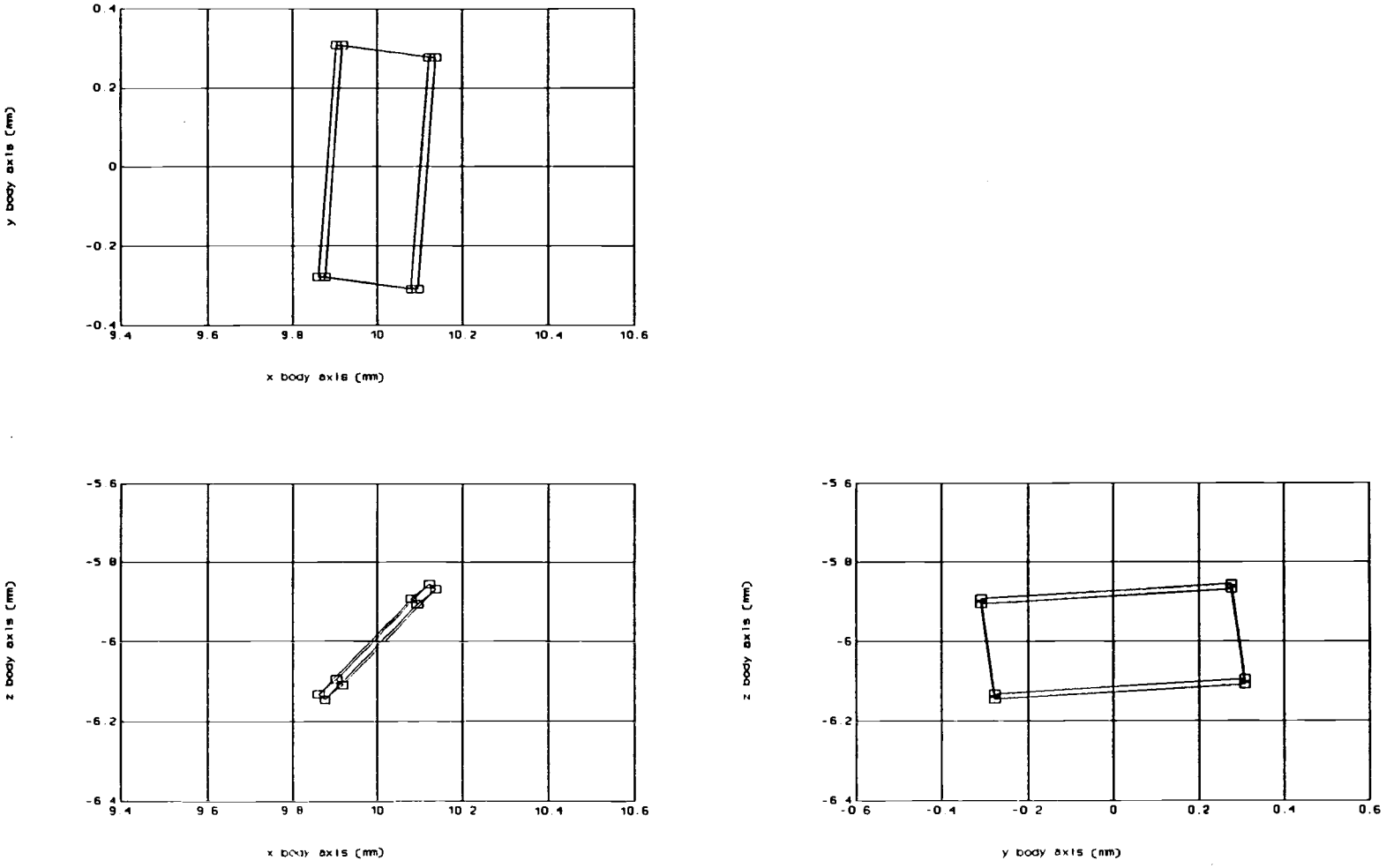

Figure 5.28. Approximate error volume surrounding actual foot position considering only dimensional errors of femur joint frame.

described above but at one of the extreme error orientations of x_b (see ϵ_x in Figure 5.6). When the points are transformed to frame f, their center of mass is quite different from the actual foot position (Figure 5.29). At the other extreme of x_b, a mirror image of points in Figure 5.29 are generated through xz-plane. The largest absolute values in directions x_f, y_f and z_f in both extreme cases produce the same size error volume about the actual foot position (Figure 5.30). Error volumes resulting from the coxa, femur and tibia joints are shown in Figures 5.31 - 5.33.

Having defined all error volumes for each frame (i.e. body to tibia) about the actual foot position, one volume is superposed onto the other. First, the error volume generated from dimensional errors in coxa frame are superposed onto those from the body frame. The eight corners from both volumes generate 64 points from which a new error volume box is defined using the above procedure. Superposed onto this volume is the error volume generated from femur frame dimensional errors. Superposition is continued until the last joint of the leg is reached. Error volume approximation resulting from all dimensional errors is seen in Figure 5.34.

When actual foot position changes, so does size and orientation of the error volume surrounding it. Figures 5.35 - 5.40 show various foot positions, each moved from

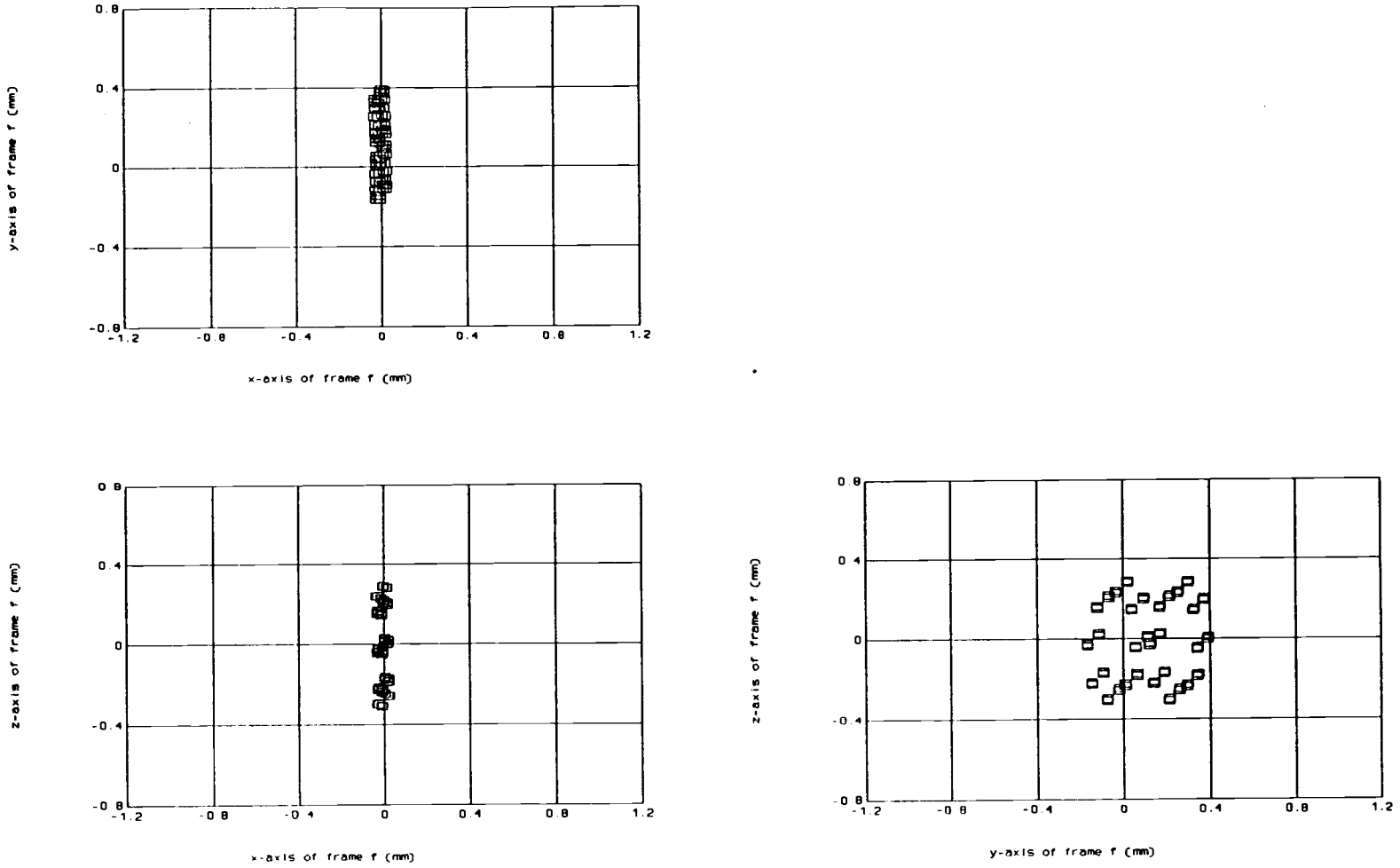

Figure 5.29. 64 error positions generated from the error box and cone of the body frame.

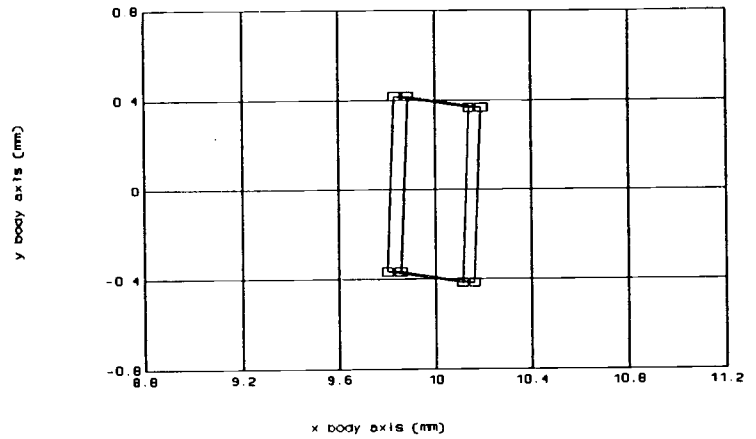

$$ {}^{b}T_{f} = \begin{bmatrix} .862 & -.505 & -.040 & 10.00 \\ -.001 & .079 & -.997 & 0.00 \\ -.506 & -.860 & -.068 & -6.00 \\ 0 & 0 & 0 & 1 \end{bmatrix} $$

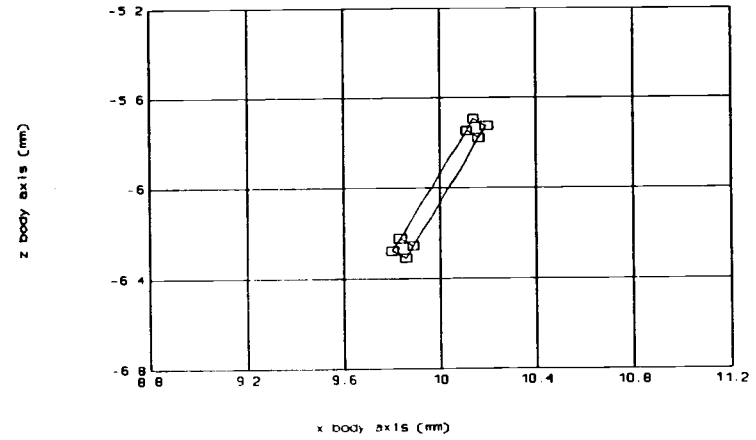

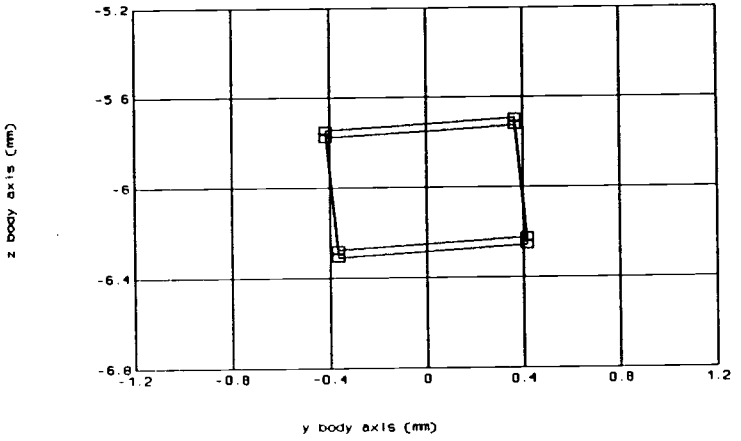

Figure 5.30. Approximate error volume surrounding actual foot position considering only dimensional errors of body frame. a=.032 mm, b=.308 mm, c=.392 mm.

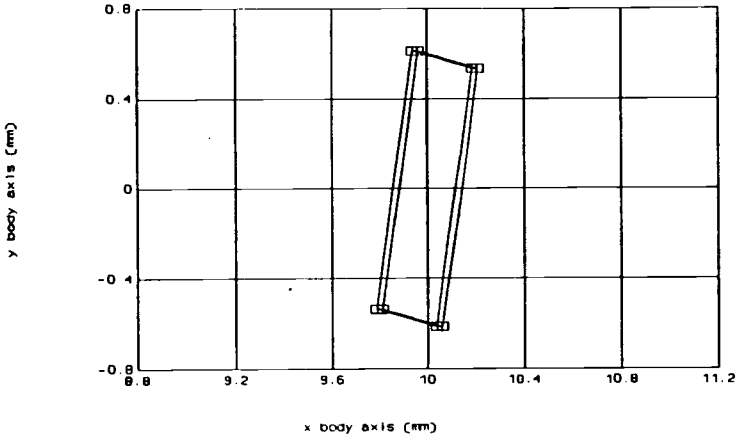

$$ {}^{b}\mathbf{T}_{f} = \begin{bmatrix} .757 & .640 & -.129 & 10.00 \\ .001 & -.198 & -.980 & 0.00 \\ -.653 & .742 & -.151 & -6.00 \\ 0 & 0 & 0 & 1 \end{bmatrix} $$

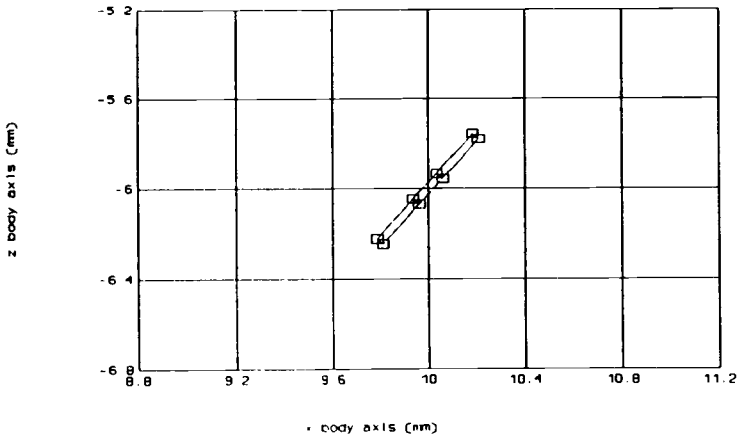

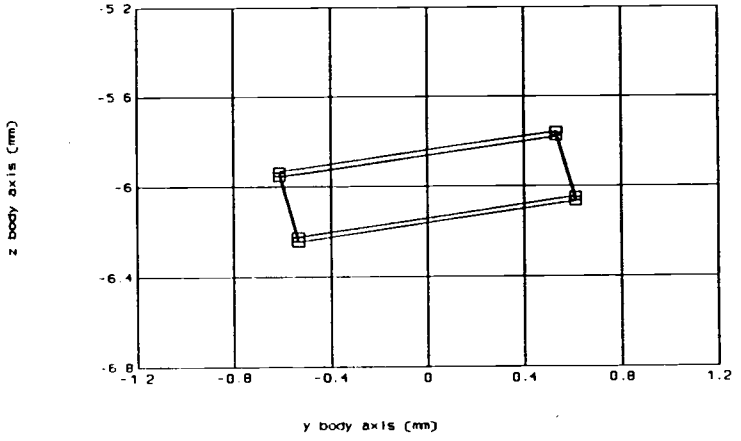

Figure 5.31. Approximate error volume surrounding actual foot position considering only dimensional errors of coxa joint frame. a=.017 mm, b=.195 mm, c=.585 mm.

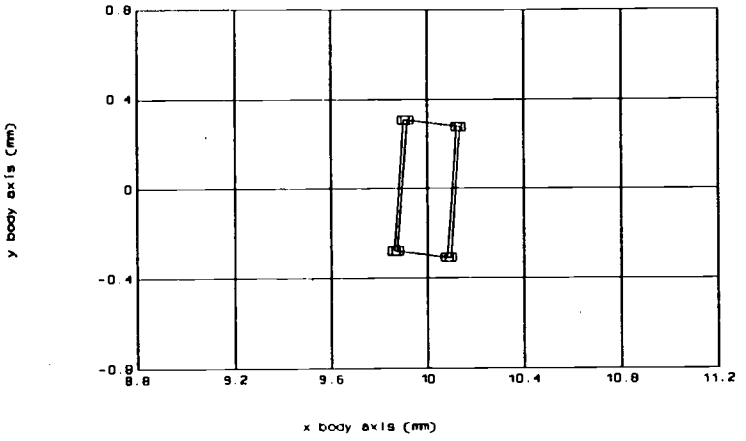

$$ {}^{b}T_{f} = \begin{bmatrix} .753 & .674 & -.071 & 10.00 \\ -.009 & -.095 & -.995 & 0.00 \\ -.678 & .732 & -.063 & -6.00 \\ 0 & 0 & 0 & 1 \end{bmatrix} $$

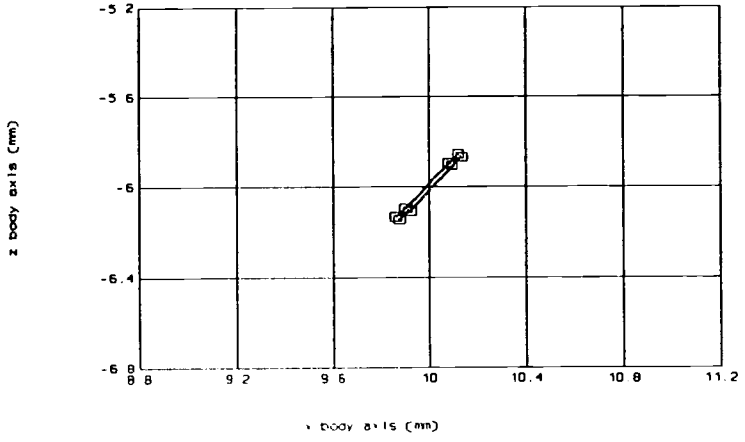

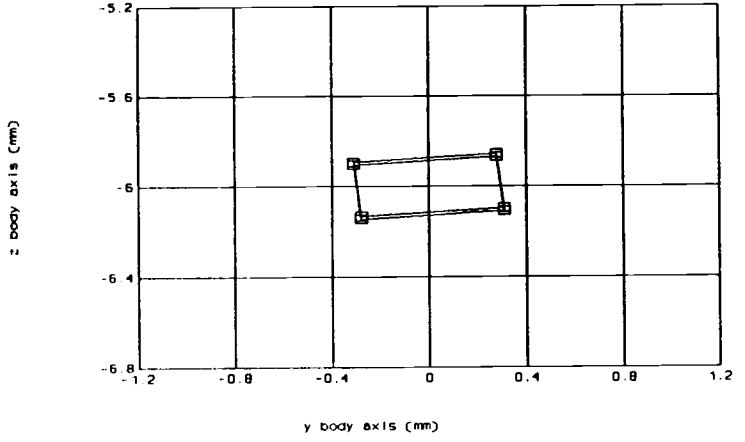

Figure 5.32. Approximate error volume surrounding actual foot position considering only dimensional errors of femur joint frame. a=.010 mm, b=.163 mm, c=.294 mm.

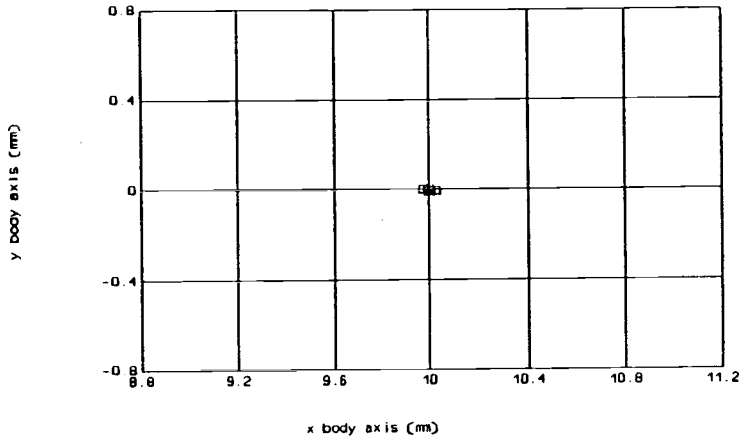

$$ {}^{b}\mathbf{T}_{f} = \begin{bmatrix} .191 & .811 & .553 & 10.00 \\ .957 & -.279 & .080 & 0.00 \\ .219 & .514 & -.829 & -6.00 \\ 0 & 0 & 0 & 1 \end{bmatrix} $$

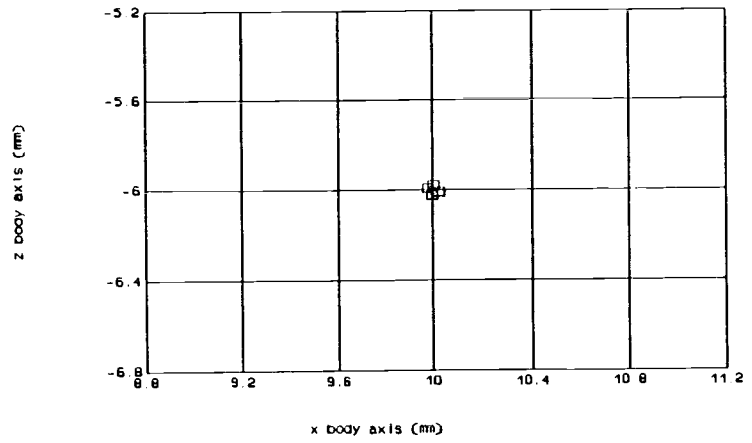

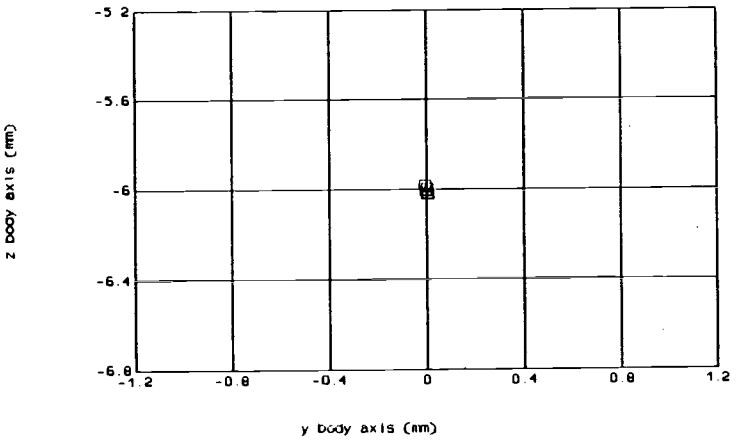

Figure 5.33. Approximate error volume surrounding actual foot position considering only dimensional errors of tibia joint frame. a=.000 mm, b=.015 mm, c=.018 mm.

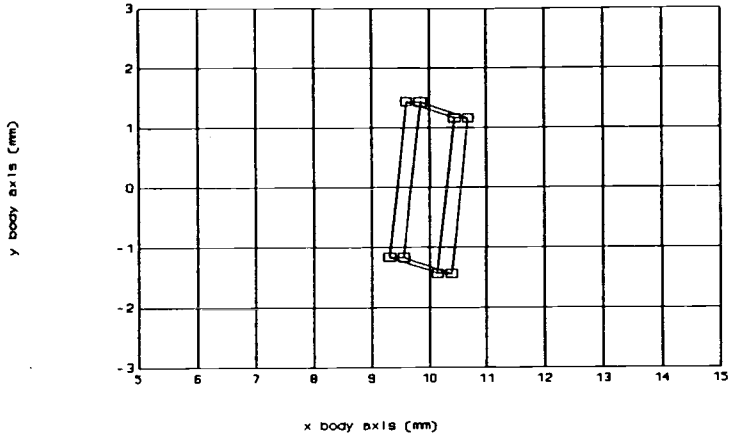

$$ {}^{b}T_{f} = \begin{bmatrix} .826 & .552 & -.113 & 10.00 \\ -.013 & -.181 & -.983 & 0.00 \\ -.563 & -.814 & -.143 & -6.00 \\ 0 & 0 & 0 & 1 \end{bmatrix} $$

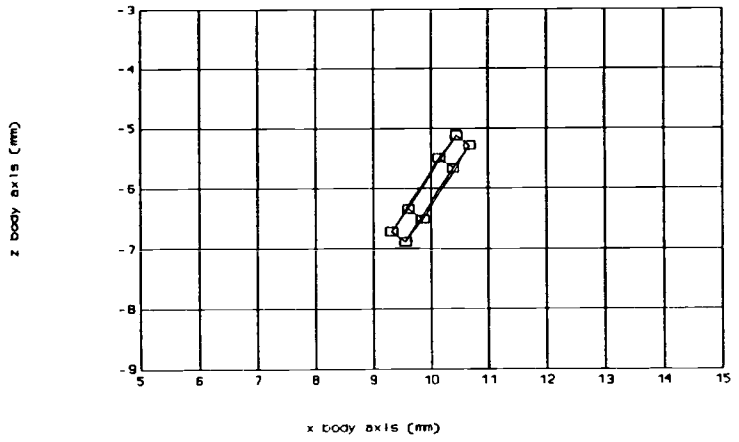

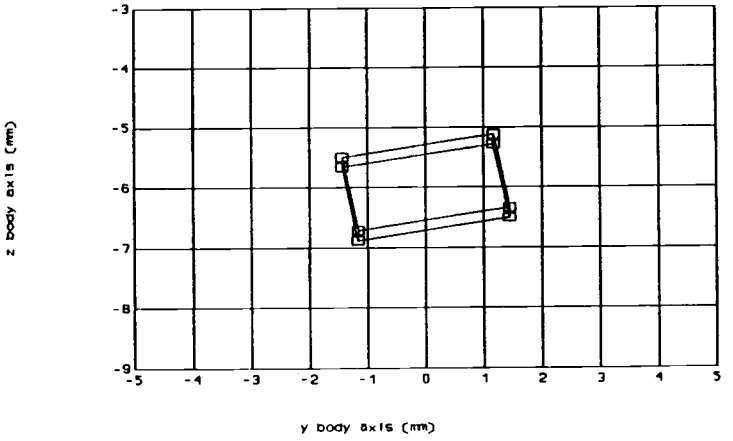

Figure 5.34. Approximate error volume surrounding actual foot position 10,0,-6 after superposing all errors. a=.170 mm, b=.770 mm, c=1.326 mm.

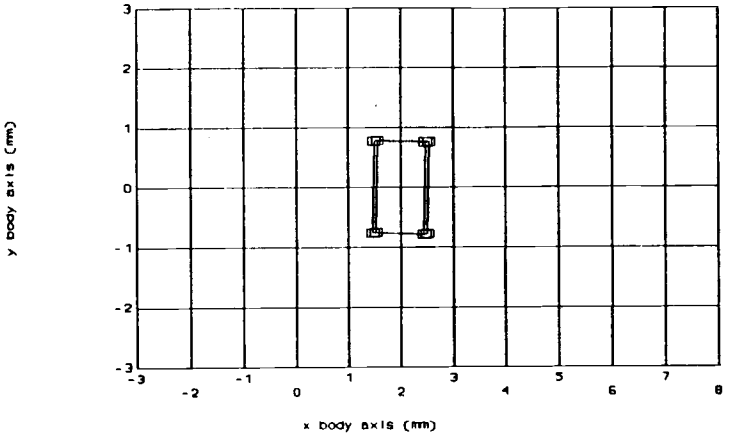

$$ {}^{b}\mathbf{T}_{f} = \begin{bmatrix} .165 & -.986 & -.018 & 2.00 \\ .024 & -.022 & -.999 & 0.00 \\ -.986 & -.165 & -.027 & -6.00 \\ 0 & 0 & 0 & 1 \end{bmatrix} $$

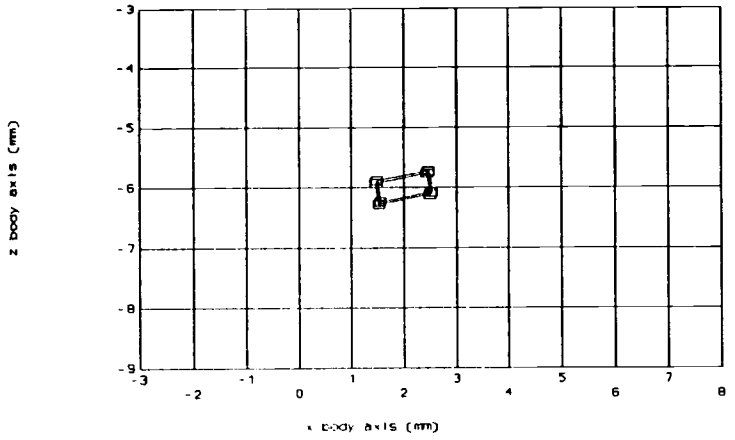

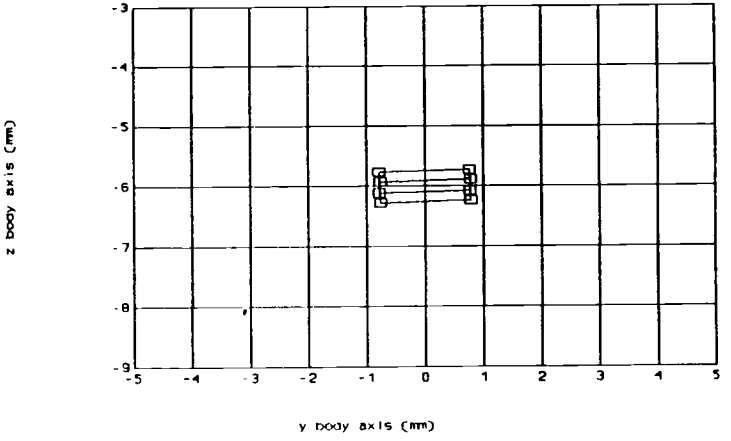

Figure 5.35. Approximate net error volume surrounding actual foot position 2,0,-6. a=.206 mm, b=.521 mm, c=.800 mm.

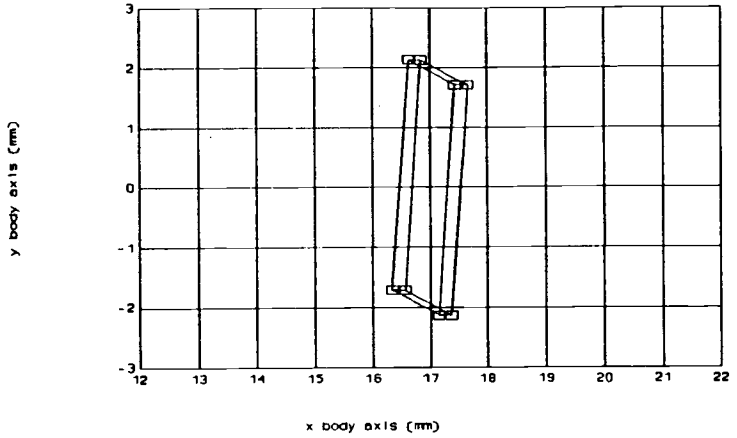

$$ {}^{b}\mathbf{T}_{f} = \begin{bmatrix} .934 & .350 & -.074 & 17.00 \\ -.009 & -.183 & -.983 & 0.00 \\ -.358 & .918 & -.168 & -6.00 \\ 0 & 0 & 0 & 1 \end{bmatrix} $$

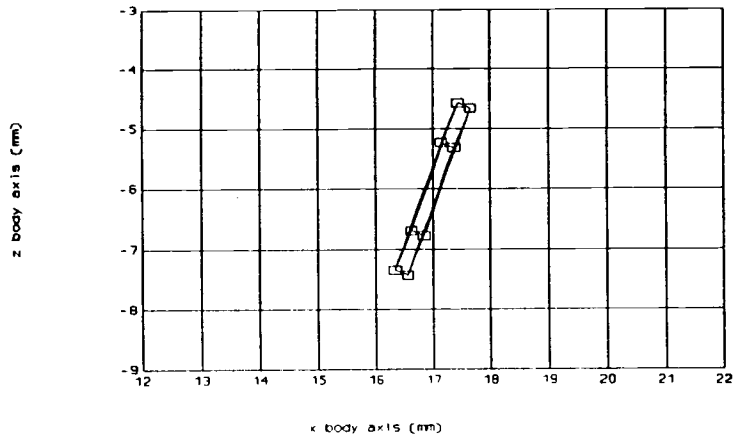

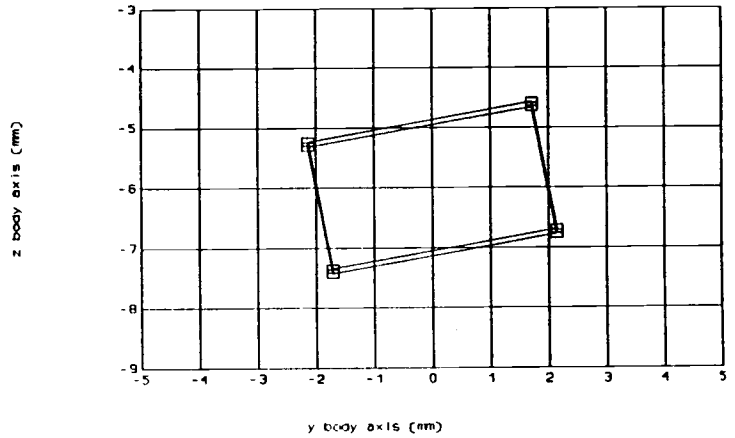

Figure 5.36. Approximate net error volume surrounding actual foot position 17,0,-6. a=.148 mm, b=1.166 mm, c=2.003 mm.

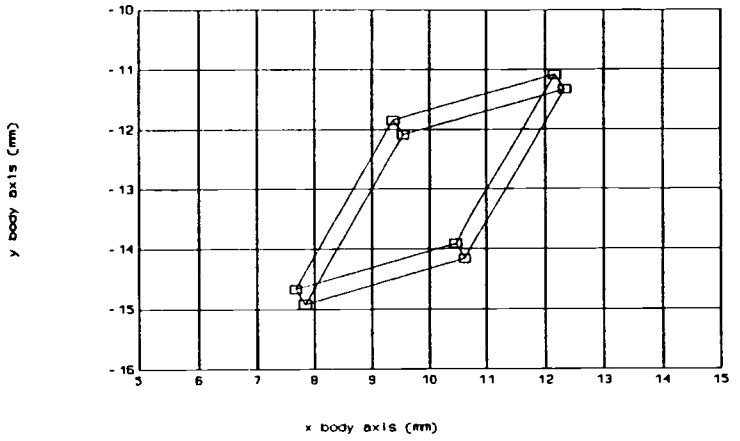

$$ {}^{b}T_{f} = \begin{bmatrix} .517 & .771 & -.372 & 10.00 \\ -.757 & .210 & -.618 & -13.00 \\ -.398 & .602 & .692 & -6.00 \\ 0 & 0 & 0 & 1 \end{bmatrix} $$

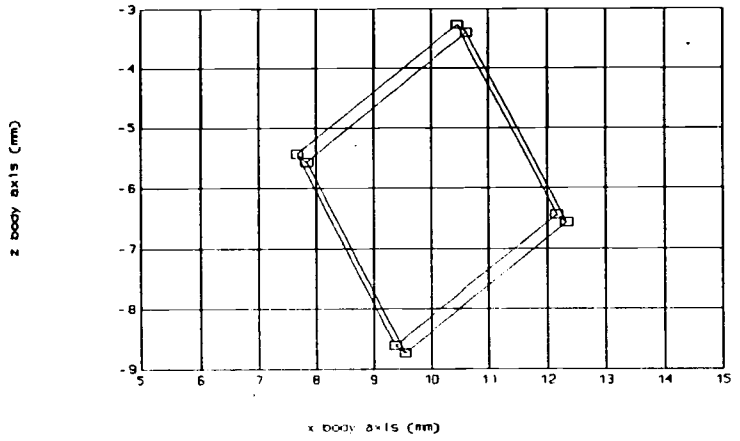

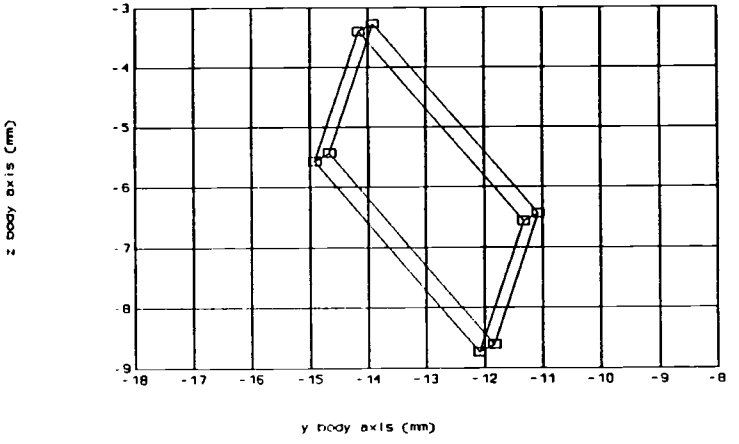

Figure 5.37. Approximate net error volume surrounding actual foot position 10,-13,-6. a=.197 mm, b=1.842 mm, c=2.335 mm.

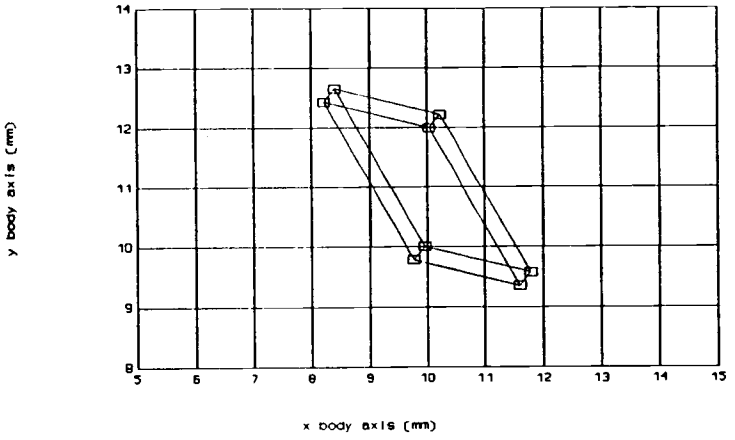

$$ {}^{b}\mathbf{T}_{f} = \begin{bmatrix} .577 & .706 & .409 & 10.00 \\ .698 & -.167 & -.696 & 11.00 \\ -.423 & .688 & -.590 & -6.00 \\ 0 & 0 & 0 & 1 \end{bmatrix} $$

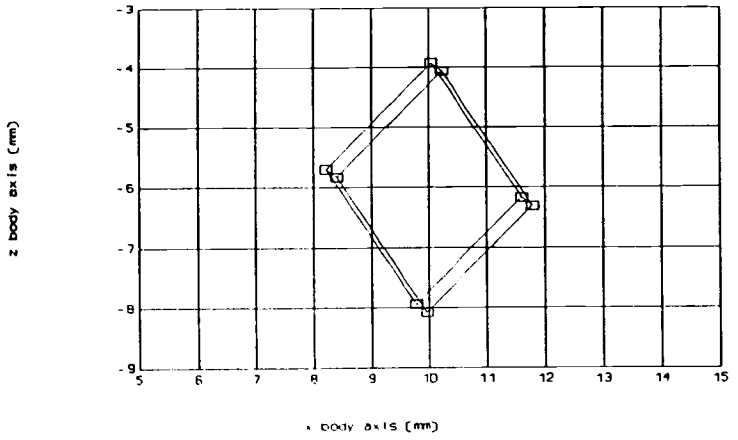

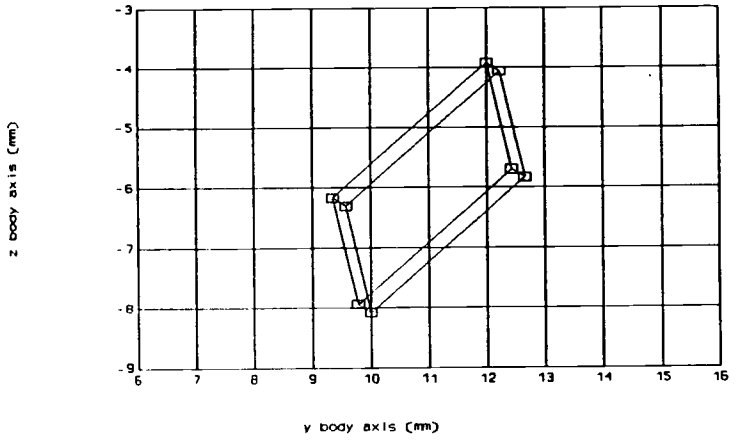

Figure 5.38. Approximate net error volume surrounding actual foot position 10,11,-6. a=.192 mm, b=1.313 mm, c=1.932 mm.

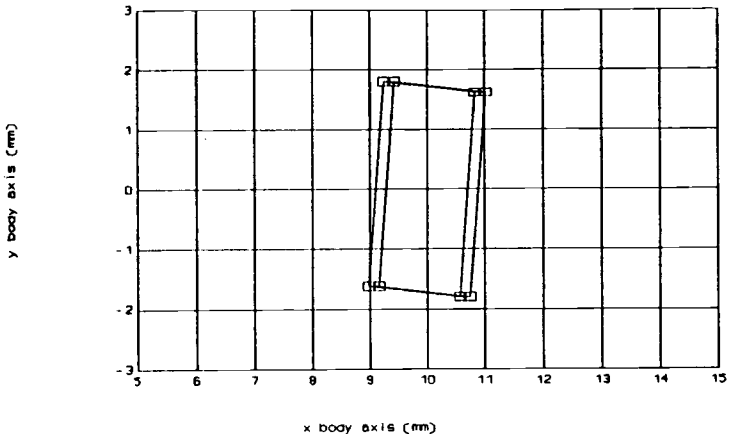

$$ {}^{b}T_{f} = \begin{bmatrix} .557 & .827 & -.077 & 10.00 \\ .001 & -.093 & -.996 & 0.00 \\ -.831 & .554 & -.053 & -13.00 \\ 0 & 0 & 0 & 1 \end{bmatrix} $$

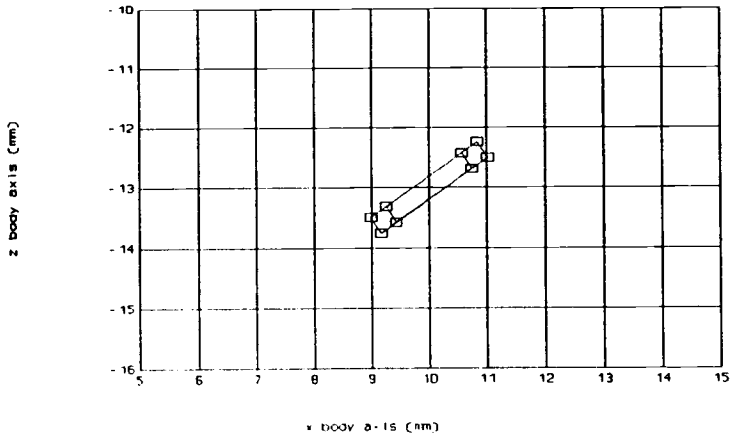

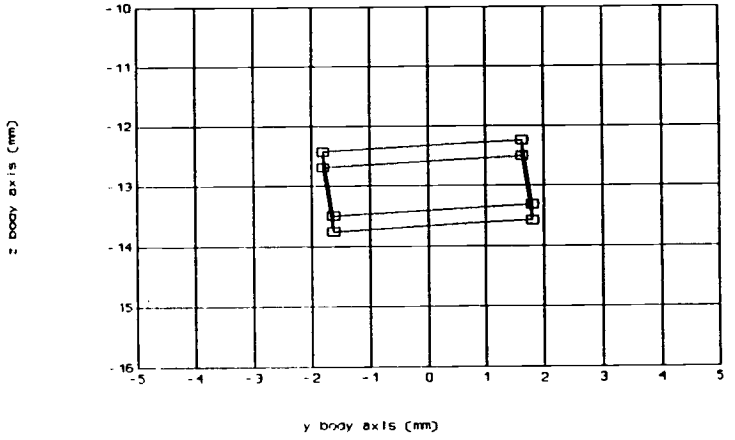

Figure 5.39. Approximate net error volume surrounding actual foot position 10,0,-13. a=.190 mm, b=.983 mm, c=1.761 mm.

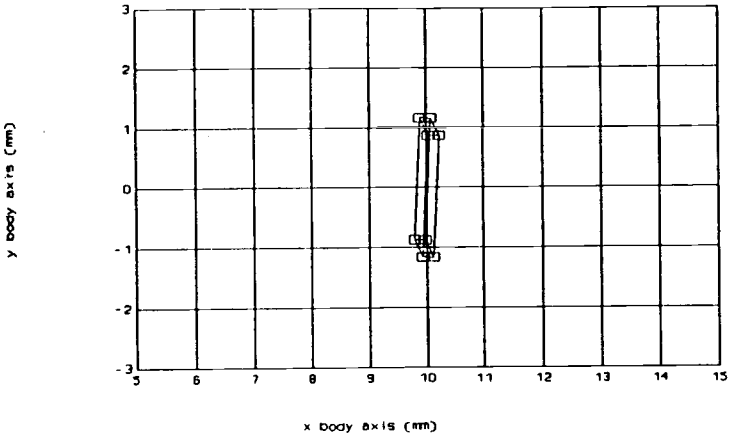

$$ {}^{b}\mathbf{T}_{f} = \begin{bmatrix} .992 & .114 & -.050 & 10.00 \\ -.024 & -.224 & -.974 & 0.00 \\ -.122 & .968 & -.219 & -1.00 \\ 0 & 0 & 0 & 1 \end{bmatrix} $$

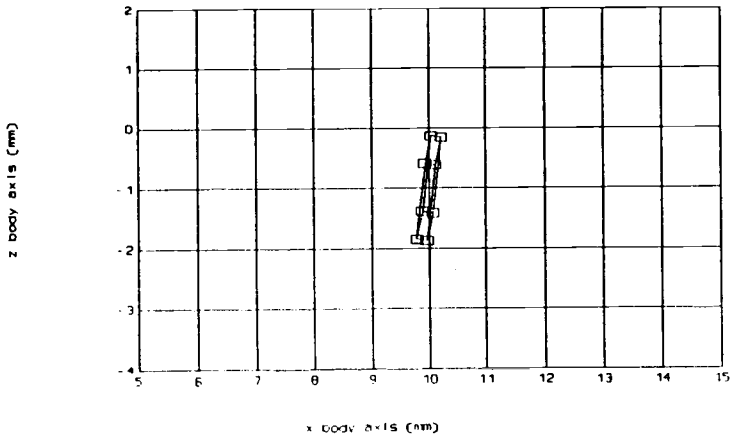

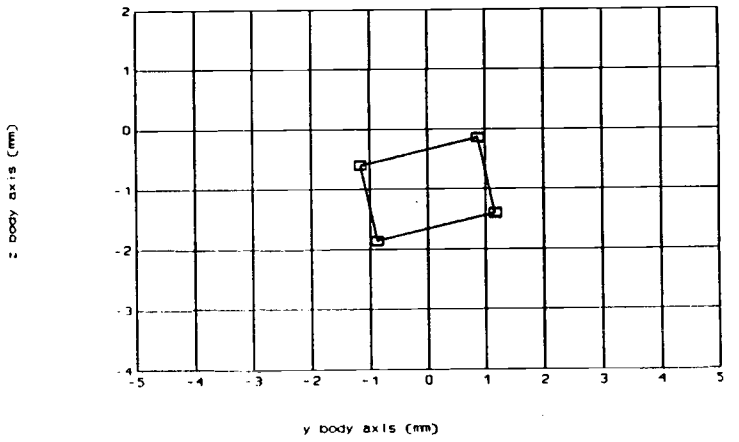

Figure 5.40. Approximate net error volume surrounding actual foot position 10,0,-1. a=.111 mm, b=.667 mm, c=1.058 mm.

x=10, y=0, z=-6 to an extreme x, y or z direction. As the foot moves away from the coxa joint, the error dimensions in general increase. Also seen in each figure is a change in the box orientation. These figures exemplify how the error in predicted foot position can be characterized by its size and orientation. An error characterization method such as this may also be used to approximate the error in predicting the position of mechanical mechanisms.

At the beginning of the chapter the assumption was made that errors in measuring the actual alignment of turntable axes 1 and 2 in chapter 4 have a negligible effect on parameter errors. This is generally true where joint axis orientation errors are concerned but is somewhat misleading in terms of joint position errors. The assumption was used, however, to simplify the explanation of the foot position error approximation method. Now the implications of this assumption and its probable effects on foot position error are revealed.

The actual directions of the turntable axes were determined within a maximum error of $\pm 0.04^{\circ}$ (± 0.0005 of their direction cosines). This error results in possible orientation and position errors when transforming a measured joint axis from frame p to frame s, dependent on the joint axis orientation measurement β and σ. Assuming the worst error case for turntable axes 1 and 2, the maximum error can be written

$$\text{max. error} = \arctan\left[\, 2*(0.0005)^2 \,\right]^{1/2} \qquad (5.27)$$

or max. error = 0.041°. This is four times less than the minimum orientation error of the tibia which contributed essentially no error in foot position. For this reason, errors in the measurement of turntable axes 1 and 2 can be ignored.

Transforming the joint axis from frame p to frame s causes a dimensional error in joint frame position due to the error in measurement of dx (the common perpendicular between turntable axes 1 and 2). Since the uncertainty in dx is ±0.02 mm, the size of the error changes box as much as 0.02 mm in a direction dependent on β and σ (see column 4 of 4.26). To account for this error the error box at each joint frame might be expanded in all directions by 0.02 mm. Since position error is critical in the measurement of the coxa and femur, as seen above, this can have a significant effect on the resulting foot position error.

6. DISCUSSION

Presented in this thesis is a method to identify the kinematic geometry of arthropod legs. The method focuses on leg modeling, leg measurement for model-parameter determination and model parameter accuracy.

Because the leg model is to be used in motion simulation studies and as a comparative tool for a wide variety of arthropods, it must have characteristics which show proportionality to differences in leg geometry, physically resemble the leg being modeled, and be adaptable to the various joint types found in arthropods. In successfully addressing these concerns, the A-model developed in chapter 2 is an improvement over other available models. As with all other models known to this author, a condition does exist where proportionality breaks down. When joint axis i+1 of leg segment i passes through the joint i position then parameter μ_i is undefined and its value is considered zero. As this condition is approached, parameter Ω_i approaches 90° and serves as a signal to the proportionality problem where parameter μ_i is considered unimportant in describing a leg's physical characteristics.

As a result of meeting the conditions of an appropriate leg model, the A-model is more difficult to handle mathematically than models containing fewer rotation parameters such as the Denavit-Hartenberg model. This was evident in

determining an analytic solution to the inverse kinematics of a 3-link manipulator. The solution appears more clean when using a mathematically simple model such as the one developed by Denavit and Hartenberg (D-H model) but it does not show physical resemblance to a manipulator of general geometry. If mathematics do require the simplicity of the D-H model then it can be extracted from the measurements used to determine the A-model, as shown by Fichter, Albright and Fichter (1988).

The measuring equipment and technique developed allows the calculation of several types of models by determining the position and orientation of each joint axis individually with respect to a common reference frame. Since this equipment is designed to measured small legs it may also prove useful for small mechanical mechanisms.

No matter what mechanism is being measured, be it biological or mechanical, all joint axis positions are measured with the same accuracy. The measurement accuracy of joint axis orientations, however, varies with effective alignment length and joint range-of-motion. For very small coxa segment, the maximum calculated orientation error was 2.9° while the longer femur axis error was only 0.64°. The coxa error had a large influence on error when translated to the foot while that of the femur was small in comparison.

In chapter 5, a method was developed for evaluating the accuracy of parameters computed from measurement.

Measurement errors were represented as dimensional errors in position and orientation of each joint axis. The boundary of these errors, the error box and error cone, were translated to the foot resulting in a volume surrounding the foot position. The size of the error is an indication of the accuracy of the computed model parameters. For small mechanical manipulators measured with this method, the foot position errors can be used to characterize the positioning accuracy of the mechanism. It can help locate regions and directions where positioning accuracy is increased.

The method not only opens doors but also raises interesting questions. Such as, what precipitates changes in shape of the error surrounding the foot? This knowledge could aid in the design of a mechanism to optimize its positioning precision in a specific direction.

Another question is, how can foot position error be used in motion planning? Foot placement of walking machines can be critical when attempting to avoid obstacles or traversing narrow beams. Foot locations where the error surrounding it is great may not be acceptable options.

Finally, when modeling a small mechanism, parameters from several different types of models can be determined using the measuring technique and equipment developed for arthropod legs. With this in mind, is any one model, determined from measurements, more accurate than another for analyzing position, motion or force transmission? The

method used for analyzing foot position error might offer a clue for answering this question.

To begin with, errors in measurement can be represented as dimensional errors of a mechanism. These are errors in the position of a joint (error box) and errors in the orientation of a joint axis (error cone). A procedure for translating these errors to the foot has been presented. The procedure was demonstrated using the A-model of a beetle leg. It resulted in a graphical view of the volume of error surrounding a foot position.

The error volume around the foot is a result of superposing the error contributions of each error box and each error cone of the individual joints. An error box has its center at the joint and four of its edges are aligned with the joint axis. The error cone has its vertex at any point within the error box and its center axis is parallel to the joint axis. After translating an error box to the foot, the box changes in size and shape depending on the position of the foot. The error cone translated to the foot is a surface bounded by a closed line roughly the shape of an ellipse. Combining boxes and cones results in a volume.

Now consider what these errors may mean for a D-H model. After a joint is aligned for measurement, its measured coordinate positions and orientations are determined all with respect to frame p. The measurement parameters are used to transform the joint axis and its

position into the reference frame s. The position and orientation of the joint axis in this frame are dependent on measurement parameters x, y, β and σ but not on z. Measurement parameter z determines only the location of the joint. The D-H model disregards the position of the joint and its parameters are dependent only on position and orientation of joint axes. Having the ability to define a line's position and orientation with just four parameters (α,a,d,θ) was the basic idea on which the D-H model was developed. Since measurement z has no effect on joint axis position and orientation, it could have any value and not affect the parameter values of the D-H model.

As opposed to the error box used with the A-model, the joint position errors of the D-H model may be represented with just an "error square" eliminating the need to consider errors in z measurement. The error squares and error cones would not be represented on the D-H model itself but on the S-model from which D-H model parameters are extracted (see Fichter, Albright and Fichter, 1988). The position of the joint frame's origin along the joint axis in the S-model is arbitrary, again allowing any value of measurement-parameter z. This could result in a more accurate method of analyzing position errors of a leg mechanism, depending how joint errors translate to the foot using the D-H model. If so, then two models would be necessary to do an accurate study of arthropod legs.

BIBLIOGRAPHY

Broderick, P.L. and Cipra, R.J., "A Method for Determining and Correcting Robot Position and Orientation Errors Due to Manufacturing," Journal of Mechanisms, Transmissions, and Automation in Design, March 1988, vol. 110, pp. 3-10.

Chen, J. and Chao, L.M., "Positioning Error Analysis for Robot Manipulators With All Rotary Joints," Proceedings of IEEE International Conference on Robotics and Automation, 1986, vol. 2, pp. 1011-1016.

Cimino, W.W. and Pennock, G.R., "Workspace of a Six-Revolute Decoupled Robot Manipulator," Proceedings of the IEEE Conference on Robotics and Automation, 1986, pp. 1848-1852.

Denavit, J. and Hartenberg, R.S., "A Kinematic Notation for Lower-Pair Mechanisms BAsed on Matrices," Journal of Applied Mechanics, June 1955, vol. 77, pp. 215-221.

Everett, L.J., Driels, M. and Mooring, B.W., "Kinematic Modelling for Robotic Calibration," International Conference on Robotics and Automation," 1987, vol. 1, pp. 183-189.

Fichter, E.F., Fichter, B.L. and Albright, S.L., "Arthropods: 350 Million Years of Successful Walking Machine Design," Proceeding of IFToMM 7th World Congress, Sevilla, Spain, Sept. 1987, pp 1877-80.

Fichter, E.F. and Fichter, B.L., "A Survey of Legs of Insects and Spiders From a Kinematic Perspective," Proceedings of IEEE International Conference on Robotics and Automation, 1988

Fichter, E.F., Albright, S.L., and Fichter, B.L., "Determining Kinematic Parameters of Arthropod Legs," 20th Biennial ASME Mechanisms Conference, 1988

Hayati, S.A., "Robot Arm Geometric Link Parameter Estimation," Proceedings of the 22nd IEEE Conference on Decision and Control, 1983, pp. 1477-1483.

Hemami, H., "Book Review: Kinematic Modeling, Identification, and Control of Robotic Manipulators," IEEE Transactions on Robotics and Automation, April 1989, pp.

Hsu,T-W, and Everett, L.J., "Identification of the Kinematic Parameters of a Robot Manipulator for Positional Accuracy Improvement," Proceedings of the ASME International Computers in Engineering Conference, 1985, vol. 1, pp. 263-267.

Ibarra, R. and Perreira, N.D., "Determination of Linkage Parameter and Pair Variable Errors in Open Chain Kinematic Linkages Using a Minimal Set of Pose Measurement Data," Journal of Mechanisms, Transmissions, and Automation in Design, June 1986, vol. 108, pp. 159-166.

Judd, R.P. and Knasinski, A.B., "A Technique to Calibrate Industrial Robots With Experimental Verification," Proceedings of IEEE International Conference on Robotics and Automation," 1987, vol. 1, pp. 351-357.

Kinzel, G.L. and Gutkowski, L.J., "Joint Models, Degrees of Freedom, and Anatomical Motion Measurement," Journal of Biomechanical Engineering, Feb. 1983, vol. 105, pp. 55-62.

Manton, S.M., "Habits of Life and Evolution of Design in Arthropoda," Journal of Linnean Society, 1958, vol. 44, pp. 58-72.

Manton, S.M., "The Arthropoda: Habits, Functional Morphology, and Evolution," Clarendon Press - Oxford, 1977.

Manton, S.M., "The Evolution of Arthropodan Locomotory Mechanisms," Journal of Linnean Society, 1973, vol. 53, pp. 257-375.

Mooring, B.W. and Tang, G-R., " An Improved Method For Identifying The Kinematic Parameters In A Six Axis Robot," Proceedings of the ASME International Computers in Engineering Conference, 1984, vol. 1, pp. 79-84.

Paul, R.P., "Robot Manipulators: Mathematics, Programming, and Control," The MIT Press, 1981, pp. 25-29.

Roth, Z.S., Mooring, B.W. and Ravani, B. " An Overview of Robot Calibration," IEEE Journal of Robotics and Automation, Oct. 1987, vol. RA-3 (5), pp. 377-384.

Song, S.-M. and Waldron, K.J., "Machines That Walk," 1989, MIT Press.

Sheth, P.N. and Uicker, J.J., "A Generalized Symbolic Notation for Mechanisms," Journal of Engineering for Industry, Feb. 1971, vol. 93 srs B, 102-112.

Stone, H.W. and Sanderson, A.C., "Kinematic Modeling, Identification, and Control of Robotic Manipulators," Kluwer Academic Publishers, 1987.

Vaishnav, R.N. and Magrab, E.B., "A general Procedure to Evaluate Robot Positioning Errors," The International Journal of Robotics Research, Spring 1987, vol. 6 (1), pp. 59-74.

Veitschegger, W.K. and Wu, Chi-haur, "A Method For Calibrating and Compensating Robot Kinematic Errors," Proceedings of IEEE International Conference on Robotics and Automation, 1987, vol. 1, pp. 39-44.

Wang, H.H.S. and Roth, B., "Position Errors Due to Clearances in Journal Bearings," Journal of Mechanisms, Transmissions, and Automation in Design, Sept. 1989, vol. 111, pp. 315-320.

Whitney, D.E., Lozinski, C.A. and Rourke, J.M., " Industrial Robot Calibration Method and Results," Proceedings of the International Computers in Engineering Conference, 1984, vol. 1, pp. 92-100.

Ziegert, J. and Datseris, P., "Basic Considerations For Robot Calibration," Proceedings of IEEE International Conference on Robotics and Automation, 1988, vol. 2, pp. 932-938.

APPENDICES

APPENDIX A

DIFFERENTIAL APPROACH TO DETERMINING ERRORS IN A-MODEL PARAMETERS

An approach taken to determine errors in A-model parameters resulting from errors in measurements of a leg was to calculate model-parameter differentials in terms of measurement-parameter differentials. The model-parameter differentials would then represent errors in the A-model parameter errors. The four fixed parameters of the A-model describing the shape of a leg segment, τ, s, μ, and Ω, are extracted from the transformation matrix ${}^{i}U_{i+1}{}'$ as described in the chapter 3 and expressed as

$$ {}^{i}U_{i+1}{}' = \begin{bmatrix} nx & ox & cx & px \\ ny & oy & cy & py \\ nz & oz & cz & pz \\ 0 & 0 & 0 & 1 \end{bmatrix} \qquad (3.12) $$

To simplify the problem at hand, the arbitrary parameter Θ used to aid the extraction of model parameters will be considered zero. The errors in determining Θ only influence the joint range-of-motion results and do not effect the

determination of model parameters describing a leg segment's shape. When θ is zero, py in 4.1 also has a value of zero and the A-model's four fixed parameters are related to only five elements in this matrix; cx, cy, cz, px and pz. The elements are then expressed as

$$\tau_i = \text{atan2}(-pz/px) \tag{A.1}$$

$$s_i = px \cos \tau_i - pz \sin \tau_i \quad \text{or} \quad (px^2 + pz^2)^{1/2} \tag{A.2}$$

$$\mu_i = \text{atan2}\left[- \frac{cy}{cx \sin \tau_i + cz \cos \tau_i} \right] \tag{A.3}$$

$$\Omega_i = \text{atan2}\left[\frac{cx \cos \tau_i - cz \sin \tau_i}{-cy \sin \mu_i + \cos \mu_i \, (cx \sin \tau_i + cz \cos \tau_i)} \right] . \tag{A.4}$$

Next is to determine the differential of each parameter in terms of the known ${}^{i}U_{i+1}'$ matrix elements and their differentials reflecting measurement errors. Each differential is dependent not only on element changes but also on the shape of the link defined by τ, s, μ, and Ω. The resulting parameter differentials can be expressed as follows.

$$d\tau_i = \frac{- dpx \sin \tau_i \; - dpz \cos \tau_i}{s_i} \tag{A.5}$$

$$ds_i = dpx \cos \tau_i \; - dpz \sin \tau_i \tag{A.6}$$

$$d\mu_i = [dcx \sin \tau_i \sin \mu_i + dcy \cos \mu_i + dcz \cos \tau_i \sin \mu_i - \sin \mu_i \sin \Omega_i (dpx \sin \tau_i + dpz \cos \tau_i)/s_i]/\cos \Omega_i \quad (A.7)$$

$$d\Omega_i = dcx (\cos \tau_i \cos \Omega_i - \sin \tau_i \cos \mu_i \sin \Omega_i) + dcy (\sin \mu_i \sin \Omega_i) - dcz (\sin \tau_i \cos \Omega_i + \cos \tau_i \cos \mu_i \sin \Omega_i) + \cos \mu_i (dpx \sin \tau_i + dpz \cos \tau_i)/s_i \quad (A.8)$$

where the prefix d indicates the differential.

The elements px and pz locate the origin of frame i+1 with respect to frame i. The elements cx, cy and cz are the direction cosines of the z_{i+1} coordinate axis with respect to frame i. These five elements are themselves functions of ten measurement parameters; ${}^{p}x_i$, ${}^{p}y_i$, ${}^{p}z_i$, σ_i, β_i, ${}^{p}x_{i+1}$, ${}^{p}y_{i+1}$, ${}^{p}z_{i+1}$, σ_{i+1} and β_{i+1}, plus the arbitrary angle δ_{fi}. The five elements are related to the measurements as follows.

$$\begin{aligned} px = & -{}^{p}x_i c\delta_{fi} - {}^{p}y_i s\delta_{fi} \\ & + {}^{p}x_{i+1}[c\delta_{fi}(c\beta_i c\beta_{i+1} c(\sigma_{i+1} - \sigma_i) + s\beta_i s\beta_{i+1}) \\ & - s\delta_{fi} c\beta_{i+1} s(\sigma_{i+1} - \sigma_i)] + {}^{p}y_{i+1}[c\delta_{fi} c\beta_i s(\sigma_{i+1} - \sigma_i) \\ & + s\delta_{fi} c(\sigma_{i+1} - \sigma_i)] \\ & + {}^{p}z_{i+1}[c\delta_{fi}(-c\beta_i s\beta_{i+1} c(\sigma_{i+1} - \sigma_i) + s\beta_i c\beta_{i+1}) \\ & + s\delta_{fi} s\beta_{i+1} s(\sigma_{i+1} - \sigma_i)] \end{aligned} \quad (A.9)$$

$$pz = -{}^{P}z_i - {}^{P}x_{i+1}[s\beta_i c\beta_{i+1} c(\sigma_{i+1} - \sigma_i) - c\beta_i s\beta_{i+1}]$$
$$- {}^{P}y_{i+1}[s\beta_i s(\sigma_{i+1} - \sigma_i)]$$
$$+ {}^{P}z_{i+1}[s\beta_i s\beta_{i+1} c(\sigma_{i+1} - \sigma_i) + c\beta_i c\beta_{i+1}] \qquad (A.10)$$

$$cx = -c\delta_{fi}(c\beta_i s\beta_{i+1} c(\sigma_{i+1} - \sigma_i) - s\beta_i c\beta_{i+1})$$
$$+ s\delta_{fi} s\beta_{i+1} s(\sigma_{i+1} - \sigma_i) \qquad (A.11)$$

$$cy = s\delta_{fi}(c\beta_i s\beta_{i+1} c(\sigma_{i+1} - \sigma_i) - s\beta_i c\beta_{i+1})$$
$$+ c\delta_{fi} s\beta_{i+1} s(\sigma_{i+1} - \sigma_i) \qquad (A.12)$$

$$cz = s\beta_i s\beta_{i+1} c(\sigma_{i+1} - \sigma_i) + c\beta_i c\beta_{i+1} \qquad (A.13)$$

where

$c\beta_i = \cos\beta_i$, $s\beta_i = \sin\beta_i$, $c\sigma_i = \cos\sigma_i$, $s\sigma_i = \sin\sigma_i$, $c\delta_{fi} = \cos\delta_{fi}$, and $s\delta_{fi} = \sin\delta_{fi}$

To complete this error evaluation approach, the differentials of A.9 to A.13 must be determined. However, an analytical error analysis of this nature becomes difficult to interpret when using the above expressions due to their obvious complexity and to the dependence some measurements have on others. For instance, the magnitude of the error in σ_i is dependent on the value of β_i when aligning joint axis i. If β_i=0° then σ_i can range in value from 0° to 360° and not change the resulting alignment. If β_i=90° then β_i and σ_i have a comparable effect on the

alignment the joint axis. In addition, because the origin of a joint coordinate frame is measured with respect to the positioner frame and the arthropod specimen is rigidly attached the stage frame, the axis alignment errors in β_i and σ_i are reflected in the relative position measurements ${}^{p}x_i$, ${}^{p}y_i$, ${}^{p}z_i$. This dependency is dramatized in the case where z_i is parallel but not coincident to z_s. Because σ_i can have any value in this axis orientation, ${}^{p}x_i$ and ${}^{p}y_i$ also have an infinite number of possible values. All would exist on a circle lying on a plane perpendicular to the z_i axis whose center is z_i and whose radius is equal to the perpendicular distance between z_i and z_s.

The difficulties of this approach stem from trying to analyze expressions which relate one joint frame to another.

APPENDIX B

ANALYTIC INVERSE KINEMATIC SOLUTION TO 3-LINK MANIPULATOR DESCRIBED BY THE A-MODEL

The beetle leg is modeled as a spatial three-link manipulator connected by revolute joints and has an analytic inverse kinematic solution. Cimino and Pennock (1986) presented an analytic solution to the first three joint displacements of a six-revolute decoupled manipulator with a general geometry. Using D-H parameters to describe the manipulator, they formulated 3x3 dual transformation matrices for use in expressing the orientation and position of the wrist joint frame relative to a base frame. Each dual transformation matrix $\hat{A}$ defines the backward transformation from one frame on the linkage to its preceding frame. $\hat{A}$ is written as $\hat{A} = A + A^{\circ}$ where A expresses the relative orientation of the frames and A° their relative position. From these matrices, three nonlinear equations in terms of the first three joint displacements were determined. By eliminating the second and third joint displacements and making various substitutions, a fourth order polynomial as a function of the first joint displacement was found. Knowing the solution to joint displacement one, joint displacement 2 then 3 could be solved.

For the three-link darkling beetle leg, only position of the origin of frame uvw_4 (i.e. the foot position) is considered here in an inverse kinematic solution. Given the foot position of a beetle leg, Yoon-Su Baek (unpublished), O.S.U. Ph.D candidate, found an analytic inverse kinematic solution to the three joint displacements. He obtained three nonlinear equations as functions of the three joint angles from 4x4 transformation matrices formulated by using a D-H model of the leg. In the elimination of variables, Baek's solution does not use the dual matrix concept of Cimino and Pennock but still results in a 4th order polynomial in terms of one joint displacement.

The D-H model contains two orientation parameters, twist and joint variable, and two displacement parameters, link length and link offset, which make it well suited to an inverse kinematic solution formulated from 3x3 dual transformation matrices. Since the A-model description does not have this same feature, the following solution uses the approach taken by Baek. It should be noted that the inverse solution using D-H model parameters is less complex than the following routine due to its simpler transformation matrix. If D-H parameters are available, then it may be advisable to use the D-H model solution. Due to the complexity of the A-model, much of the equation reduction in following solution was accomplished with aid of MACSYMA, a symbolic equation solver software package.

Coordinate frames are attached to each joint axis of the beetle (see Figure 2.5) as described in chapter 2 section 4. The position of the foot at the origin of frame 4 is described relative to the base frame (i.e. body frame of the beetle) by ${}^{b}\mathbf{P}_4$ and is expressed as

$$ {}^{b}\mathbf{P}_4 = \mathbf{A}\ {}^{4}\mathbf{P}_4 \qquad \text{(B.1)} $$

where ${}^{4}\mathbf{P}_4$ is the foot position relative to frame uvw_4 and $\mathbf{A}$ is the transformation matrix relating the frame uvw_4 to the body frame. Since position ${}^{4}\mathbf{P}_4$ is coincident to the origin of frame uvw_4 it is expressed as column matrix ${}^{4}\mathbf{P}_4 = [0,0,0,1]^T$. From equation 2.1, $\mathbf{A}$ is defined in terms of the pair and shape matrices of each link as

$$ \mathbf{A} = \mathbf{B}\ \mathbf{\$}_1\ \mathbf{S}_1\ \mathbf{\$}_2\ \mathbf{S}_2\ \mathbf{\$}_3\ \mathbf{S}_3 \qquad \text{(B.2)} $$

where $\mathbf{B}$ is the transformation matrix defined by equation (2.4).

Substituting equation (B.2) into (B.1) and pre-multiplying both sides of the equation by $\mathbf{B}^{-1}$, the position of the foot relative to frame uvw_1, ${}^{1}\mathbf{P}_4$, is defined in terms of the joint displacements 1, 2 and 3.

$$ {}^{1}\mathbf{P}_4 = \mathbf{\$}_1\ \mathbf{S}_1\ \mathbf{\$}_2\ \mathbf{S}_2\ \mathbf{\$}_3\ \mathbf{S}_3\ {}^{4}\mathbf{P}_4 \qquad \text{(B.3)} $$

The pair matrix $\mathbf{\Phi}$ and shape matrix $\mathbf{S}$ are defined by transformations (2.5) and (2.3) respectively. Transformation matrix 2.3 is rewritten here as

$$\mathbf{S}_i = \begin{bmatrix} ax_i & bx_i & cx_i & px_i \\ ay_i & by_i & cy_i & 0 \\ az_i & bz_i & cz_i & pz_i \\ 0 & 0 & 0 & 1 \end{bmatrix} \tag{B.4}$$

where

$$ax_i = c\tau_i c\Omega_i - s\tau_i c\mu_i s\Omega_i \tag{B.5}$$

$$ay_i = s\mu_i s\Omega_i \tag{B.6}$$

$$az_i = -s\tau_i c\Omega_i - c\tau_i c\mu_i s\Omega_i \tag{B.7}$$

$$bx_i = s\tau_i s\mu_i \tag{B.8}$$

$$by_i = c\mu_i \tag{B.9}$$

$$bz_i = c\tau_i s\mu_i \tag{B.10}$$

$$cx_i = c\tau_i s\Omega_i + s\tau_i c\mu_i c\Omega_i \tag{B.11}$$

$$cy_i = -s\mu_i c\Omega_i \tag{B.12}$$

$$cz_i = -s\tau_i s\Omega_i + c\tau_i c\mu_i c\Omega_i \tag{B.13}$$

$$px_i = c\tau_i s_i \tag{B.14}$$

$$pz_i = -s\tau_i s_i \tag{B.15}$$

and where i = 1, 2 and 3.

Position ${}^1\mathbf{P}_4$ is also expressed as a known quantity by the column matrix ${}^1\mathbf{P}_4 = [{}^1Px, {}^1Py, {}^1Pz, 1]^T$ and is determined from the expression

$$ {}^{1}\mathbf{P}_4 = \mathbf{B}^{-1}\ {}^{b}\mathbf{P}_4 \qquad \text{(B.16)} $$

By substituting equations (2.5) and (B.4) into (B.3) and then expanding, three nonlinear equations are obtained which relate the three coordinates of ${}^{1}\mathbf{P}_4$ in terms of the three joint displacements.

$$ {}^{1}Px = E1 \cos \phi_1 - E2 \sin \phi_1 \qquad \text{(B.17)} $$

$$ {}^{1}Py = E1 \sin \phi_1 + E2 \cos \phi_1 \qquad \text{(B.18)} $$

$$ {}^{1}Pz = E3 \qquad \text{(B.19)} $$

where

$$ E1 = ax_1 (F1 \cos \phi_2 - F2 \sin \phi_2) + bx_1 (F1 \sin \phi_2 + F2 \cos \phi_2) + cx_1 F3 + px_1 \qquad \text{(B.20)} $$

$$ E2 = ay_1 (F1 \cos \phi_2 - F2 \sin \phi_2) + by_1 (F1 \sin \phi_2 + F2 \cos \phi_2) + cy_1 F3 \qquad \text{(B.21)} $$

$$ E3 = az_1 (F1 \cos \phi_2 - F2 \sin \phi_2) + bz_1 (F1 \sin \phi_2 + F2 \cos \phi_2) + cz_1 F3 + pz_1 \qquad \text{(B.22)} $$

and where

$$ F1 = ax_2\ px_3 \cos \phi_3 + bx_2\ px_3 \sin \phi_3 + cx_2\ pz_3 + px_2 \qquad \text{(B.23)} $$

$$ F2 = ay_2\ px_3 \cos \phi_3 + by_2\ px_3 \sin \phi_3 + cy_2\ pz_3 \qquad \text{(B.24)} $$

$$ F3 = az_2\ px_3 \cos \phi_3 + bz_2\ px_3 \sin \phi_3 + cz_2\ pz_3 + pz_2 \qquad \text{(B.25)} $$

Joint displacement 1 is eliminated by squaring then adding equations (B.17) - (B.19). After some manipulation this yields:

$$Psqr = K1 + K2 \sin \phi_3 + K3 \cos \phi_3 \qquad (B.26)$$

where

$$Psqr = {}^1Px^2 + {}^1Py^2 + {}^1Pz^2 \qquad (B.27)$$

and

$$K1 = M1 + M2 \sin \phi_2 + M3 \cos \phi_2 \qquad (B.28)$$

$$K2 = M4 + M5 \sin \phi_2 + M6 \cos \phi_2 \qquad (B.29)$$

$$K3 = M7 + M8 \sin \phi_2 + M9 \cos \phi_2 \qquad (B.30)$$

and where

$$M1 = s_1^2 + s_2^2 + s_3^2 - 2\, s_1\, s\Omega_1\, s\tau_2\, s_2 + 2\, s_1\, s\Omega_1\, s\tau 3\, s_3\, (s\tau_2\, s\Omega_2 - c\tau_2\, c\mu_2\, c\Omega_2) - 2\, s_2\, s\Omega_2\, s\tau_3\, s_3$$

$$M2 = -2\, s_1\, c\Omega_1\, s\mu_2\, c\Omega_2\, s\tau_3\, s_3$$

$$M3 = 2\, s_1\, c\Omega_1\, c\tau_2\, s_2 - 2\, s_1\, c\Omega_1\, s\tau_3\, s_3\, (c\tau_2\, s\Omega_2 + s\tau_2\, c\mu_2\, c\Omega_2)$$

$$M4 = 2\, s_1\, s\Omega_1\, c\tau_2\, s\mu_2\, c\tau_3\, s_3$$

$$M5 = -2\, s_1\, c\Omega_1\, c\mu_2\, c\tau_3\, s_3$$

$$M6 = 2\, s_1\, c\Omega_1\, s\tau_2\, s\mu_2\, c\tau_3\, s_3$$

$$M7 = -2\, s_1\, s\Omega_1\, c\tau_3\, s_3\, (s\tau_2\, c\Omega_2 + c\tau_2\, c\mu_2\, s\Omega_2) + 2\, s_2\, c\Omega_2\, c\tau_3\, s_3$$

$$M8 = -2\ s_1\ c\Omega_1\ s\mu_2\ s\Omega_2\ cY_3\ s_3$$

$$M9 = -2\ s_1\ c\Omega_1\ cY_3\ s_3\ (-cY_2\ c\Omega_2 + sY_2\ c\mu_2\ s\Omega_2)$$

The s and c followed by angles Y, μ, and Ω are the sin and cos of these angles respectively.

The z coordinate of the foot position with respect to frame uvw_1 is redefined as

$$^1Pz = K4 + K5 \sin \phi_3 + K6 \cos \phi_3 \qquad (B.31)$$

where

$$K4 = R1 + R2 \sin \phi_2 + R3 \cos \phi_2 \qquad (B.32)$$

$$K5 = R4 + R5 \sin \phi_2 + R6 \cos \phi_2 \qquad (B.33)$$

$$K6 = R7 + R8 \sin \phi_2 + R9 \cos \phi_2 \qquad (B.34)$$

and where

$$R1 = cz_1\ (cz_2\ pz_3 + pz_2) + pz_1$$

$$R2 = bz_1\ (cx_2\ pz_3 + px_2) - az_1\ cy_2\ pz_3$$

$$R3 = az_1\ (cx_2\ pz_3 + px_2) + bz_1\ cy_2\ pz_3$$

$$R4 = cz_1\ bz_2\ px_3$$

$$R5 = (bz_1\ bx_2 - az_1\ by_2)\ px_3$$

$$R6 = (bz_1\ by_2 + az_1\ bx_2)\ px_3$$

$$R7 = cz_1\ az_2\ px_3$$

$$R8 = (bz_1\ ax_2 - az_1\ ay_2)\ px_3$$

$$R9 = (bz_1\ ay_2 + az_1\ ax_2)\ px_3$$

Solving equations (B.26) and (B.31) simultaneously for sin ϕ_3 and cos ϕ_3 we find

$$\sin \phi_3 = (K6\ Psqr - K6\ K1 - K3\ {}^1Pz + K3\ K4)/(K2\ K6 - K3\ K5) \tag{B.35}$$

$$\cos \phi_3 = (-K5\ Psqr + K5\ K1 + K2\ {}^1Pz - K2\ K4)/(K2\ K6 - K3\ K5) \tag{B.36}$$

Equations (B.35) and (B.36) are now squared and added to eliminate ϕ_3. Substituting (B.28) - (B.30) and (B.32) - (B.34) into this sum with extensive rearrangement we get

$$N1\ s^2\phi_2 + N2\ c^2\phi_2 + N3\ s\phi_2\ c\phi_2 + N4\ s\phi_2 + N5\ c\phi_2 + N6 = 0 \tag{B.37}$$

where

$$N1 = Q1^2 - Q4^2 - Q7^2$$

$$N2 = Q2^2 - Q5^2 - Q8^2$$

$$N3 = 2\ (Q1\ Q2 - Q4\ Q5 - Q7\ Q8)$$

$$N4 = 2\ (Q1\ Q3 - Q4\ Q6 - Q7\ Q9)$$

$$N5 = 2\ (Q2\ Q3 - Q5\ Q6 - Q8\ Q9)$$

$$N6 = Q3^2 - Q6^2 - Q9^2$$

and where

$$Q1 = M4\ R8 + M5\ R7 - M7\ R5 - M8\ R4$$

$$Q2 = M4\ R9 + M6\ R7 - M7\ R6 - M9\ R4$$

$$Q3 = M5\ R8 + M4\ R7 - M8\ R5 - M7\ R4$$

$$Q4 = R8\ Psqr - M1\ R8 - M2\ R7 + M7\ R2 + M8\ R1 - {}^1Pz\ M8$$

$$Q5 = R9\ Psqr - M1\ R9 - M3\ R7 + M7\ R3 + M9\ R1 - {}^1Pz\ M9$$

$$Q6 = R7\ Psqr - M2\ R8 - M1\ R7 + M8\ R2 + M7\ R1 - {}^1Pz\ M7$$

$$Q7 = -R5\ Psqr + M1\ R5 + M2\ R4 - M4\ R2 - M5\ R1 + {}^1Pz\ M5$$

$$Q8 = -R6\ Psqr + M1\ R6 + M3\ R4 - M4\ R3 - M6\ R1 + {}^1Pz\ M6$$

$$Q9 = -R4\ Psqr + M2\ R5 + M1\ R4 - M5\ R2 - M4\ R1 + {}^1Pz\ M4$$

Finally, substituting the half-angle relationships

$$\sin \phi_2 = \frac{2T}{1 + T^2} \quad \text{and} \quad \cos \phi_2 = \frac{1 - T^2}{1 + T^2} \tag{B.38}$$

where $T = \tan \phi_2/2$, into equation (B.37), we get

$$T^4 + C1\ T^3 + C2\ T^2 + C3\ T + C4 = 0 \tag{B.39}$$

where

$$C1 = 2\ (N4 - N3)/(N6 - N5 + N2)$$

$$C2 = 2\ (N6 - N2 + 2\ N1)/(N6 - N5 + N2)$$

$$C3 = 2\ (N4 + N3)/(N6 - N5 + N2)$$

$$C4 = (N6 + N5 + N2/(N6 - N5 + N2)$$

The quartic equation (B.39) has four possible solutions which may all be real, complex or a combination of the two. The real solutions of T are substituted back into (B.38) from which ϕ_2 is determined by

$$\phi_2 = \text{atan2}\ (\sin \phi_2,\ \cos \phi_2) \tag{B.40}$$

The solutions of joint displacement ϕ_2 are used in equations (B.28) - (B.30) and (B.32) - (B.34) which are then substituted into (B.35) and (B.36). Joint displacement ϕ_3 is solved from

$$\phi_3 = \text{atan2}\ (\sin \phi_3,\ \cos \phi_3) \tag{B.41}$$

The solutions of ϕ_3 are substituted into equations (B.20) - (B.25). Solving (B.17) and (B.18) for sin ϕ_1 and cos ϕ_1 then making the appropriate substitutions of (B.20) - (B.25) into these equations, ϕ_1 is found from

$$\phi_1 = \text{atan2}\ (\sin \phi_1,\ \cos \phi_1) \tag{B.42}$$

A valid set of joint displacement solutions exists if

$$\phi_{L1} \le \phi_1 \le \phi_{H1}, \quad \phi_{L2} \le \phi_2 \le \phi_{H2} \quad \text{and} \quad \phi_{L3} \le \phi_3 \le \phi_{H3} \tag{B.43}$$